Electromagnetic Transient Modelling of Power Transmission Line Tower and Tower-Footing Grounding System

by

Bamdad Salarieh

A thesis submitted to the Faculty of Graduate Studies of
The University of Manitoba
in partial fulfilment of the requirements of the degree of

Master of Science

Department of Electrical and Computer Engineering
University of Manitoba
Winnipeg, MB, Canada

Abstract

Lightning is known to be a major cause of outage in power systems. It may result in damage to equipment, high repair costs, and loss of revenue to utility companies. The most vulnerable component of a power system to lightning is the power transmission line system. Transmission lines expand over hundreds of kilometers and are exposed to lightning discharge. When a lightning strike directly hits either the top of a transmission tower or the ground wires, surge waves are generated that flow through the tower structure that has been hit and propagate to adjacent towers. This leads to an increased voltage difference across the string of insulators that may lead to a backflashover. Backflashover may occur when the voltage difference on the string of insulators exceeds the withstand of the insulators due to a lightning surge and it is the main outage mechanism. There is a significant need in the power system community for the accurate electromagnetic transient (EMT) analysis of lightning discharge phenomena through complex power installations such as transmission towers and their grounding system. The tower-footing grounding systems consists of long conductors, in different shapes and arrangements, buried in either homogeneous or stratified ground to obtain the lowest tower-footing grounding impedance. Moreover, the impedance of the tower's structure contributes to the total impedance of the system when subjected to lightning surges. Currently, existing simulation tools make various approximations in

the process of lightning analysis that result in modeling inaccuracies in many important practical scenarios. Such errors make unreliable predictions about the failure rates of the system resulting in costly power outages.

In this thesis, simulation models are developed for the determination of the response of typical arrangements of grounding electrodes and transmission towers subjected to lightning and calculate the impedance of these structures over the frequency range of interest in lightning studies. Time-domain macro-models will then be developed that are compatible with EMT-type simulators (such as PSCAD/EMTDC) and enable the calculation of voltages along the tower structure considering several geometric factors and ground parameters. The objectives of this research are to accurately estimate the overvoltages/surge in the transmission tower, and to develop a model for the prediction of backflashovers. The developed model will significantly improve the accuracy of EMT analysis of lightning discharge and its impacts on complex power systems.

Acknowledgements

Firstly, I would like to express my gratitude to my advisor, Dr. Behzad Kordi, for his guidance, motivation, and encouragement throughout this research. I deeply appreciate all his valuable comments and guidance.

Many thanks to my thesis examination committee, Dr. Ani Gole and Dr. Dharshana Muthumuni for their comments and suggestions to improve my thesis. I also want to thank Dr. Ian Jeffrey, who provided me with an exceptional computational recourse to perform simulations. The cooperation and support of Dr. Jeewantha De Silva, Dr. Akihiro Ametani, and Ryan Bridges are appreciated.

Financial support from University of Manitoba, Faculty of Graduate Studies, Mitacs, and Manitoba Hydro International (MHI) is gratefully acknowledged.

Last but not least, I would like to thank my wife, Farnaz, for her kindness, patience and full support through my studies.

Dedication

To my loving wife who encouraged me to pursue my dreams.

Table of Contents

List of Figures

List of Tables

Chapter 1

Introduction

1.1 Motivation

Lightning strike to transmission line towers or overhead conductors is one of the major causes of outage in power systems. Seven out of twelve major blackouts happened in 2019 were reported to be due to a lightning strike to power lines [1]. Such blackouts can affect the lives of millions of people for several days and even weeks, and cost billions of dollars to utility companies. Accurate electromagnetic transient modelling of lightning discharge through complex power systems requires accounting for the 3D geometric details of the power system components, effect of the grounding system, and the impact of the material parameters on the injected charge relaxation. All of the mentioned features must be included into a computational model to adequately describe the physical electromagnetic interactions occurring in the actual power system. The model of transmission line tower currently available in EMT-type simulators adopts several simplifications that restrict its applicability. Furthermore, the impedance of the grounding system is approximated by a resistor which is not accurate for

studies that involve the injection of currents with high frequency components in to the system, such as lightning currents [2]. As a result, the existing model is unable to estimate the surge behaviour of the transmission line with sufficient accuracy. The electrical behaviour of a transmission tower considering lightning discharge at its top depends on several factors, such as the geometry of tower or its transient impedance, grounding impedance, and the current waveform injected in to the tower. In this context, the surge impedance of the tower and its grounding system play a fundamental role in the determination of lightning-induced electrical potential rise in the tower and across the string of insulators. There is a need to develop a model for the transmission line tower and its grounding system to calculate the overvoltage and predict the occurrence of a backflashover. Using the developed model, the end-user of the time domain simulators (such as PSCAD/EMTDC) does not need to perform any electromagnetic field analysis to obtain the transient voltages across the string of insulators. Furthermore, the backflashover rate of the system can be determined and the length of grounding electrodes can be calculated to ensure a desired outage rate.

1.2 Problem Definition

Power transmission line networks, due to their vast physical dimensions, are the most critical components of a complex power system from the reliability point of view in relation to direct lightning strike. The outages due to a lightning strike are caused by three different mechanisms: flashover, midspan-flashover, and backflashover [3]. The first type occurs when lightning strikes directly on the phase conductors due to the absence of a shielding wire. A midspan-flashover occurres when a lightning strikes the shield wires at midspan and the distance between the shield wire and phase conductors is not enough to prevent a flashover.

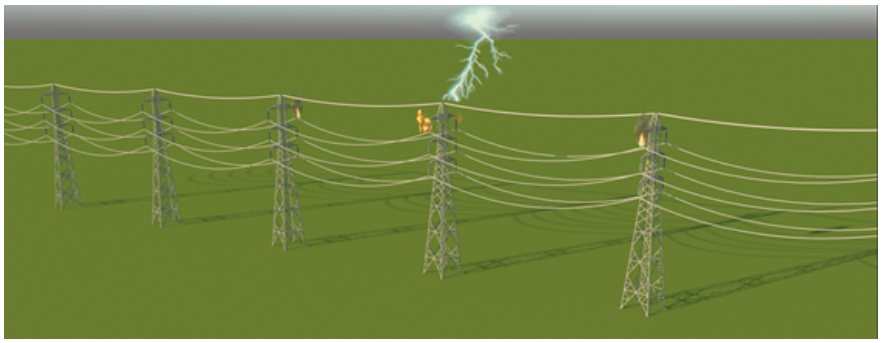

Fig. 1.1: A schematic of the occurrence of a backflashover due to a lightning strike to the top of a double circuit transmission line tower.

On the other hand, when a lightning strike directly hits either the top of a transmission tower or the ground wires as shown in Fig. 1.1, voltage surge waves are generated that flow through the tower structure that has been hit and consequently the voltage of the cross-arms raises and a flashover occurs if the electric field across the string of insulators exceeds the air dielectric strength. This phenomenon is called backflashover and is the main cause of outages for lines of voltages below 500 kV [4]. Although the characteristics of the transmission line grounding system are practically irrelevant in terms of flashover and midspan-flashover, they play a fundamental role in mitigating the backflasover [5].

There are three approaches to the modeling of a grounding system, 1) theoretical, 2) numerical, and 3) experimental. The theories are either based on the circuit [6–13] or transmission-line formulations [14–28]. These approaches are based on quasi-static approximation, which restricts their validity at high frequencies. The numerical solution of Maxwell's equations is based on the Finite Element Method (FEM) [29–36], the Method of Moments (MOM) [37–51], the Finite-Difference Time-Domain (FDTD) method [52–54], or the Partial Electric Equivalent Circuit (PEEC) [55, 56]. When the full-wave Maxwell's equations are considered in these approaches, they can be considered as the most rigorous and accurate

modeling procedures over a wide frequency range. The measurements are performed using the fall-of-potential (FOP) method. This method is based on passing a current through a grounding system using an auxiliary current probe and then measuring the voltage between the ground electrode and a potential probe [10, 57–61].

There are several references in the published literature that have tried to take into account the inherent features of soil which may affect the response of grounding systems to lightning currents. Typically, earth is an inhomogeneous medium, containing several layers oriented vertically or horizontally, each having different values of resistivity and electrical permittivity [62]. Attempts to model the grounding electrodes in multilayer soil structures can be found in [63–66]. The other important quality of soil is the frequency dependence of its electrical parameters (conductivity and permittivity). In lightning studies of grounding systems, the electrical parameters of the medium in which they are buried have a high importance and they need to be determined accurately. It has been shown through experiments that the conductivity and dielectric constant of soil are both very dependent on the moisture content of the soil which is known to be between 4% to 30% of the total soil weight over the greater part of the year [67]. An accurate model for grounding electrodes should consider the characteristics above to provide accurate results under different system conditions.

Besides the characteristics of the grounding system, the transient impedance of the tower is of great importance in the calculation of the induced voltage along the string of insulators. The tower components, such as cross arms, slant bars, and shield wires have a considerable effect on the transient response of the system. A model that takes into account these details can provide very accurate results for the lightning studies.

1.3 Objectives of the Thesis

The main objective of this research is to obtain macro-models for the transmission line tower and its grounding system to be used in time-domain simulations. To achieve this, a simulation model is developed for the analysis of grounding electrodes. Using this model, the full-wave Maxwell's equations are solved in the frequency domain to obtain the impedance of grounding systems. Both vertical and horizontal arrangements of grounding electrodes with different lengths are considered. Moreover, the effect of variation of soil electrical parameters and their frequency dependence on the response of the grounding electrodes are included. Next, the transmission line tower is added to the grounding electrodes to obtain a detailed model of the system in the frequency domain.

An automated process is developed to obtain the wire network of the transmission towers for the analysis in the Numerical Electromagnetic Code (NEC), which is based on the thin wire approximation and uses the Method of Moments (MOM) to solve for the currents in the system in the frequency domain. Further, a complete model of the tower, its grounding system, overhead conductors, and shield wires is analyzed using the Finite Element Method (FEM). The impedance of tower/grounding electrode is evaluated in a frequency range of 10 kHz to 10 MHz, as it is the frequency range where the most part of the frequency contents of typical lightning strokes are [68]. The developed macro-model will be implemented in an EMT-type simulator (such as PSCAD/EMTDC) and the probability of occurrence of a backflashover in different soil conditions is assessed.

1.4 Research Contributions

The contributions of this thesis can be categorized in two parts: i) grounding system, and ii) transmission line towers as follows:

i. Grounding System

- A simulation configuration is developed for the analysis of grounding electrodes using Finite Element Method (FEM). A sensitivity analysis is performed to find the optimum value of the parameters that can affect the accuracy of the numerical analysis.
- The frequency-domain response of vertical and horizontal grounding electrodes of different lengths buried in soil is obtained considering a wide range of soil electrical parameters (conductivity σ and permittivity ε). Both constant and frequency dependent soil parameters are considered.
- The accuracy of theoretical approaches, *i.e.* circuit and transmission line theories, is evaluated through comparison with the results obtained using the developed full-wave approach.
- Equivalent time-domain model of the considered grounding systems is developed, and the voltage at the top of the grounding electrodes is calculated in the time domain.

ii. Transmission Line Tower

- An automated process is developed to obtain the wire network model of transmission towers to be used in simulations using NEC4, which needs the system under simulation to be represented as a network of thin wires.

- After verifying the simulation model in NEC4, the accuracy of the previous theoretical tower models are compared with the results of NEC4, considering both a PEC and lossy ground.

- A simulation model is developed for the full-wave transient analysis of transmission towers in the frequency domain using Finite Element Method (FEM). The accuracy of the model is verified by reproducing some measured voltages and currents.

- Simulations are performed to solve the Full-wave Maxwell's equations considering all tower details, the real geometry of grounding system, a realistic equivalent representation of the string of insulators, shield wires, and phase conductors.

- A macro-model in the form of a black-box is developed for the transmission line tower and its grounding system and implemented in an EMT-type simulator (PSCAD/EMTDC in this thesis) using a state-space model.

- Backflashover studies are performed in different soil conditions to calculate the required length of counterpoise grounding electrodes to ensure an acceptable rate of outage.

1.4.1 Publications

- Conference Paper

    1. "Wideband EMT-Compatible Model for Grounding Electrodes Buried in Frequency Dependent Soil," B. Salarieh, H. M. J. De Silva, B. Kordi, International Conference on Power Systems Transients (IPST) - 2019.

       The main focus of the paper is on development of a FEM model for the analysis of the grounding electrodes. Sensitivity analysis is performed on the affecting pa-

rameters on the accuracy of the model, and the grounding impedance considering constant and frequency dependent soil is obtained. This paper received the Best Student Paper Award (Young Scientist Award) at the conference.

An extended version of the paper is also invited to be submitted to the especial issue of Electronic Power System Research (EPSR) journal, 2020.

- Jorunal Paper

1. "On the High Frequency Response of Grounding Electrodes: Effect of Soil Dielectric Constant," B. Salarieh, H. M. J. De Silva, B. Kordi, submitted to IET Generation, Transmission and distribution (GTD).

   In this paper, the developed FEM model is used to assess the effect of soil permittivity and water content on the high frequency behavior of the grounding electrodes. Further, the accuracy of the theoretical approaches in modeling the dynamic behavior of grounding electrodes is examined.

2. "An Electromagnetic Model for the Calculation of Tower Surge Impedance Based on Thin Wire Approximation," B. Salarieh, H. M. J. De Silva, A. Gole, A. Ametani, B. Kordi, submitted to IEEE Transactions on Power Delivery.

   This paper contains a thorough review of the previous models for transmission towers, and uses the Method of Moments (MOM) to show the effect of counterpoise grounding electrodes on the developed voltage on top of a tower. This paper assess the accuracy of theoretical tower models in predicting the tower top voltage and its transient behavior.

3. "A Black-box Approach to Interface Transmission Tower Model with EMT Simulators for the Assessment of Backflashover," B. Salarieh, B. Kordi, submitted

to the IEEE Transactions on power delivery. The development of a black-box model for transmission line tower is covered in this paper. A multi-port network in the form of a black-box is proposed for the tower, which includes the effect of grounding system, frequency dependency of soil electrical parameters, the overhead conductors and shield wires. Furthermore, the model is implemented in PSCAD/EMTDC to calculate the backflashover rate in a typical 400 kV double circuit tower, due to the injection of first lightning strokes at the tower top.

1.5 Thesis Outline

This thesis is divided into 5 chapters as stated below:

Chapter 1: Introduction, background information, problem definition, existing solutions, objectives, and contributions.

Chapter 2: Literature review of this study completed on the definition of grounding and tower impednace, theoretical approaches to the modeling of grounding electrodes, an overview of the previous tower models, and inclusion of frequency-domain responses to the time-domain simulators.

Chapter 3: A proposed model for the simulation of grounding electrodes is represented in this chapter. Sensitivity analysis is performed to determine the influencing parameters on the accuracy of the numerical simulations. Moreover, the time-domain overvoltage is calculated using Vector Fitting (VF) and recursive convolution.

Chapter 4: The wire diagram of a double circuit tower is developed for the simulations using NEC4, which is based on the Method of Moments (MOM). The validation of the model proposed for the analysis of transmission line towers is represented. The simulation of the

tower on a PEC and a lossy ground is performed to obtain the tower top voltage in respect to a remote ground. Previous tower models are compared with the results of NEC4.

Chapter 5: A simulation model is proposed for the full-wave analysis of transmission line tower using FEM to obtain a black-box equivalent model of the tower. This model includes the effect of grounding system, frequency dependency of soil electrical parameters, the equivalent model of string of insulators, shield wires and the overhead phase conductors. Next, the model is implemented in time domain simulations to assess the backflashover performance of a 400 kV line in different soil conditions.

Chapter 2
Literature Review

In this chapter, the background and past research related to the modeling of grounding system and transmission line towers is provided. The definition of grounding impedance and theoretical approaches on modeling of grounding electrodes, an overview of existing tower models, and a description of interfacing frequency-domain response to time-domain simulators are covered.

2.1 Definition of Grounding Impedance

Approaches to the modeling of grounding electrodes are either in the time- or frequency-domain. There are different definitions for the time-domain (transient) surge impedance of grounding electrodes. Suppose that a voltage source $v(t)$ is connected to the top of the grounding electrode and its other terminal is attached to a remote ground located infinitely far away. In such a condition, if the injected current into the top of the electrode is $i(t)$, three definitions for the impedance of grounding electrode can be found in the literature [69]

as

$$z(t) = \frac{v(t)}{i(t)} \tag{2.1a}$$

$$z(t) = \frac{v(t)}{\max(i(t))} \tag{2.1b}$$

$$z(t) = \frac{\max(v(t))}{I} \tag{2.1c}$$

where I is the value of $i(t)$ when the voltage $v(t)$ is maximum. Equation (2.1a) is a time-domain impedance called the *transient surge impedance* [70]. This definition only works for purely resistive circuits, where the voltage and current have the same waveshapes. In (2.1b), a step or ramp current is assumed to be injected into the electrode [71], and (2.1c) is the commonly-used definition [72], which is constant and not a function of time.

The above time-domain definitions of the surge impedance are dependent on the waveshape of the injected current [69]. In other words, one gets different values for the grounding impedance using double-exponential excitation, Heidler's excitation [73] or a step pulse current input. In order to mitigate this issue and to define a general impedance for any grounding system, the frequency-domain surge impedance given by

$$Z(j\omega) = \frac{V(j\omega)}{I(j\omega)} \tag{2.2}$$

is used in this thesis, where $I(j\omega)$ is the injected current at the top of the electrode and $V(j\omega)$ is the voltage at the top of the electrode in respect to a remote ground. This definition depends only on the geometry and electromagnetic properties of the grounding system and

the medium they are buried in, and is not dependent on the excitation waveshape.

2.2 Grounding Impedance based on Theoretical Approaches

Two theoretical approaches can be employed to model the grounding electrodes, namely, circuit (lumped-parameters) and transmission line theories (distributed parameters). Sections 2.2.1 and 2.2.2 discuss their modeling approach and the equations to be used to obtain the wideband frequency response of grounding electrodes.

2.2.1 Circuit Theory Approach

According to Sunde [14], to derive a formula for the DC resistance of a vertical cylindrical conductor located near the surface of the earth, two assumptions are made: Firstly, it is assumed that the conductors are surrounded by a conducting medium of infinite extent in all directions. In other words, the effect of the soil-air interface is neglected. Secondly, a constant leakage current is assumed along the length of the electrode. These assumptions lead to an equation for the DC resistance R_v of a vertical conductor buried in ground given by [14]

$$R_v = \frac{\rho}{2\pi\ell}(\ln\frac{4\ell}{a} - 1) \tag{2.3}$$

where ρ (Ωm) is the resistivity of the soil, ℓ and a are the length and radius of the electrode, respectively ($\ell \gg a$). The capacitance of the conductor is obtained assuming a uniform

distribution of charge on the surface of the electrode along its length as [14]

$$C = \frac{\rho\varepsilon}{R} \tag{2.4}$$

where ε (F/m) is the permittivity of the soil. Finally, the inductance of the electrode is obtained with the longitudinal current taken as constant along the length of the electrode [14]

$$L_v = \frac{\mu\ell}{2\pi}(\ln\frac{2\ell}{a} - 1) \tag{2.5}$$

in which μ is the permeability of the soil.

In the case of a horizontal grounding electrode, the DC resistance is obtained using image theory. When the conductor is buried at a depth of d, its resistance is obtained by assuming two conductors $2d$ apart buried in a medium of infinite extent in all directions. Therefore, the DC resistance of a horizontal electrode buried d meters under the surface of the ground ($d \ll \ell$) is given by [14]

$$R_h = \frac{\rho}{\pi\ell}(\ln\frac{2\ell}{\sqrt{2ad}} - 1). \tag{2.6}$$

The self inductance of a hypothetical horizontal electrode buried in an infinite depth is less than 5% smaller than the inductance of the same electrode placed near the surface of the ground. As a result, to calculate the inductance of wires at ordinary depths of up to around 1 m (as stated in [14]), the inductance of a wire at the surface of the ground will be used as

$$L_h = \frac{\mu\ell}{2\pi}(\ln\frac{2\ell}{a} - 1). \tag{2.7}$$

The capacitance of a horizontal buried conductor is obtained using (2.4). Using the circuit theory approach leads to a representation of a grounding electrode with an inductance in

series with a parallel resistance and capacitance as shown in Fig. 2.1, when $N = 1$. An alternative to this simple circuit will be obtained if the electrode is divided into N fictitious segments, and each segment is represented by the RLC equivalent circuit. As $N \to \infty$, this model will be equivalent to the Transmission-Line approach introduced in detail in the next section.

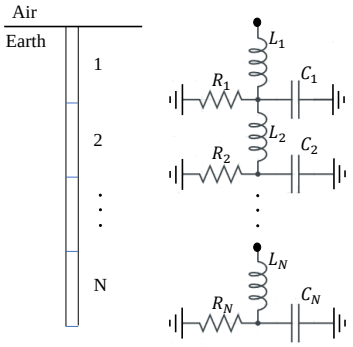

Fig. 2.1: Equivalent circuit of a grounding electrode obtained by dividing it in to N fictitious segments.

2.2.2 Transmission-Line Theory

The transmission-line approach is based on the quasi-static hypothesis which assumes that the electrical dimensions of the problem is much smaller than the smallest wavelength of the flowing current [25]. The buried conductor is assumed to have an infinite conductivity, and its internal resistance is therefore equal to zero. The per-unit-length parameters of the electrode are then calculated as

$$G' = \frac{1}{R\ell}[S/m] \tag{2.8a}$$

$$C' = \frac{C}{\ell}[F/m] \tag{2.8b}$$

$$L' = \frac{L}{\ell}[H/m] \tag{2.8c}$$

where R, C, and L are calculated using (2.3) to (2.7), and ℓ is the length of the electrode. Given the per-unit-length parameters, one can calculate the impedance of a grounding electrode by finding the input impedance of the open-ended equivalent transmission line. In the frequency domain, the harmonic grounding impedance is given by [74]

$$Z(j\omega) = Z_c coth(\gamma\ell) \tag{2.9}$$

where $Z_c = \sqrt{\frac{j\omega L'}{G'+j\omega C'}}$ and $\gamma = \sqrt{j\omega L'(G'+j\omega C')}$ are the characteristic frequency and the propagation constant of the transmission line, respectively.

The transmission line theory approach does not take into account the mutual coupling between the adjacent segments, so it is expected that they might lead to errors in the high frequency response of grounding electrodes when their length is increased. However, as they divide the electrode into a higher number of segments compared to the circuit theory approach, the transmission line theory approach is expected to have more accurate results for higher length of electrodes than circuit theory approach.

2.3 Overview of Tower Models

The large number of existing models for transmission line towers [70, 72, 75–95] can be classified in three categories based on the underlying assumptions and the components used to represent the tower as follows.

2.3.1 Vertical Lossless Frequency-Independent Models

These types of models approximate the tower body, *i.e.* its main legs and cage, with a simple geometric shape such as a cylinder [70, 72, 77–81, 84, 85] or a cone [72, 78]. The characteristic impedance of the whole tower as a function of the height above ground is derived using basic electromagnetic field analysis. In some, the current that is injected to the tower is assumed to be of a specific shape, such as a ramp [72, 84], a double exponential [72, 76], or a rectangular wave shape [70, 81], that restricts the applicability of such tower models to other waveshapes. Furthermore, the effect of tower cross arms and bracings is neglected, and the criteria for the selection of the radius of the equivalent structure is not well established. Figure 2.2A shows a typical double circuit tower, and Fig. 2.2B shows its representation by such models. Table 2.1 shows the surge impedance of the double-circuit tower calculated based on these models.

2.3.2 Multisection Lossless Transmission Line Models

In this group of models, similar to the previous, only the main body of the tower is considered, but it is divided into a number of lossless transmission lines, usually 4, and the characteristic impedance of each part is derived by analysing the tower elements as a multiconductor system [85–87, 95]. Table 2.2 shows the value of the surge impedance of each section for a 4-story tower model as shown in Fig. 2.2C. In the model of Hara & Yamamoto [85], the tower cross arms are also modeled by horizontal lossless transmission lines (Z_{Ai}), and the bracings are modeled by a surge impedance ($Z_{Li} = 9Z_{Ti}$) in parallel to the tower main body in each section, as shown in Fig. 2.2D.

2.3.3 Multistory Tower Models

As shown in Figs. 2.2E and 2.2F, these tower models divide the tower at the upper, middle, and lower phase arm positions into four sections. Each section consists of a lossless transmission line Z_T in series with a parallel RL circuit [88–91, 93, 94, 96]. The resistance

Table 2.1: Surge impedance of a typical double circuit tower (Fig. 2.2A) calculated by lossless frequency-independent tower models.

No	Model	Expression	$Z_T(\Omega)$
1	Wagner & Hileman [70]	$60\ln(\sqrt{2}\frac{2h}{r_0})$	205
2	Jordan [72]	$60\ln(\frac{h}{r_1})-60$	129
3	Sargent & Darveniza [72]	$60\ln(\sqrt{2}\frac{2h}{r_3})-60$	195
4	Sargent & Darveniza [72]	$60\ln(\sqrt{2}\frac{\sqrt{h^2+r_0^2}}{r_0})$	160
5	Menemenlis & Chun [76]	$50+35\sqrt{h}$	285
6	Chisholm*et al.* [78]	$60\ln(\cot(\frac{\tan^{-1}(\frac{r_0}{h})}{2}))$	184
7	Chisholm*et al.* [78]	$60\ln(\cot(\frac{\tan^{-1}(\frac{r_0}{h})}{2}))-60$	124
8	Chisholm*et al.* [77]	$60\ln(\cot(\frac{\tan^{-1}(T)}{2}))$	190
9	Flash version 1.7 [79]	$60\sqrt{\frac{\pi}{4}}\ln(\frac{1}{\sqrt{2}}\cot(\frac{\tan^{-1}(T)}{2}))$	150
10	Hara & Yamamoto [85]	$60\ln(\sqrt{2}\frac{2h}{r_0})-120$	167
11	De conti [80], Takahashi [81]	$60\ln(\frac{4h}{r_0})-60$	166
12	IEEE WG [84]	$60\ln(\frac{h}{r_0})$	142
13	Takahashi [81]	$60[\ln(\sqrt{2}\frac{2h}{r_0})-1.54]$	112

[1] The radius of the tower at its base, waist and top are r_0, r_1, r_2, respectively. r_3 is the radius of the cylinder approximating the tower.

[2] The height of the tower is h, height from base to waist is h_1 and height from waist to top is h_2.

[3] $T=(r_2h_2+r_1h+r_0h_1)/h^2$.

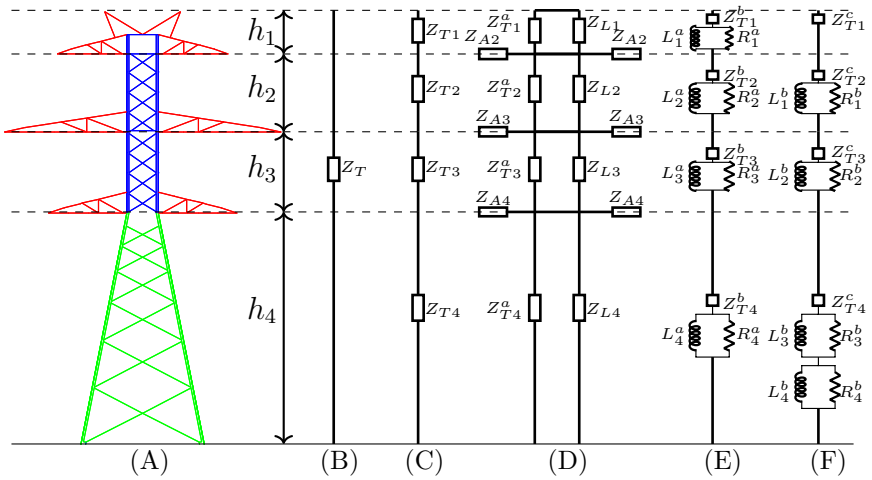

Fig. 2.2: (A) 400 kV double circuit transmission line tower, and its equivalent circuits: (B) lossless frequency-independent equivalent circuit, (C) multisection lossless line, (D) the model of Hara & Yamamoto [85] which considers the cross arms and bracings, (E) Multistory tower model, and (F) is the model of Baba [91].

represents the attenuation of traveling waves in the tower, and the inductance makes the resistance ineffective as time passes by and also adjusts the propagation velocity along the tower [88]. These models are derived based on the results of field measurements on actual towers and the values of the tower surge impedance and attenuation coefficients have to be determined by a trial and error process such that the response of the circuit representing the tower would be the same as the measured ones. There are limitation in extending the results of such models to other types of transmission towers [88]. Table 2.3 shows the values of tower parameters calculated based on these models, and the equivalent circuit of the tower is shown in Fig. 2.2E. In the model of Baba [91], two parallel RL elements are considered in the lower tower section as shown in Fig. 2.2F.

Table 2.2: Surge impedance of the double circuit tower calculated by lossless tower models (multi conductor system).

No	Model	$Z_{T1}(\Omega)$	$Z_{T2}(\Omega)$	$Z_{T3}(\Omega)$	$Z_{T4}(\Omega)$
14	Ametani [95]	95	112	102	87
15	Ametani simplified [95]	88	108	96	75
16	Gutierrez [86], [87]	270	253	230	167
17	Hara & Yamamoto [85]	128	120	106	83
		$Z_{L1}(\Omega)$	$Z_{L2}(\Omega)$	$Z_{L3}(\Omega)$	$Z_{L4}(\Omega)$
		1152	1080	954	747
		$Z_{A1}(\Omega)$	$Z_{A2}(\Omega)$	$Z_{A3}(\Omega)$	$Z_{A4}(\Omega)$
		-	305	282	257

Table 2.3: Surge impedance of the double circuit tower calculated by multistory tower models.

No	Model	Z^b_{T1}	Z^b_{T2}	Z^b_{T3}	Z^b_{T4}	R^a_1	R^a_2	R^a_3	R^a_4	L^a_1	L^a_2	L^a_3	L^a_4
18	Ishii [88]	220	220	220	150	8.32	20.37	20.37	33.47	3.49	8.53	8.53	14.01
19	Yamada [89]	120	120	120	120	9.30	16.45	17.06	42.80	2.79	4.94	5.13	12.86
20	Motoyama [90]	120	120	120	120	5.83	11.7	9.32	26.8	2.31	4.61	3.69	10.6
21	Baba [91]	200	200	180	150	20	30	25	25	6	9	15	1.5
22	Hashimoto [93]	195	182	149	121	13.3	32.5	28.1	76.1	7.42	18.1	15.7	52.7

[1] The impedances Z_{Ti} and R_i values are in Ω and L_i are in μH.

2.4 Interface to Time-Domain Simulators

After obtaining the frequency domain simulation results, in order to calculate the time-domain voltage at the top of a grounding electrode or across the string of insulators of a tower, it is needed to transform the frequency-domain responses so they can be interfaced with electromagnetic transient simulators. One approach is to use vector fitting to represent a frequency-domain impedance $Z(s)$, given at n_0 frequency points, with rational function

approximations [97] in the state-space form as

$$Z(s) = D + \mathbf{C}(s\mathbf{I} - \mathbf{A})^{-1}\mathbf{B} + sE \tag{2.10}$$

or in the pole-residue form

$$Z(s) = D + \sum_{m=1}^{N} \frac{\mathbf{R_m}}{s - a_m} + sE. \tag{2.11}$$

where N poles are used in the vector fitting, and the dimensions of A, B, and C in (2.10) are $N \times N$, $N \times 1$, and $1 \times N$, respectively. Then, the recursive convolution method [98] is used to obtain the time domain voltage $v(t)$ from the input current $i(t)$ in a time-domain simulation based on a fixed time-step Δt given by [99]

$$\mathbf{x}_k = \boldsymbol{\alpha}\mathbf{x}_{k-1} + \mathbf{B}i_{k-1} \tag{2.12a}$$

$$v_k = \hat{\mathbf{C}}\mathbf{x}_k + \mathbf{G}i_k \tag{2.12b}$$

where

$$\boldsymbol{\alpha} = (\boldsymbol{I} - \boldsymbol{A}\frac{\Delta t}{2})^{-1}(\boldsymbol{I} + \boldsymbol{A}\frac{\Delta t}{2}) \tag{2.13a}$$

$$\hat{\boldsymbol{C}} = \boldsymbol{C}(\boldsymbol{\alpha}\boldsymbol{\lambda} + \boldsymbol{\mu}) \tag{2.13b}$$

$$\boldsymbol{G} = (\boldsymbol{D} + \boldsymbol{C}\boldsymbol{\lambda}\boldsymbol{B}) \tag{2.13c}$$

$$\boldsymbol{\lambda} = \boldsymbol{\mu} = (\boldsymbol{I} - \boldsymbol{A}\frac{\Delta t}{2})^{-1}\frac{\Delta t}{2}. \tag{2.13d}$$

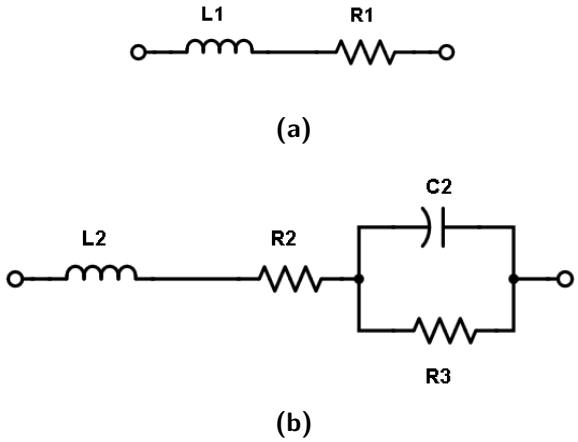

Fig. 2.3: Series equivalent circuit for a real pole (a), and a complex pole pair (b).

The subscripts $k-1$ and k denote the past and present time-steps, respectively. $\mathbf{x}$ is the vector of state space variables.

2.5 Equivalent Circuit Implementation

An alternative way for the implementation of a frequency-domain response in time-domain simulators is to find circuit equivalents that could reproduce the same frequency domain response. The method presented in [100] is used to generate an RLC circuit equivalent for the simulated grounding electrodes which can be incorporated in EMT-type simulators. The constant term R_0 and the proportional term E in (2.11) are represented with a conductance and a capacitance of values R_0 and E, respectively. The equivalent circuit for real poles is a series RL circuit as shown in Fig. 2.3a and the equivalent circuit for a pair of complex-conjugate poles is a series RLC circuit given in Fig. 2.3b [100]. The value of components in

Fig. 2.3a are given by

$$L_1 = 1/R_n \tag{2.14a}$$

$$R_1 = -a_n/R_n \tag{2.14b}$$

and for Fig. 2.3b, the value of the elements can be calculated using [31]

$$L_2 = 1/(R_{n1} + R_{n2}) \tag{2.15a}$$

$$R_2 = (-a_{n1}R_{n1} - a_{n2}R_{n2})/(R_{n1} + R_{n2})^2 \tag{2.15b}$$

$$C_2 = -(R_{n1} + R_{n2})^3/(R_{n1}R_{n2}(a_{n1} + a_{n2})^2) \tag{2.15c}$$

$$R_3 = -(R_{n1} + R_{n2})/[(R_{n1}a_{n2} + R_{n2}a_{n1})C_2]. \tag{2.15d}$$

2.6 Summary

In this chapter, different definitions of grounding impedance available in the literature were provided, and it was mentioned that in contrast to the time-domain definitions, the frequency-domain definition does not depend on the waveshape of the excitation. The representation of towers and grounding electrodes using circuit and transmission-line theories was provided in detail, and the required equations for the wideband modelling of grounding electrodes were given. An overview of tower models, their underlying assumptions and their restrictions were provided. Finally, the method of interfacing frequency-domain responses with time-domain simulators was introduced.

Chapter 3
Grounding Electrodes

In this chapter, the development of an equivalent time-domain macro-model for grounding electrodes of different lengths and orientation buried in soil is presented. First, a simulation model is proposed to numerically solve for the grounding impedance in the frequency domain. Next, the full-wave Maxwell's equations are solved using Finite Element Method (FEM). Both cases of constant and frequency dependent soil electrical parameters are considered. In order to have an estimation about the effect of weather change on the grounding impedance, the variation of soil electrical parameters in the permissible range of soil water contents are calculated. Time-domain voltage of grounding electrodes due to the injection of a current at the top of the electrode is then obtained using Vector fitting and recursive convolutions. Both first and subsequent lightning strokes are considered and the effect of electrode dimensions and soil parameters on the waveshape and peak of the induced voltages are examined.

3.1 Soil Electrical Parameters

In the study of electromagnetic wave propagation in a homogeneous, isotropic medium, three properties of the medium are considered: electrical conductivity, dielectric constant,

and magnetic permeability. The attenuation of electromagnetic waves propagating in such a medium is defined as [14]

$$\alpha = \omega \sqrt{\frac{\mu\varepsilon}{2}(\sqrt{(1+\frac{\sigma^2}{\omega^2\varepsilon^2}}) - 1)}. \tag{3.1}$$

In (3.1), α is the attenuation constant (nepers/m), ω is angular frequency (rad/s), μ is the magnetic permeability (H/m), ε is the dielectric constant (F/m), and σ is the conductivity (S/m) of the medium. The attenuation constant α is important to evaluate the strength of electromagnetic waves in a specific distance from its source. This equation highlights the importance of accurate determination of the electrical properties of the soil in studying the performance of grounding electrodes.

3.1.1 Electrical Conductivity

Soil conductivity is determined by field measurements of apparent resistivity at very low frequencies, often DC to 20 Hz. Four metal electrodes are driven a few meters into the soil in an inline array. A source of electric current is connected to the two outer electrodes, and the resulting potential difference between the two inner electrodes are measured. The apparent low frequency resistivity of the soil is calculated as a function of the measured voltages and current and the spacing between the electrodes. In the next step, using curve matching methods, the true resistivity of the soil layers at different depths is determined [101]. The conductivity of soil is nearly constant below a frequency of 20 Hz, and its value at higher frequencies can be estimated by knowing either its low frequency resistivity or its water content [101]. In general, it has been shown that clay soil has a high conductivity of 0.11 S/m and above, the loam and chalk soil has an average conductivity value of about

0.1 S/m, while soil of a sandy or gritty nature gives a much lower conductivity value [67]. The lowest values were obtained for the solid granite or slate subsoil with a conductivity of the order of 0.0001 S/m [67]. It is worth mentioning that the temperature of the soil also affects the value of its conductivity and permittivity. As the temperature increases, resistivity decreases at a rate of about $2-3$ percent per $^\circ$ in the range of normal soil temperatures above the freezing point [67, 102, 103].

3.1.2 Dielectric Constant

The relative dielectric constant (ε_r) is the ratio between the absolute permittivity of a material (ε) and the absolute permittivity of free space ($\varepsilon_0 = 8.854 \times 10^{-12}$ F/m), and expresses the ability of a material to polarize under an electric field. To measure this quantity, the material is placed in an alternating electromagnetic field, and the time it takes for the wave to travel through the material is measured [103].

Several factors affect the value of soil permittivity. Soil is generally consisted of air, water and solids. The permittivity of water is 80.36 at 20° C which is much larger than the permittivity of most common soil minerals, which ranges between 3 to 5 [104]. This difference clearly shows the high ability of the water molecules to polarize compared to the soil particles. As there are significant differences between the permittivity of a soil constituent components, it stands to reason that the permittivity of a soil is highly dependent on its water content. The measurements of the dielectric properties of soil have shown that the variation of dielectric constant with moisture content depends on the type of soil. The observed dielectric constant increases slowly with soil 's water content up to a transition point, beyond which a rapid increase occurs [105]. For moisture contents below the transition moisture, the water in soils is thought to behave like ice and, consequently, the dielectric

constant for ice is used in the mixing, while above the transition moisture the dielectric properties of the liquid water is used. In was also observed that the dielectric constant of 12 samples of soil with different water contents (from dry soil to 30% of moisture content) show the range of its variation to be between 3 to near 30, with its trend being dependent on the soil type or texture [67]. In another measurement, when precautions were taken to remove all the moisture from a sample of soil by drying it out, the minimum observed dielectric constant was equal to 2 [106]. Regarding the texture, the clay soils have a high dielectric constant, while it reaches to 20 for loam and chalk soils [67]. As a final remark, it is worth noting that the temperature effect on the dielectric constant is negligible for temperatures above the freezing point [67, 103]. It must be remembered that the surface variations are not completely followed by the temperature of the ground below the surface, and that the variation of the effective conductivity of the ground with surface temperature will depend upon the depth to which the electric waves penetrate the earth.

3.1.3 Magnetic Permeability

Magnetic permeability is determined by measuring magnetic susceptibility of soil samples under a weak magnetic field [107]. Relative magnetic permeability of rock and soil is less important than its conductivity and dielectric constant in studies of electromagnetic pulse propagation, because for most earth materials it is only slightly greater than unity (between 1.0006 and 1.001) [108]. Due to this fact, the permeability of soil is considered equal to 1 in all studies involving the ground [107].

3.1.4 Frequency Dependence of Soil Electrical Parameters

Considering the electrical conductivity, permittivity, and magnetic permeability of soil, the first two parameters are strongly frequency dependent, whereas the last one is similar to the magnetic permeability of air in most cases. It has been found that the resistivity and permittivity of soil has a decreasing trend as the frequency increases [109]. Additionally, it was realized that the decrease of soil resistivity and permittivity, resulting from the frequency dependent effects, is responsible for significant decrease of the grounding impedance [110]. There have been many laboratory measurements done to determine the frequency dependence of soil parameters [109–112].

Based on low frequency measurements together with statistical correlations of laboratory measurements of conductivity and permittivity in the frequency range of 100 Hz to 1 MHz, Scott *et al.* [111] developed plots for permittivity, conductivity and permeability as functions of frequency and soil water content. The measurements were performed on a group of rock and soil samples. The proposed expressions where derived based on additional measurements as follows [101]

$$\log_{10}(\varepsilon_r(f)) = 5.491 + 0.946\log_{10}(\sigma_{100\text{Hz}}) - 1.097\log_{10}(f) + 0.069(\log_{10}(\sigma_{100\text{Hz}}))^2 - 0.114\log_{10}(f)\log_{10}(\sigma_{100\text{Hz}}) + 0.067(\log_{10}(f))^2 \quad (3.2a)$$

$$\log_{10}(\sigma(f)) = 0.028 + 1.098\log_{10}(\sigma_{100\text{Hz}}) - 0.068\log_{10}(f) + 0.036(\log_{10}(\sigma_{100\text{Hz}}))^2 - 0.046\log_{10}(f)\log_{10}(\sigma_{100\text{Hz}}) + 0.018(\log_{10}(f))^2(\text{mS/m}) \quad (3.2b)$$

where f (Hz) is frequency, and $\sigma_{100\text{Hz}}$ (mS/m) is the conductivity at 100 Hz. In the same

reference, there are another set of equations which determine the frequency dependence of conductivity and permittivity based on the water content of the soil instead of low-frequency conductivity.

Longmire and Longley [113] developed another set of equations based on the Scott's experimental data, with the fundamental assumption that each volume element of soil could be represented by a RC network. Such assumption would backup the idea that the frequency dependence of conductivity and permittivity are not independent. They also noticed that there is only one curve for $\varepsilon_r(f)$ and in order to obtain this frequency dependence for different water contents, the curve only has to be moved to the right or left, i.e., a frequency scale should be used. Their model, which is called the *universal soil model*, is given as [114]

$$\varepsilon_r(f) = \varepsilon_\infty + \sum_{i=1}^{13} \frac{a_i}{1 + (\frac{f}{F_i})^2} \tag{3.3a}$$

$$\sigma(f) = \sigma_0 + 2\pi\varepsilon_0 \sum_{i=1}^{13} a_i F_i \frac{(\frac{f}{F_i})^2}{1 + (\frac{f}{F_i})^2} \tag{3.3b}$$

where ε_∞ and σ_0 are the high frequency limit of the dielectric constant and the low frequency conductivity, respectively. The value of $\varepsilon_\infty = 5$ is chosen and coefficient a_i are given in table 3.1. For a water content of $P = 10\%$, $F_i = 10^{n-1}$ Hz, where $n = 1, 2, ..., 13$. There are two restrictions related to this model: i) the assumption of dependency of soil conductivity only on the water content, and ii) the use of different materials than what used by Scott, to fit the results at higher frequencies.

Another representation of the frequency dependence of soil electrical parameters, which was also based on Scott's experimental data, was proposed by **Messier** [115]. The proposed

Table 3.1: Coefficients a_i for the universal soil model.

i	a_i	i	a_i
1	3.4×10^6	8	1.25×10^1
2	2.74×10^5	9	4.8×10^0
3	2.58×10^4	10	2.17×10^0
4	3.38×10^3	11	9.8×10^{-1}
5	5.26×10^2	12	3.92×10^{-1}
6	1.33×10^2	13	1.73×10^{-1}
7	2.72×10^1		

equations were modified in a later publication [116] and they are given as

$$\varepsilon_r(f) = \frac{\varepsilon_\infty}{\varepsilon_0}\left(1 + \sqrt{\frac{\sigma_0}{\pi f \varepsilon_\infty}}\right) \tag{3.4a}$$

$$\sigma(f) = \sigma_0\left(1 + \sqrt{\frac{4\pi f \varepsilon_\infty}{\sigma_0}}\right) \tag{3.4b}$$

where σ_0 and ε_∞ are defined in the same way as the previous model, except that $\varepsilon_\infty = 8$.

Visacro and Alipio developed another set of equations for the frequency dependence of soil electrical parameters based on their own measurements that are given by [110]

$$\sigma = \sigma_0\left[1 + (1.2 \times 10^{-6} \times \sigma_0^{-0.73}) \times (f - 100)^{0.65}\right] \tag{3.5a}$$

$$\varepsilon_r = 7.6 \times 10^3 f^{-0.4} + 1.3. \tag{3.5b}$$

where σ_0 is the soil conductivity at 100 Hz and ε_r is the soil relative permittivity at frequency

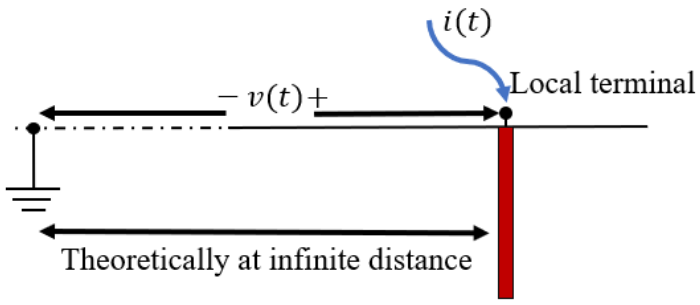

Fig. 3.1: An illustration of the grounding impedance.

f. It is worth noting that (3.5a) is valid for frequencies ranging from 100 Hz to 4 MHz, while (3.5b) is valid for frequencies ranging from 10 kHz to 4 MHz. In a later work, Alipio and Visacro developed a causal model to describe the frequency dependence of soil electrical parameters. Using these expressions, the impact of frequency dependence of soil electrical parameters on the lightning response of vertical and horizontal arrangements of electrodes can be accurately assessed.

3.2 Simulation Model for Grounding Electrodes

Suppose that an electrode is buried in soil as shown in Fig. 3.1. If a current $i(t)$ is injected at the top of the electrode, the grounding impedance is defined by defining a voltage for the same node (top of the electrode) in respect to a remote ground. In this section, two simulation models are proposed for the modelling of grounding electrodes in the frequency domain.

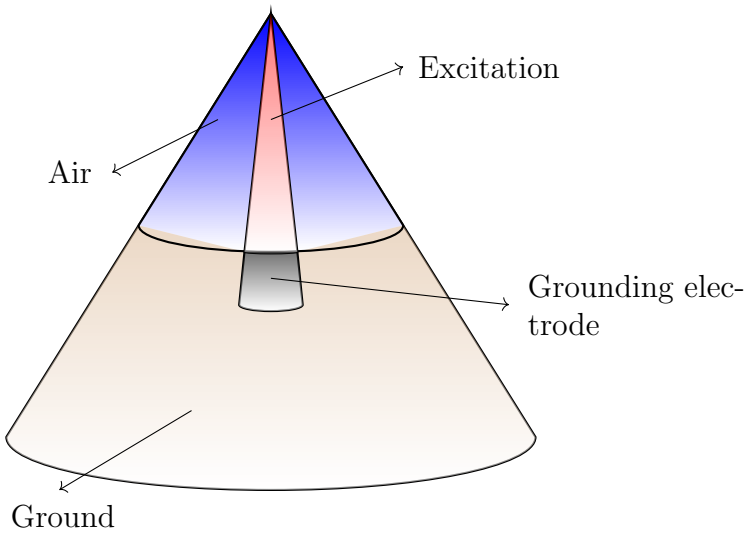

Fig. 3.2: Simulation model for the analysis of grounding electrodes using conical transmission lines.

3.2.1 Conical Transmission Line

In this model, the ground and air region are modelled using conical transmission lines. The motivation is that if the air region can be modelled as a transmission line, then given the input impedance of the line, one can find the load impedance, which is the grounding impedance. Further, the effect of the parasitic capacitance between the inner and outer conductors of the line can be deduced from the grounding impedance. The classical equation for the input impedance of a transmission line is valid only under the assumption that the electromagnetic field is of the transverse electromagnetic (TEM) type. This is the reason why the conical transmission lines are investigated instead of the more commonly used cylindrical transmission lines (coaxial). Is is known that the cutoff frequency in conical transmission lines is not abrupt like normal guides, but occurs gradually [117]. Furthermore, it is known that the cutoff frequency of non-TEM modes are much higher in conical transmission lines

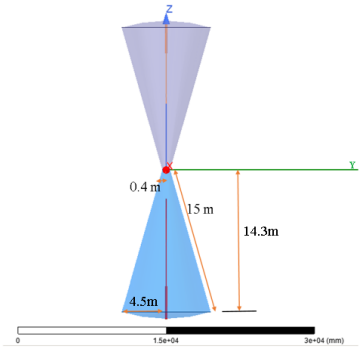

Fig. 3.3: Two series conical transmission lines considered for numerical simulation using FEM.

compared to cylindrical transmission lines. Firstly, in order to validate the accuracy of the FEM simulations, two series conical transmission lines are considered as shown in Fig. 3.3. A port is defined between the two lines and each line is short circuited at its end. A theoretical solution is obtained by halving the input admittance of one short-circuited conical transmission line. Figures 3.4 and 3.5 show the magnitude and phase angle of the admittance seen from the port calculated by FEM and the theoretical solution. It can be seen that the simulation and theoretical results match both in the magnitude and frequency of resonances up to a frequency of 20 MHz. This result proves that in such condition, non-TEM modes are not propagating in the conical line, and the transmission line theory is providing accurate results.

If we can determine the cut-off frequency of higher order TE and TM modes, one can consider the ground region in the FEM simulation model in a way that only TEM modes will propagate in the frequency range of interest. To find the cut-off frequency of non-TEM

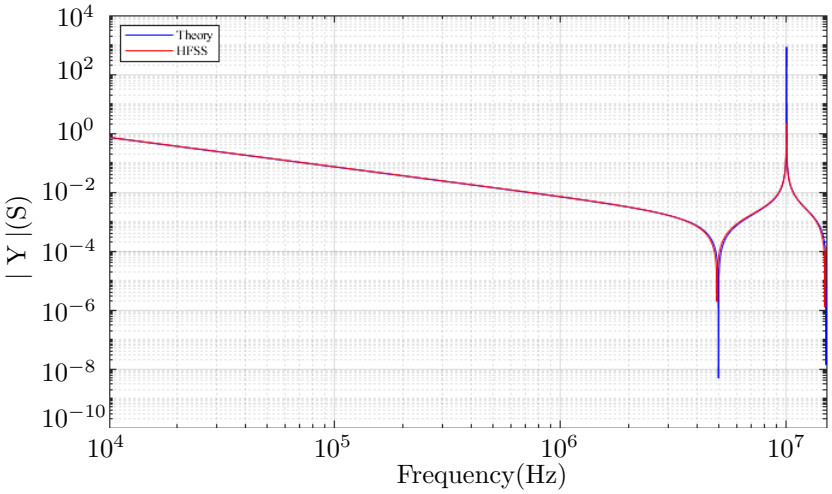

Fig. 3.4: Magnitude of the admittance seen by the port located between two conical transmission lines, which are short circuited at their ends.

modes, the nth root of

$$\frac{dP_v^m(\cos\theta_1)}{d\theta_1}\frac{dQ_v^m(\cos\theta_2)}{d\theta_2} - \frac{dQ_v^m(\cos\theta_1)}{d\theta_1}\frac{dP_v^m(\cos\theta_2)}{d\theta_2} = 0 \tag{3.6a}$$

and

$$P_v^m(cos(\theta_1))Q_v^m(cos(\theta_2)) - Q_v^m(cos(\theta_1))P_v^m(cos(\theta_2)) = 0 \tag{3.6b}$$

are found to obtain the value of v for TE_{mn} and TM_{mn} modes, respectively. In (3.6b), θ_1 and θ_2 are the half angles of the inner and outer cones, and P_v^m and Q_v^m are the associated Legendre functions of first and second kind of degree v and order m. Knowing the value of v, the cutoff frequency is found using:

$$f_{\text{cutoff}} = \frac{c \times \sqrt{v(v+1)}}{2\pi r} \tag{3.7}$$

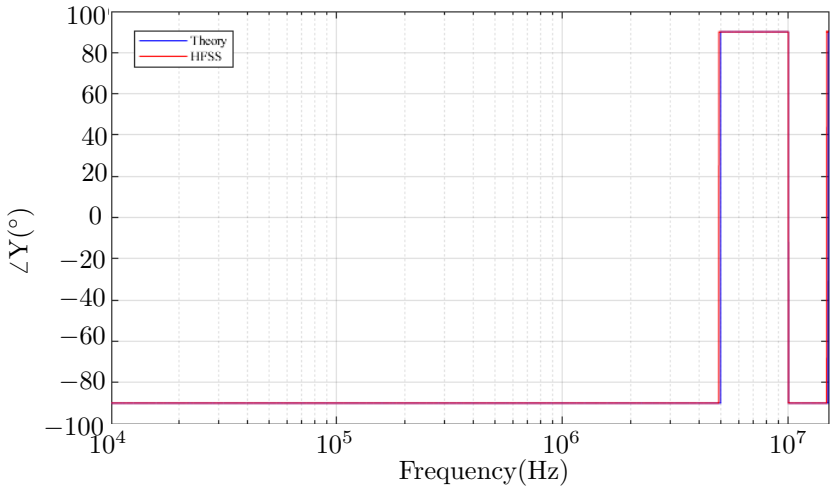

Fig. 3.5: Phase angle of the admittance seen by the port located between two conical transmission lines, which are short circuited at their ends.

one can conclude that if the lower radius of the conical line (which is equal to the radius of the hemisphere representing the soil part of the simulation model) can not be equal to a small value, the height of the line should be as small as possible, so that non-TEM modes wont propagate. However, as this approach for the modelling of grounding electrodes was not successful, it was not further investigated.

3.2.2 Cone and Sphere Model

In this developed model, to analyze the performance of grounding electrodes subjected to a lightning surge, the calculation region can be divided into two sections: one is the conductor domain including the electrode of radius r_1 buried in soil with relative permeability of μ_r, relative permittivity of ε_r, and conductivity of σ. The unbounded ground is represented by a hemisphere of radius r_0. The other part is the air region, which is represented by a cone of height h, a lower radius of r_0, and an upper radius equal to the electrode's diameter. A

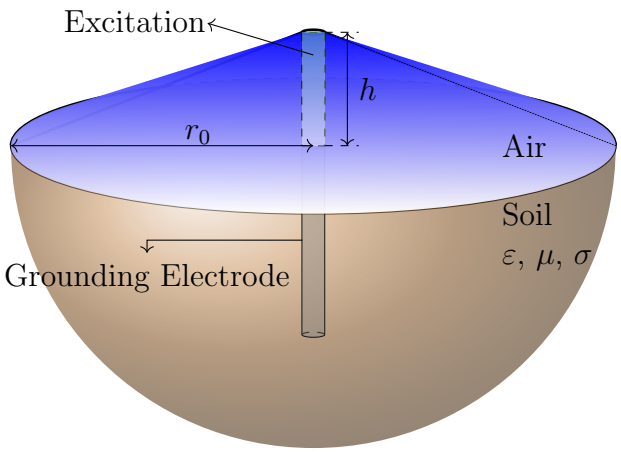

Fig. 3.6: Proposed FEM model for the calculation of the grounding impedance. The air region is represented by the blue cone of height h, the brown hemisphere with radius r_0 is representing the ground region, and a rectangular port is defined for the excitation. The excitation is equivalent to a voltage source of 1V in amplitude (Note that the dimensions are not exact in the figure).

voltage source of amplitude 1 V is applied between the electrode's top surface and the upper face of the cone by means of defining a port between them. The port is a rectangle with a width equal to the electrode's diameter and a length of h. The solution of (3.13) using FEM needs suitable boundary conditions in order to represent the electromagnetic model in an accurate way. The electric field is forced to be normal to the port edges which interface with conductors and also at the reference point, while it is tangential to all remaining edges. Perfect electric conductor (PEC) boundary condition is applied to all outer surfaces of the cone and the hemisphere. A 3D view of the proposed model is shown in Fig.3.6. The sensitivity analysis described in Section 3.3 aims to justify the size of the computational domain and to select the optimum value for the radius and other parameters that impact the accuracy of results.

3.3 Sensitivity Analysis and Convergence

In this section, first the selection of the size of the computational domain is justified for the consideration of different soil resistivities and then the parameters influencing the accuracy of the proposed model are assessed and their optimum value is obtained. The variables considered here are the truncation radius r_0, the length of the port used to excite the electrodes h, and the frequency dependence of soil parameters.

3.3.1 Shape and Size of the Computational Domain

The outermost surface of the computational domain serves as the current closing path. There is no such truncation in reality, so the effect of size of the computational region should be minimized in the surge response of the electrode. The ground has been modeled by a hemisphere, because there should be a symmetry around the electrode in order to avoid forcing the current to go in a particular direction. The sensitivity analysis done to find the suitable hemisphere radius tries to minimize the effect of this imaginary ground around the electrode. The air region is modeled as a nonuniform coaxial cable. The current going through this coaxial cable can be considered as a wave which will be scattered cylindrically at high frequencies. The waves reflected back from the air's outer surface, propagate into the computational region and could cause an error. These errors show themselves as resonances in the simulated frequency-domain impedance of the electrode. To minimize this error, the air region is modeled as a cone, which is equivalent to having a non-uniform axial cable. As the distance between the PEC wall and the source of scattered waves (central conductor) decreases, the resonances will occur at higher frequencies. This will cause these unwanted resonances to occur in frequencies outside the frequency range of ineterest.

3.3.2 Truncation Radius

In order to have a quantitative estimate about the wave propagation in a lossy medium, the TEM wave propagation constant should be considered which is given by [118]

$$\gamma = \alpha + j\beta = \sqrt{j\omega\mu_0(\sigma + j\omega\varepsilon)} \tag{3.8}$$

where α is the attenuation constant given by (3.1), and β is the phase constant. The skin depth can be calculated from the attenuation constant as

$$\delta = \frac{1}{\alpha}. \tag{3.9}$$

The strong dependence of skin depth on the soil conductivity is shown in Fig. 3.7, where a relative permittivity of $\varepsilon_r = 10$ is considered. As the resistivity of the soil increases from 10 to 10000 Ωm, attenuation of the electromagnetic waves propagating in the soil increases, which causes the skin depth to increase. Furthermore, at higher frequencies, the fields tend to localize around the source, so the maximum skin depth is seen in dc. The skin depth shows a saturation in the very high frequencies and becomes constant as the frequency increases further, the starting point of which depends on the soil resistivity.

In Fig. 3.8, the effect of soil permittivity on the skin depth while considering a constant conductivity is shown. As expected, the value of permittivity has no influence in the low frequency region, no matter what the soil conductivity is. However, as the frequency of the waves increases, for lower soil conductivities, *i.e.* $\sigma = 0.0001$ S/m, the effect of soil permittivity on the wave propagation appeares as an increase in the value of the skin depth. There is still no change in the high frequency region for high soil conductivities of $\sigma =$

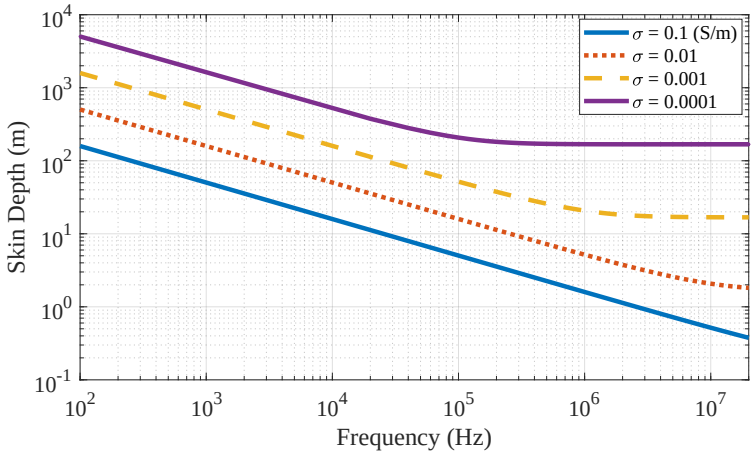

Fig. 3.7: Skin depth in soil as a function of frequency when different values of conductivity is considered and $\varepsilon_r = 10$..

0.1 S/m.

It can be concluded from Figs. 3.7 and 3.8 that if a specific radius for the ground part of the FEM model simulates the case of DC currents accurately, it can be assured that it is acceptable to simulate the high frequency propagation with no error due to the truncation. By truncation error it is meant that enough soil volume for the current dissipation has been considered, so no current will reach the artificial Perfect Electric Conductor (PEC) surface enclosing the model.

Two cases are considered for the dc simulation. First, consider a PEC hemispherical electrode of radius a buried in homogeneous soil with a conductivity of σ_{Soil} as shown in Fig. 3.9. The reason for considering such configuration is the availability of an exact analytical solution with no approximations. Assuming that the conductivity of the electrode is much higher than the soil, the resistance of the electrode is negligible in comparison with that of the soil. By integrating the resistance of differential shells, the dc resistance of such electrode/soil configuration is calculated as

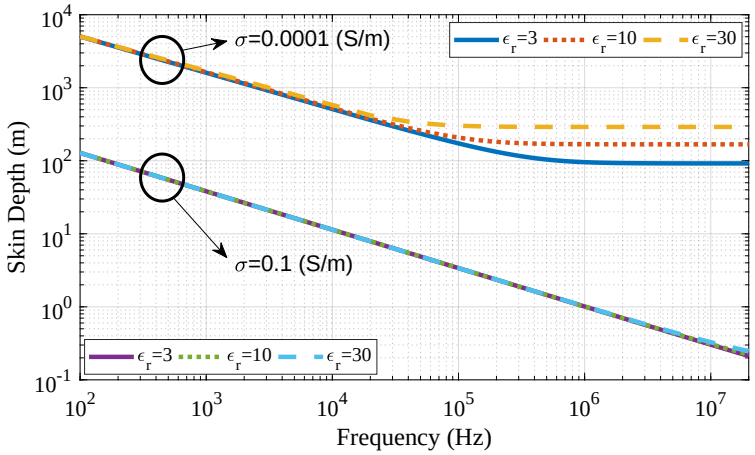

Fig. 3.8: Skin depth in soil as a function of frequency for $\sigma = 0.1$ S/m and $\sigma = 0.0001$ S/m.

$$R_{\mathrm{DC}} = \int_a^{\infty} \frac{dr}{2\pi r^2 \sigma_{\mathrm{Soil}}} = \frac{1}{2\pi a \sigma_{\mathrm{Soil}}} \,. \tag{3.10}$$

The simulation of the grounding system shown in Fig. 3.9 considering the truncation radius as the variable will allow us to determine the effect of the truncation radius. The analytic dc resistance obtained from (3.10) is $1,273\ \Omega$ assuming $a = 12.5$ mm and $\sigma_{\mathrm{Soil}} = 0.01$ S/m.

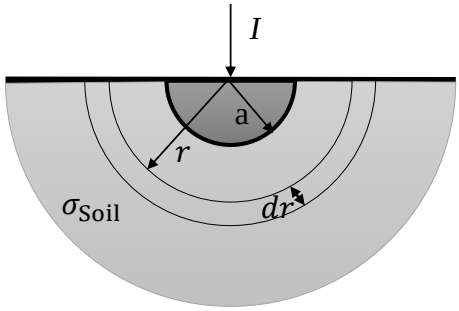

Fig. 3.9: A perfect conducting hemispherical electrode of radius r_0 buried in homogeneous soil with conductivity of σ_{Soil}. A differential segment with a radial length of dr is shown.

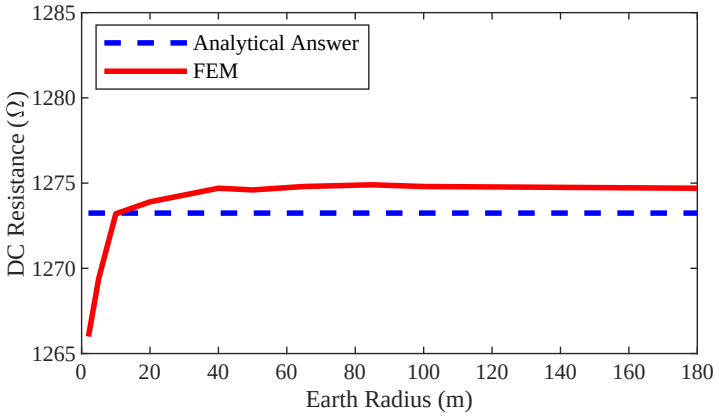

Fig. 3.10: DC resistance of a PEC hemispherical electrode buried in homogeneous soil as a function of the ground's radius obtained from FEM.

Fig. 3.10 shows the simulated DC resistance as a function of ground's truncation radius. From this figure it can be concluded that considering a hemisphere of radius 60 m would be sufficient to model the resistance of the hemispherical grounding electrode accurately with an error of less than 0.2%. As the frequency increases, the skin depth of the soil will decrease that means if the truncation radius is large enough at $f = 0$ (DC), it is sufficiently large at any other frequency.

For the second case considered for the verification of the ground radius, an electrostatic analysis on the vertical and horizontal grounding electrodes buried in a hemisphere of soil with a specific conductivity (any permittivity) is performed. Figure 3.11 shows the results of such a DC analysis for vertical grounding electrodes. A ground radius of 30 m to 600 m has been considered with a PEC grounding electrode buried in. It can be concluded that for the modeling of vertical grounding electrodes with lengths of 1,3, and 5 m, a radius of 50, 55, and 70 m is sufficient for the ground to achieve en error of less than 1% in the value of the DC resistance with reference to the case of a 600 m radius, where the results seem to converge. Is is worth mentioning that the assumptions made in the derivation of theoretical

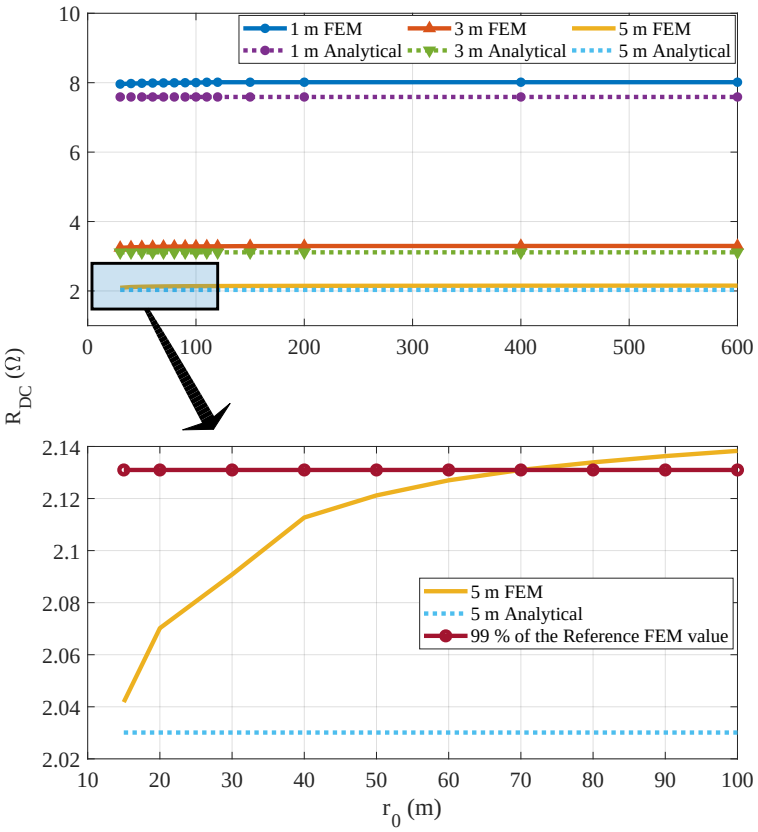

Fig. 3.11: Electrostatic analysis of a vertical electrode buried in a homogeneous soil with conductivity of $\sigma = 0.1$ S/m as a function of ground radius obtained with FEM, and analytical formulae (2.3) and (2.6) as the reference values.

equations (2.3) and (2.6) lead to a maximum error of 5.3% and 4% (for a burial depth of 0.5 m) in comparison to the exact numerical solution, respectively. Less error is observed as the length of the electrode increases.

Table 3.2: The magnitude of impedance for a port with width of 25 mm and varying length.

Port length (mm)	Magnitude of Port Impedance (Ω)
10	0.20964
50	2.5104
100	6.624
1000	122.84
2000	280.36
5000	815.6

3.3.3 Port Length

The existence of the port creates a parasitic inductance that can be calculated using [119]

$$L = 0.2 \times h \times \left(\ln \frac{2h}{w} + \frac{0.223w}{h} + 0.5 \right) \text{ [nH]} \tag{3.11}$$

where h and w are the length and width of the port in millimeters, respectively. A radius of 12.5 mm for the electrode requires a port width of 25 mm. Table 3.2 shows the magnitude of port's impedance ($2\pi fL$) for a number of port lengths in the maximum frequency of concern that is 20 MHz. In this table, it can be seen that the port length has to be less than 50 mm in order to have a negligible impedance in comparison with the grounding system.

3.3.4 Significance of the Soil Permittivity in the High-Frequency Analysis

Considering the case of a grounding electrode buried in soil, as the frequency of the propagating current goes up, the term $\sigma^2/(\omega^2\varepsilon^2)$ in (3.1) decreases, lowering the effect of soil conductivity in comparison to its permittivity. In the extreme case, where this term is very small compared with unity, the conductivity has a negligible effect. Similarly when $\sigma^2/(\omega^2\varepsilon^2)$ is large compared with unity, the effect of the dielectric constant is unimportant in determining the flow of current. As a result, it is expected that at a sufficiently high frequency, the dielectric constant would play a prominent, and even a major role in determining the effect of the earth on wave propagation. It is now evident that in order to have a clear understanding of the effect of soil on the response of grounding electrodes to the flow of alternating currents, it is necessary to consider the variation of both electric conductivity and permittivity of the soil, especially the latter, in the high-frequency region.

3.3.5 Numerically Solved Equations

The Finite Element Method (FEM) is commonly used to solve partial differential equation that require the whole problem space to be divided into a number of smaller regions [120]. In this thesis, a full-wave electromagnetic solver is used for the simulation of grounding electrodes and the differential equations being solved are the well-known Maxwell's equations

given by

$$\nabla \times \mathbf{E} = -\frac{\partial \mathbf{B}}{\partial t} \tag{3.12a}$$

$$\nabla \times \mathbf{H} = \mathbf{J} + \frac{\partial \mathbf{D}}{\partial t} \tag{3.12b}$$

$$\nabla \cdot \mathbf{D} = \rho_v \tag{3.12c}$$

$$\nabla \cdot \mathbf{B} = 0. \tag{3.12d}$$

where $\mathbf{E}$, $\mathbf{B}$, $\mathbf{H}$, $\mathbf{D}$ and $\mathbf{J}$ are the electric field, magnetic flux density, magnetic field, electric flux density, and current density vector, respectively. ρ_v is the volume electric charge density. Here, we solve the wave equation in the frequency domain that is represented by [121]

$$\nabla \times \left(\frac{1}{\mu} \nabla \times \mathbf{E}(x, y, z) \right) - k^2 \, \mathbf{E}(x, y, z) = \mathbf{0} \tag{3.13}$$

where

$$k = \omega \sqrt{\varepsilon (1 - j \frac{\sigma}{\varepsilon \omega})}.$$

$\mathbf{E}(x, y, z)$ is the electric field vector in the frequency domain, μ_r is the relative permeability, and ε_r is the relative permittivity of the medium [121]. An advantage of the FEM solution of (3.13) is that one can easily incorporate the inhomogeneity and/or frequency-dependence of the medium. The other advantage of FEM is that once the electric field is obtained, other physical quantities are calculated by derivation from the phasor representation in any location of the system, including the points that might have been neglected in an analytical approach. In this process, the solved electric fields are evaluated to determine if there is an error due to the mesh's failure to capture field gradients accurately. The mesh is refined in those locations, and the new mesh is solved. This adaptive process continues until a specific output quantity,

usually based on the S-parameters, changes less than a user-specified convergence criteria between two consecutive adaptive passes.

3.4 Numerical Results

In this section, the normalized magnitude of the impedance ($Z(j\omega)/Z_{DC}$) of vertical and horizontal grounding electrodes of length 1, 3, and 5 m with a radius of 12.5 mm in the frequency region of 1 kHz to 20 MHz calculated using FEM, circuit, and transmission line theories are represented and compared. The conductivity of the soil is assumed to vary from 0.0001 to 0.1 S/m, and the values considered for its relative permittivity are 3, 5, 10, 20, and 30. The dependence of the characteristic frequency on the parameters of the electrode and the soil is discussed. Finally, the effect of frequency dependent soil electrical parameters on the grounding impedance is evaluated.

3.4.1 Frequency Response of Grounding Electrodes

The three modeling approaches outlined in Sections 2.2 and 3.3.5 are compared here, namely the circuit theory, transmission-line and the electromagnetic full-wave approach. In the figures, they are identified as "RLC", "TLine", and "FEM", respectively. The soil electrical parameters are considered to be constant throughout the considered frequency range in this section. First, the effect of varying soil electrical permittivity is ignored, and it is considered to be equal to $\varepsilon_r = 10$. The harmonic impedance of vertical grounding electrodes of different lengths with $\varepsilon_r = 10$ are shown in Figs. 3.12-3.14. The response of grounding electrodes is practically constant up to a certain frequency, which is called the characteristic or the break frequency F_c [122]. Above such frequency, the electrode wont have the low-

frequency resistive behavior anymore. Instead it shows either an inductive (increasing high-frequency magnitude) or a capacitive response (decreasing high-frequency magnitude) based on the length of the electrode and the soil conductivity. The influencing parameters on the value of F_c will be discussed in Section 3.4.2. As the conductivity increases, the effect of ground displacement current becomes less important and an inductive behavior is seen in the high frequency region. This can be qualitatively assessed in terms of the ratio $\sigma/\omega\varepsilon$. The other influencing parameter is the length of the electrode which results in an inductive behavior as it increases. Furthermore, the resonant region starts at a lower frequency with longer electrodes. Figures 3.15-3.17 are similarly organized, but for a horizontal grounding electrode. Here, the radius of the electrode is 12.5 mm and burial depth is 0.5 m. The vertical and horizontal grounding electrodes of the same length despite of having different low frequency resistances (R_v and R_h), have almost a similar high frequency response and the only difference is in the region where the resonant behavior starts.

To compare the modeling approaches, the FEM is considered as the reference, since it is the most accurate modeling approach. The highest amount of error is seen in the regions of dominant resonant behavior for both of the theoretical modeling approaches, where they predict resonances with much higher peaks. Nevertheless, traditional models lead to very small errors up to the MHz range in all considered cases. The most accurate predictions of the circuit and transmission-line methods seem to be for the highly resistive earth and shorter electrodes.

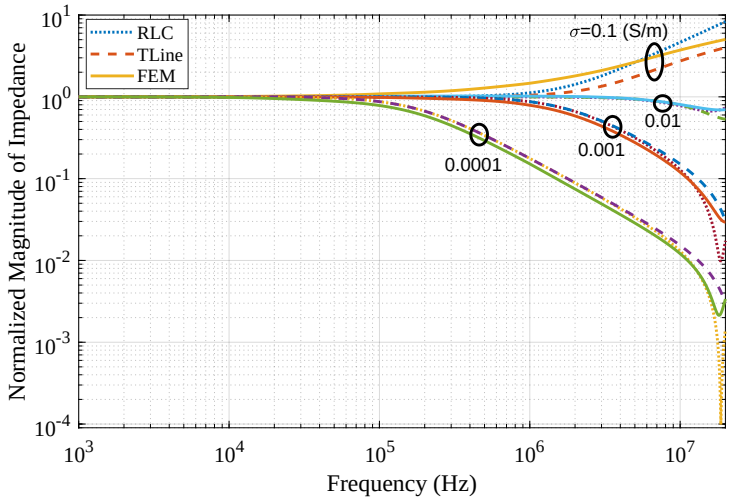

(a)

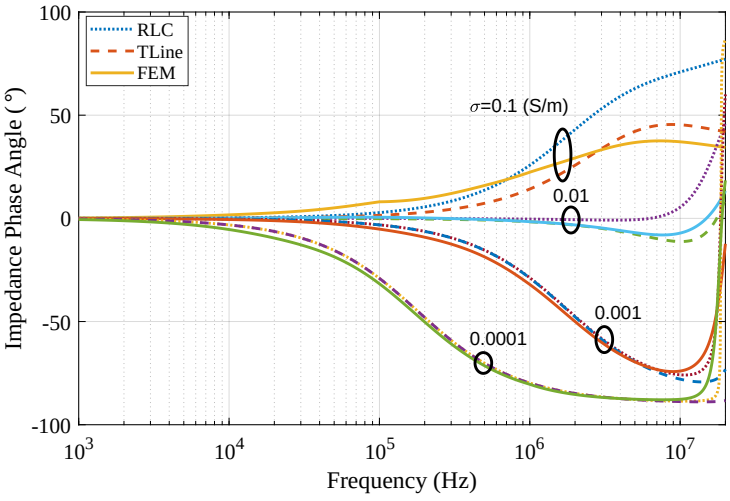

(b)

Fig. 3.12: Normalized magnitude (a) and phase angle (b) of harmonic impedance of 1 m vertical grounding electrode for $\varepsilon_r = 10$.

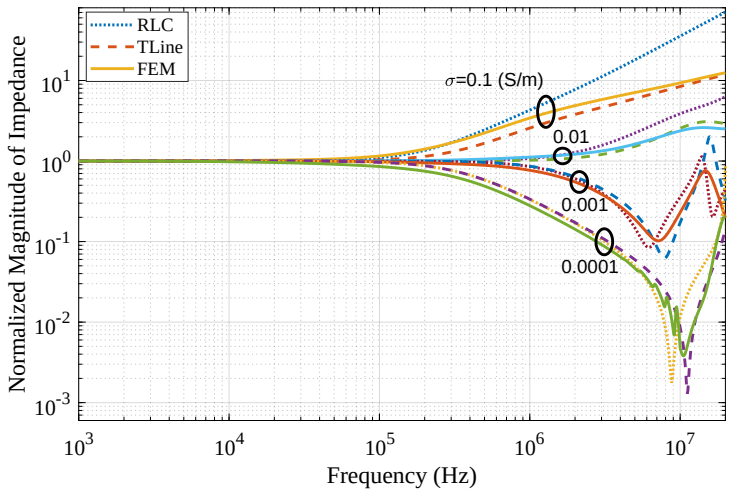

(a)

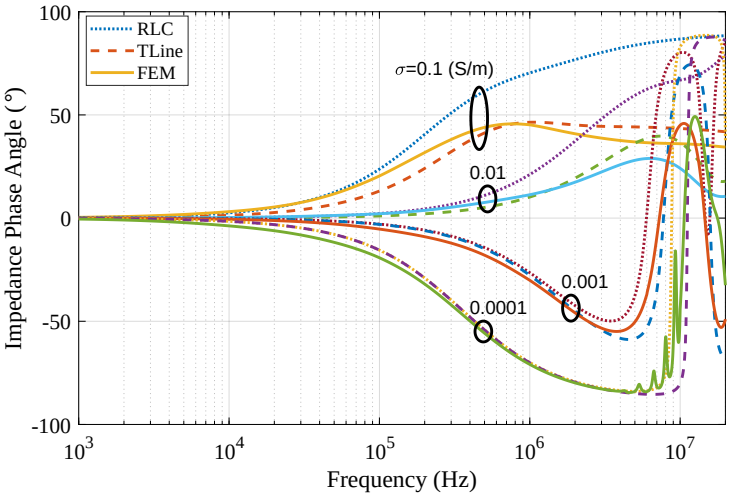

(b)

Fig. 3.13: Normalized magnitude (a) and phase angle (b) of harmonic impedance of 3 m vertical grounding electrode for $\varepsilon_r = 10$ along with its phase angle.

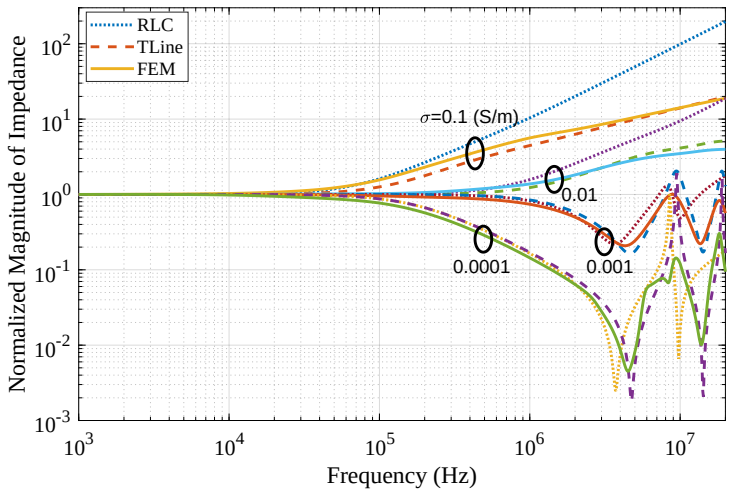

(a)

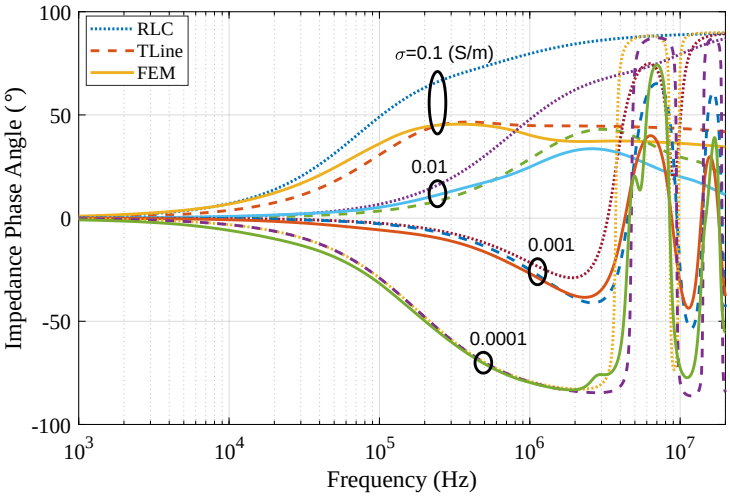

(b)

Fig. 3.14: Normalized magnitude (a) and phase angle (b) of harmonic impedance of 5 m vertical grounding electrode for $\varepsilon_r = 10$ along with its phase angle.

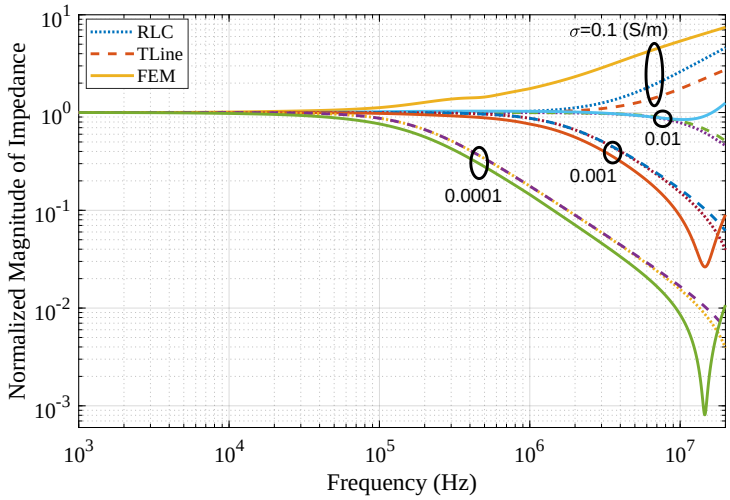

(a)

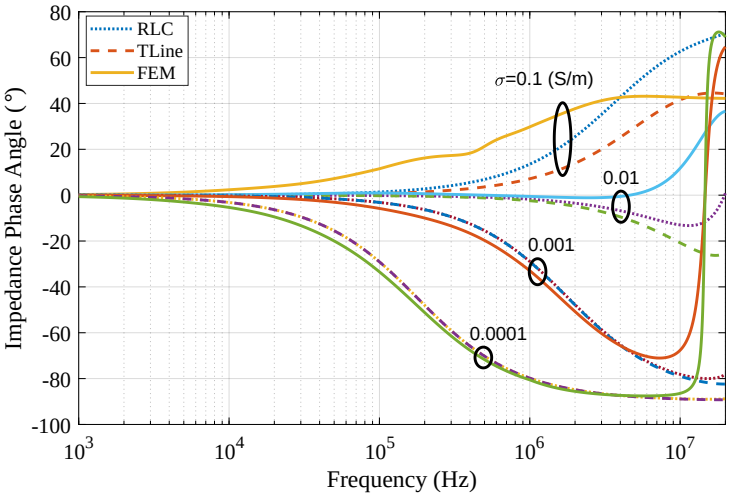

(b)

Fig. 3.15: Normalized magnitude (a) and phase angle (b) of harmonic impedance of 1 m horizontal grounding electrode for $\varepsilon_r = 10$ along with its phase angle.

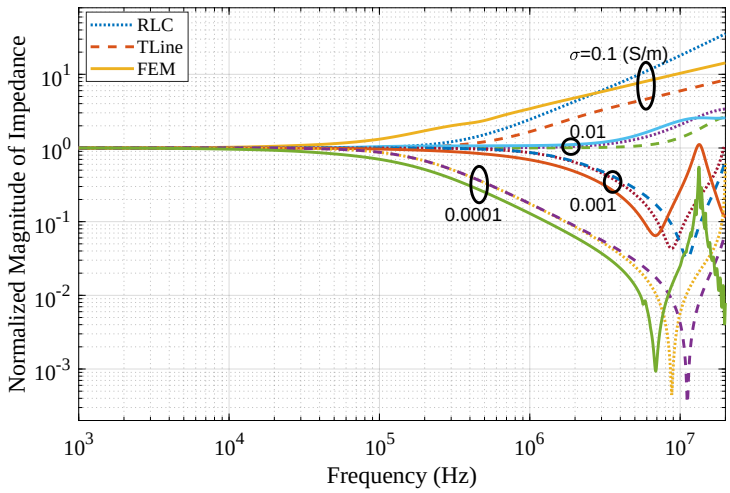

(a)

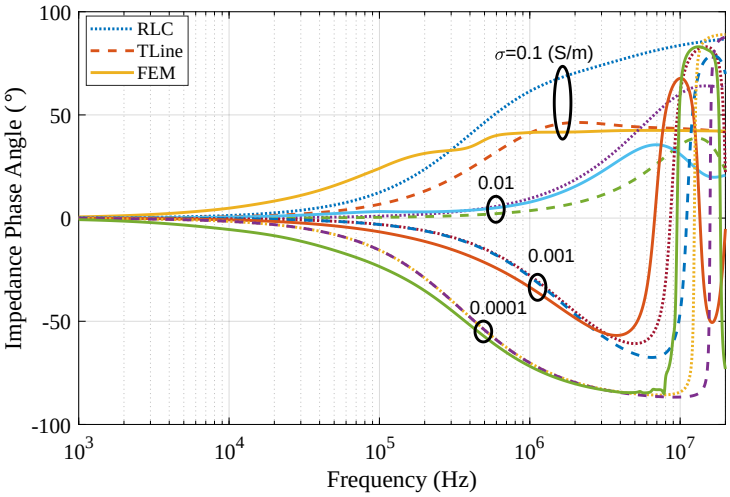

(b)

Fig. 3.16: Normalized magnitude (a) and phase angle (b) of harmonic impedance of 3 m horizontal grounding electrode for $\varepsilon_r = 10$ along with its phase angle.

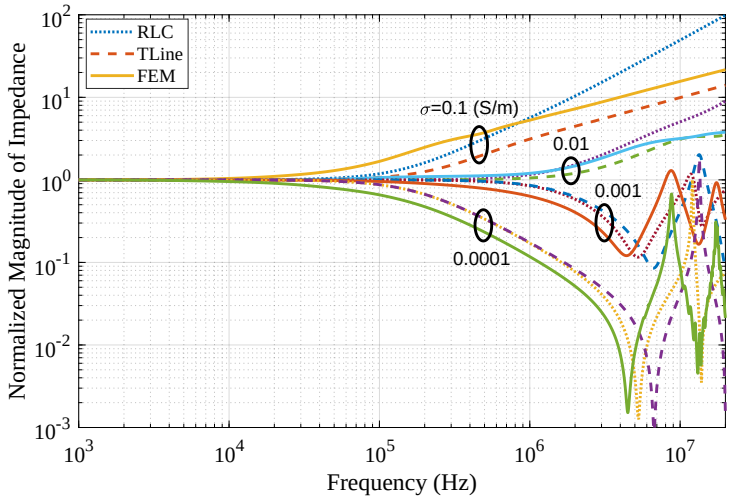

(a)

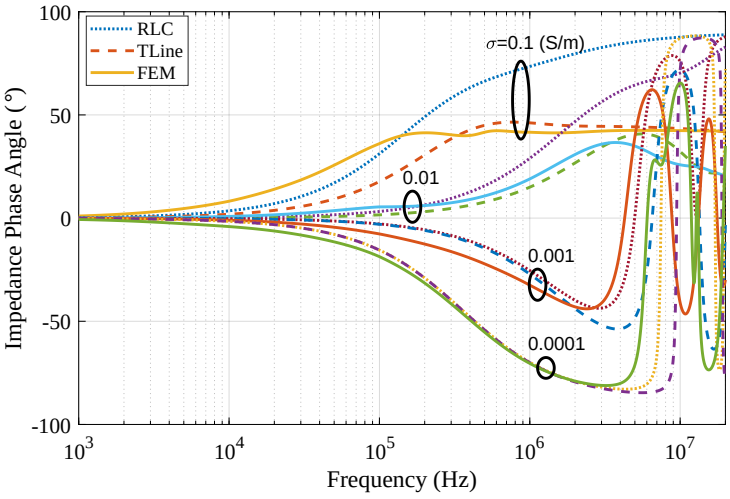

(b)

Fig. 3.17: Normalized magnitude (a) and phase angle (b) of harmonic impedance of 5 m horizontal grounding electrode for $\varepsilon_r = 10$ along with its phase angle.

Regarding the effect of soil electrical permittivity on the harmonic impedance of the grounding electrodes, Figs. 3.18 - 3.19 show how the high frequency impedance of a vertical grounding electrode of length 1 m varies as the soil relative permittivity is changed from $\varepsilon_r = 3$ to 30. Figures 3.20 and 3.21 are similarly organized, but for horizontal grounding electrodes. As discussion in Section 3.3.4, the variation of soil electrical permittivity (and so its water content) has no marked effect on the the impedance of the vertical grounding electrodes at low soil resistivity medium (10 and 100 Ωm). At high soil resistivity condition (1000 and 10000 Ωm) and low frequency range, the performance of the grounding electrodes have no significant change as the permittivity varies. However, beyond a threshold frequency of around 10 kHz, increasing the relative permittivty from 3 to 30 resulted in a significant reduction of at least 50% in the magnitude of impedance due to the capacitive effect. This decrease continues up to a frequency of 10 MHz after which an oscillatory behavior is observed for very high permittivities. The exact same variation in the impedance of horizontal grounding electrodes was observed and they are not shown here.

Figure 3.22 shows the percentage variation in the magnitude of vertical grounding impedance of the same length for the cases of $\varepsilon_r = 3$ and $\varepsilon_r = 30$ as a function of frequency and soil conductivity. The considered frequency range considered here is from 1 kHz to 10 MHz, cutting out the interval of resonant behavior. The variation in the magnitude of grounding impedance continuously increases as the frequency or the soil resistivity goes up. The steepest variation is observed in the frequency range of 50 to 200 kHz, smoothing out as the frequency increases further. This shows the importance of considering the effect of soil permittivity in high frequency analysis of grounding electrodes.

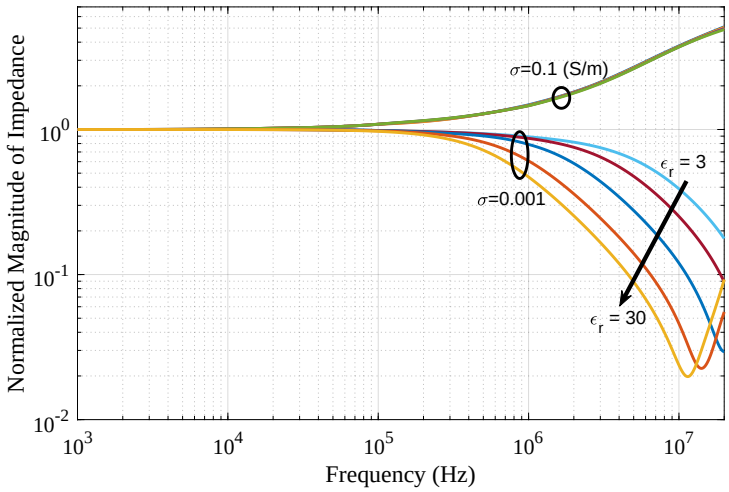

(a) $\sigma = 0.1$ and 0.001 S/m and considered relative permittivities are $\varepsilon_r = 3, 5, 10, 20, 30$.

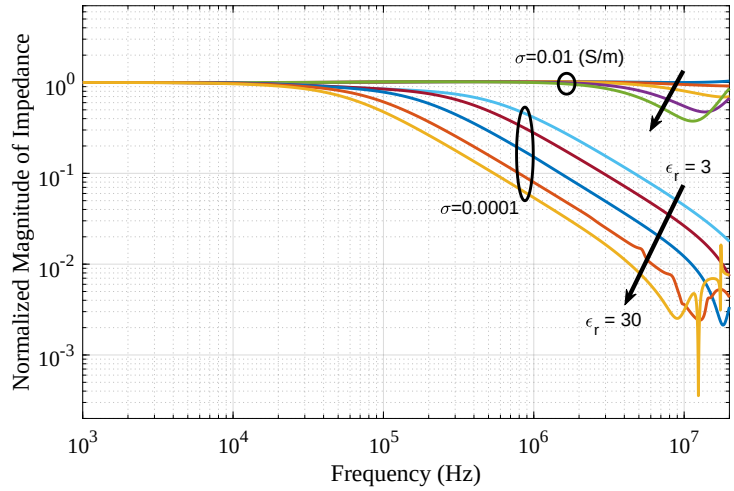

(b) $\sigma = 0.01$ and 0.0001 S/m and considered relative permittivities are $\varepsilon_r = 3, 5, 10, 20, 30$.

Fig. 3.18: Normalized magnitude of harmonic impedance of a vertical grounding electrode of 1 m in length with varying the soil permittivity.

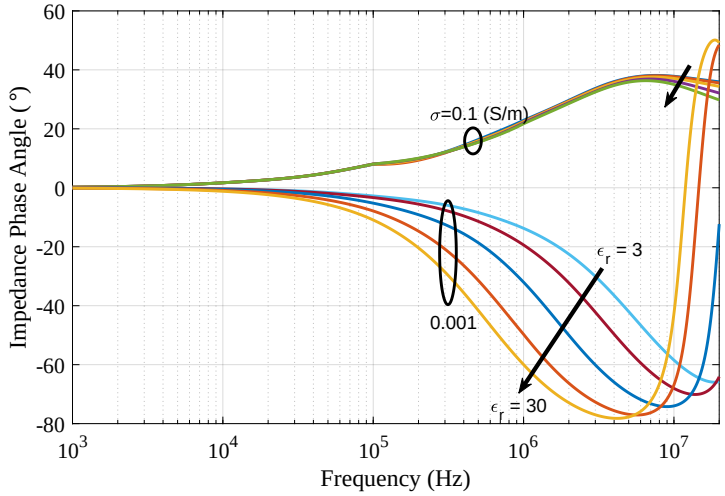

(a) $\sigma = 0.1$ and 0.001 S/m and considered relative permittivities are $\varepsilon_r = 3, 5, 10, 20, 30$.

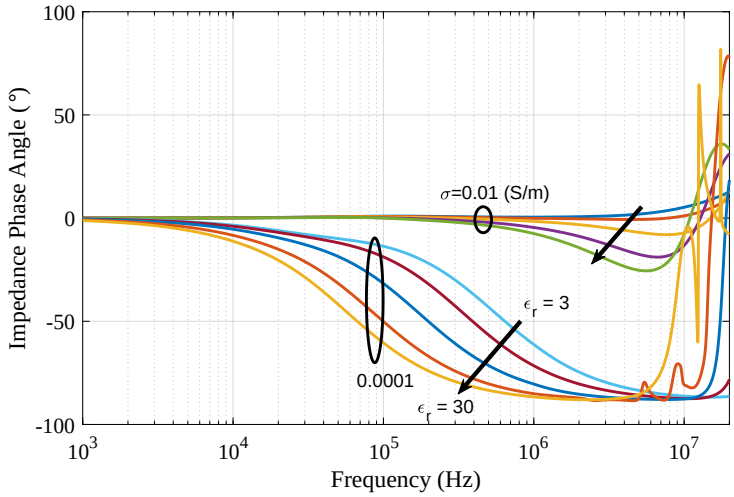

(b) $\sigma = 0.01$ and 0.0001 S/m and considered relative permittivities are $\varepsilon_r = 3, 5, 10, 20, 30$.

Fig. 3.19: Phase angle of the impedance of a vertical grounding electrode of 1 m in length with varying the soil permittivity.

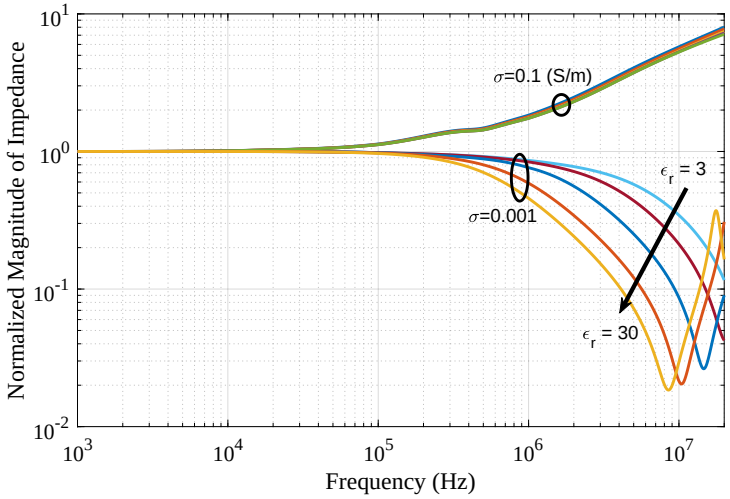

(a) $\sigma = 0.1$ and 0.001 S/m and considered relative permittivities are $\varepsilon_r = 3, 5, 10, 20, 30$.

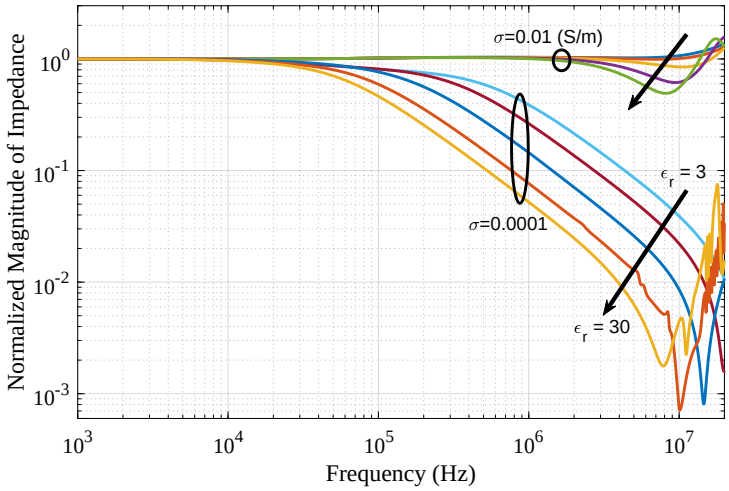

(b) $\sigma = 0.01$ and 0.0001 S/m and considered relative permittivities are $\varepsilon_r = 3, 5, 10, 20, 30$.

Fig. 3.20: Normalized magnitude of harmonic impedance of a horizontal grounding electrode of 1 m in length with varying the soil permittivity.

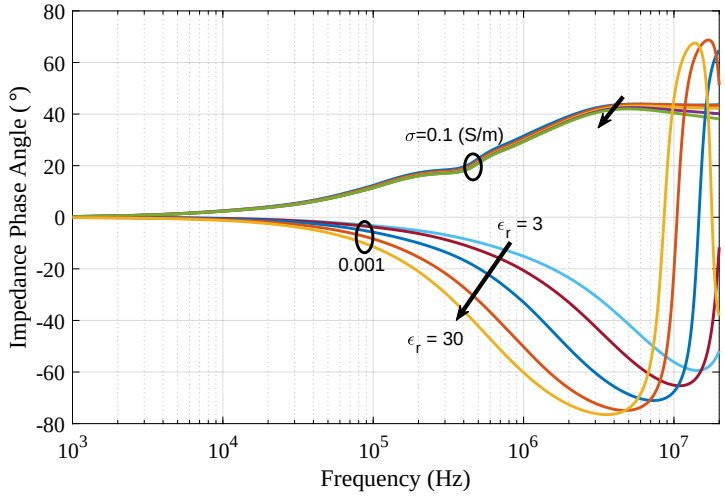

(a) $\sigma = 0.1$ and 0.001 S/m and considered relative permittivities are $\varepsilon_r = 3, 5, 10, 20, 30$.

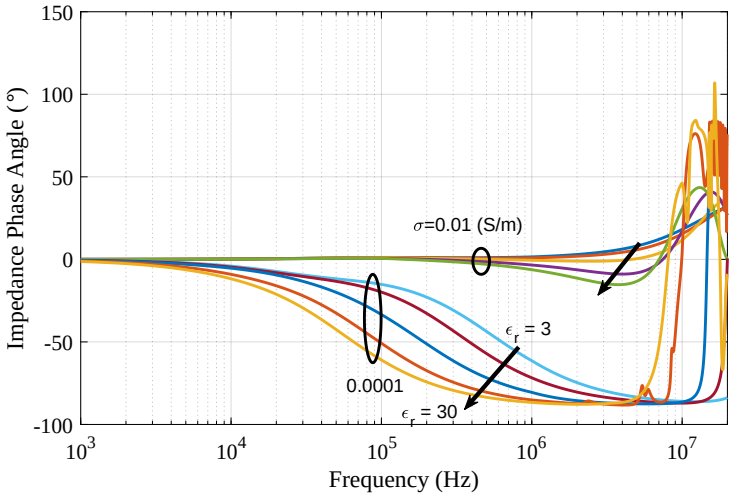

(b) $\sigma = 0.01$ and 0.0001 S/m and considered relative permittivities are $\varepsilon_r = 3, 5, 10, 20, 30$.

Fig. 3.21: Phase angle of the impedance of a horizontal grounding electrode of 1 m in length with varying the soil permittivity.

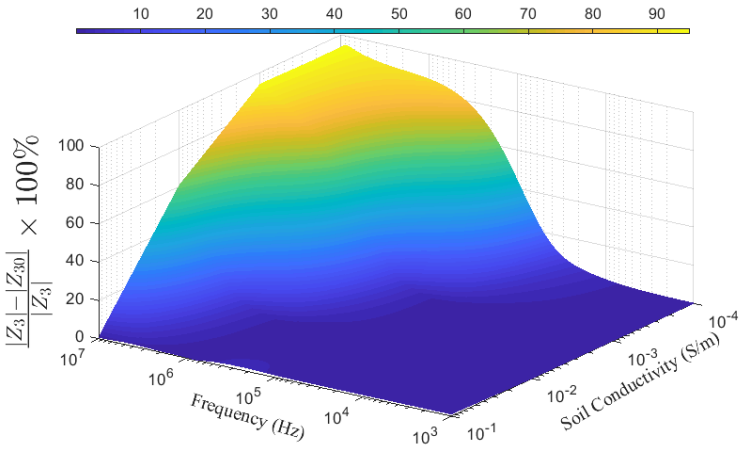

Fig. 3.22: Variation (%) in the magnitude of the grounding impedance of a vertical rod of length 1 m in soils with permittivity of $\varepsilon_r = 3$ and 30 as a function of frequency (1 kHz-10 MHz) and soil conductivity (0.0001 - 0.1 (S/m)).

3.4.2 Characteristic Frequency

The frequency limit for the resistive behavior of grounding electrodes was termed as the characteristic frequency F_c by Gary [122]. He derived a formula for the characteristic frequency based on the circuit theory [123]. Grcev [124] determined the following formula for f_c based on the electromagnetic model which is more precise than Gary's formula

$$F_c = \rho(\frac{0.6}{\ell})^{2.3} \tag{3.14}$$

In (3.14), ρ is the soil resistivity (Ωm), ℓ is the length of the electrode (m), and F_c will be in MHz. The effect of soil conductivity and electrode's length on this frequency is evident through (3.14) and Figs 3.12-3.17. The characteristic frequency increases as the length of the electrode or the soil conductivity decreases.

Increasing the permittivity makes the capacitive behavior of the grounding electrode

more pronounced, causing the magnitude and phase angle of the grounding impedance to decrease as the frequency increases. As a result, increasing the soil permittivity will make the phase angle of the grounding impedance less positive, and increases the characteristic frequency. This is the case for grounding electrodes of shorter length and lower earth resisitivity. On the other hand, a grounding electrode in highly resisitive soil shows a capacitive high frequency response, and increasing the soil permittivity makes its impedance to have a more negative phase angle, and the characteristic frequency would go down. These statements are illustrated in Fig. 3.23, showing the variation of characteristic frequency for a vertical electrode 3 m in length as the permittivity increases from 3 to 30 for various soil conductivities. As it can be seen, the characteristic frequency is more influenced by the soil permittivity in highly resisitive grounds.

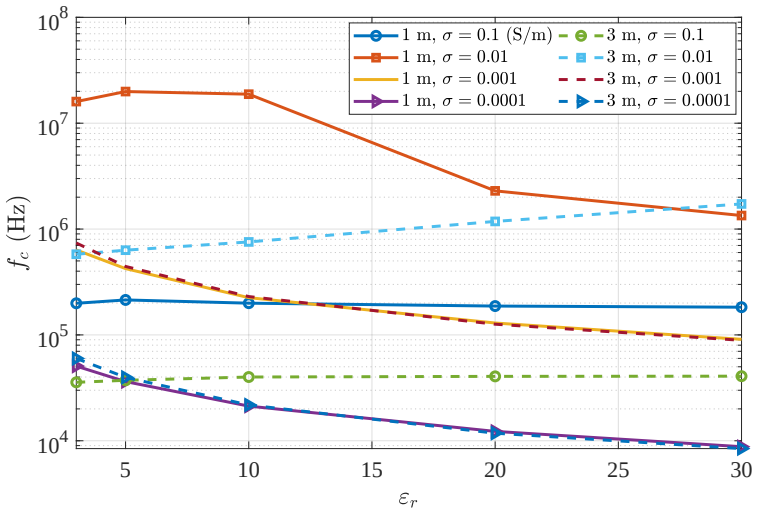

Fig. 3.23: Dependence of the characteristic frequency (f_c) on the dielectric constant and frequency for a vertical electrode of length 1 and 3 m.

3.4.3 Frequency-Dependent Soil

It has been shown that the grounding potential rise (GPR) of the simulated models matches the measured GPR when the frequency dependence of soil parameters is considered [125]. The assumption of constant parameters through the whole frequency range of interest causes considerable errors in the evaluation of the behaviour of the grounding electrodes [126, 127]. We consider the frequency dependence of conductivity and permittivity of soil in modeling the vertical and horizontal grounding electrodes using (3.5a) and (3.5b). A low frequency soil conductivity of $\sigma_0 = 0.001$ S/m and permittivity of $\varepsilon_r = 10$ have been considered here. Figure 3.24 shows the magnitude and phase of the vertical and horizontal grounding electrodes with lengths of 1 m and 5 m, taking the frequency-dependent effects in to account. In all cases, the frequency-dependent effects decrease the impedance of the grounding system, which is more evident at higher frequencies. It can be implied from the results of this section that the frequency dependence of soil parameters results in considerable improvement of the lightning performance of transmission lines. Given the frequency domain behavior of the grounding electrodes, they can be included in the lightning studies of transmission lines.

3.5 Time-Domain Computations

In this section, the influence of the dominant parameters on the dynamic behavior of grounding electrodes are analyzed in the time domain. First, the accuracy of modeling methods are compared in the time domain. Then, the importance of soil permittivity on the value of developed overvoltages is explored. Finally, the effect of frequency dependence of soil electrical parameters on the time-domain response is shown.

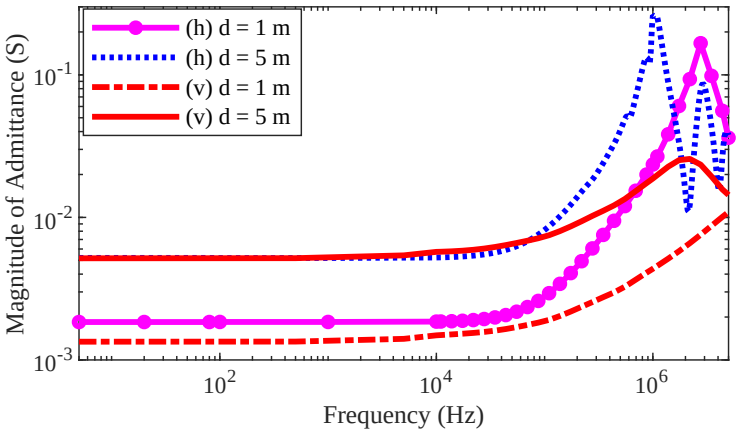

(a)

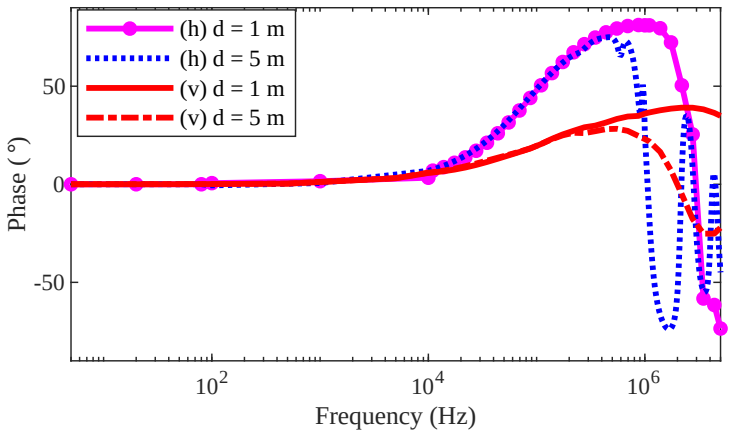

(b)

Fig. 3.24: Magnitude (a) and Phase (b) of admittance for vertical (v) and horizontal (h) grounding electrodes using FEM considering the frequency dependence of soil parameters described by (5a) and (5b).

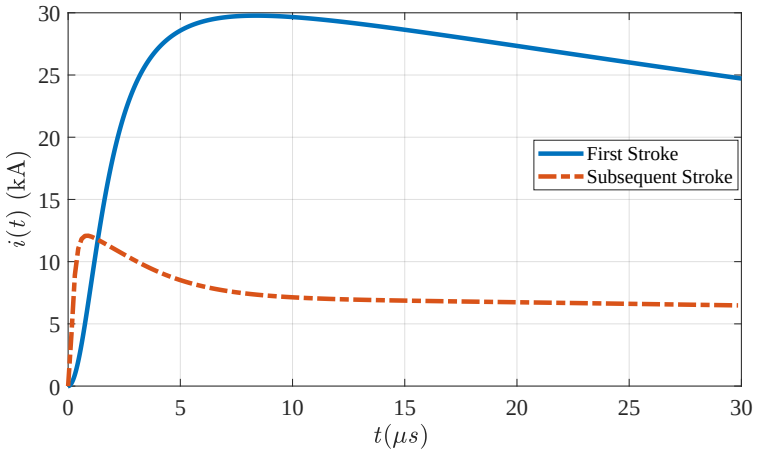

Fig. 3.25: First and subsequent return stroke current waveforms.

3.5.1 Lightning Stroke Current

An accurate knowledge of the parameters of the lightning strokes is necessary in order to predict the severity of the transient overvoltages generated across insulator strings by a direct stroke to the transmission line conductors or the tower. Lightning current is random in nature and its parameters must be expressed in probabilistic terms from the measured data in field. Measurement of lightning parameters can be done by direct measurements on actual, or rocket triggered lightning. More than 90% of the cloud-to-ground strokes are of negative polarity, except for seasonal and regional variations. There has been small number of positive lightning strokes recorded, and the recorded ones don't have enough common features to produce an acceptable mean waveshape [128]. Many researchers have collected the statistical data for the influencing parameters of negative lightning flash over many years and in different places, with most of the data taken by Berger [128]. Using these data, it is possible to generate a mean waveshape for the first and subsequent lightning strokes as shown in Fig 3.25.

Considering the waveshpae of the first stroke current, it has a concave wavefront with

the greatest rate of change near its peak as shown in Fig. 3.25. The subsequent stroke current has, in general, shorter wavefront in comparison to the first stroke and they don't show the pronounced concavity of the wavefront of the first stroke current. A number of expressions have been proposed to approximate the lightning currents using cosine or exponential functions, but these current waveshapes have been proved to be unrealistic [129]. The current waveforms which fit the experimental data to a better extent were chosen by Rachidi et al. [130] and are expressed by means of Heidler's functions [73]

$$i(t) = \frac{I_0}{\eta} \frac{(\frac{t}{\tau_1})^n}{1 + (\frac{t}{\tau_2})^n} e^{\frac{-t}{\tau_2}} \tag{3.15}$$

where

$$\eta = e^{-\frac{\tau_1}{\tau_2}(n\frac{\tau_2}{\tau_1})^{\frac{1}{n}}}. \tag{3.16}$$

In (3.15) and (3.16), I_0 is the peak of the current pulse, τ_1 is the front time constant, τ_2 is the decay time constant, n is the current steepness factor having values between 2 to 10, and τ is the amplitude correction factor. It was stated in [73] that the usual double-exponential function to represent a transient lightning waveshape has a discontinuity of its first derivative at t = 0, but such difficulty does not arise with (3.15). The first and subsequent stroke waveforms are represented by one and a sum of two Heidler's functions, respectively, with the parameters given in Table 3.3. Regarding the frequency content of lightning strokes, the first and subsequent strokes are known to have their major frequency components in the frequency range of DC to 10 MHz [68].

Table 3.3: parameters of the Heidler's functions used to produce the waveforms of the Fig. 3.25.

	I_0 (kA)	$\tau_1(\mu s)$	$\tau_2(\mu s)$	n
First Stroke	28	1.8	95	2
Subsequent	10.7	0.25	2.5	2
Stroke	6.5	2	230	2

3.5.2 Comparison of Modeling Approaches in the Time Domain

Since the vertical and horizontal grounding electrodes have very similar high-frequency behavior, only vertical grounding electrodes are considered in the rest of this chapter. This section aims at comparing the three modeling approaches based on the calculated overvoltages. Figures 3.26-3.28 show the voltage at the feed point of the grounding electrodes with respect to remote ground calculated by the three methods. Three parameters influence the accuracy of the circuit and transmission-line theory with respect to the FEM approach that are soil conductivity (σ), dielectric constant (ε), and the electrode's length. Two features of the developed overvoltages need to be considered: the peak of the voltage and the time to peak or the front time. The front time influences the withstand capability of the insulator strings and in general any other apparatus. The variation of the tail time which is several orders of magnitude longer than the front time, has less importance in the computation of the overvoltages.

In all cases, both circuit and transmission-line approaches overestimate the potential in comparison to the electromagnetic model. Figure 3.26 shows the effect of soil resistivity on the estimated overvoltages with the three methods. The graphs show the voltages developed

Table 3.4: Effect of soil resistivity on the error value of $\frac{v(t)_{max}^{RLC} - v(t)_{max}^{FEM}}{v(t)_{max}^{FEM}} \times 100\%$ for a vertical electrode of length 3 m, and $\varepsilon_r = 10$.

$\rho(\Omega m)$	First Stroke	Subsequent Stroke
10	2.6	9.5
10^4	7.17	13.27

by the first and subsequent lightning currents in case of a 3 m vertical electrode buried in a soil with a resistivity of 10 and 10000 Ωm). It can be seen that the overestimation of the theoretical methods is much larger for more resistive soil and subsequent stroke lightning current. The agreement between the two theories decreases in low resistivity soils. After the first high frequency region, which is called the surge region, the stationary period is reached, in which the behavior of the grounding electrodes can be estimated by their low frequency resistance. For this reason, the error between the models in the stationary region is less, and the overvoltages tend to converge. Back to Fig. 3.13, it was understood that the grounding electrodes exhibit a capacitive high frequency behavior in more resistive soils. This effect shows itself as a higher delay in the peak of the voltage in the time-domain when the resistivity of the soil is increased (Fig. 3.26). Table 3.4 shows the error between the estimated overvoltage peak using the circuit theory and the FEM model. It is worth noting that the difference between the results of circuit and transmission line theory is not considerable.

Considering the effect of soil permittivity, Fig. 3.27a and 3.27b show the grounding impedance for the same electrode in a soil with resistivity of $10,000$ Ωm for a relative permittivity of $\varepsilon_r = 3$, and $\varepsilon_r = 30$. Considering these two figures, along with Fig. 3.26b, it is obvious that as the soil permittivity increases, the computation error of RLC and Tline theories decreases. Again the maximum deviation is for the subsequent stroke. Table 3.5

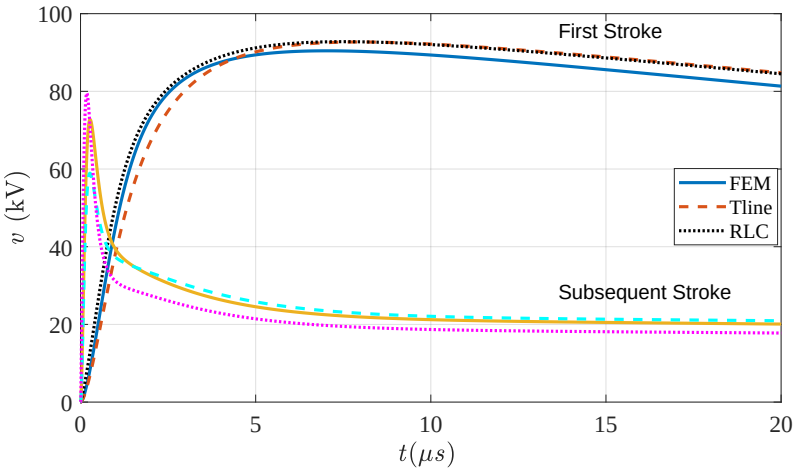

(a) $\rho = 10\ \Omega\text{m}$.

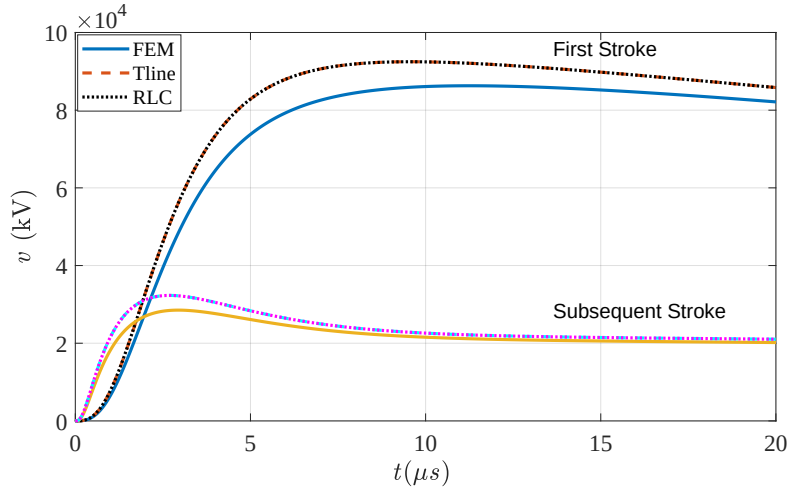

(b) $\rho = 10000\ \Omega\text{m}$.

Fig. 3.26: First and subsequent voltage of a 3 m vertical electrode in a soil of $\varepsilon_r = 10$.

Table 3.5: Effect of soil permittivity on the value of $\frac{v(t)_{max}^{RLC} - v(t)_{max}^{FEM}}{v(t)_{max}^{FEM}} \times 100\%$ for a vertical electrode of length 3 m, and $\rho = 10000\ \Omega$m.

ε_r	First Stroke	Subsequent Stroke
3	8.38	20.08
30	5.82	9.58

Table 3.6: Effect of electrode length on the value of $\frac{v(t)_{max}^{RLC} - v(t)_{max}^{FEM}}{v(t)_{max}^{FEM}} \times 100\%$ for a vertical electrode buried in a soil of $\rho = 1000\ \Omega$m and $\varepsilon_r = 10$.

$l(m)$	First Stroke	Subsequent Stroke
1	5.9	11.35
5	2.9	8.68

shows the change of the voltage peak for this case.

The dynamic behavior of two lengths of vertical electrodes, *i.e.* 1 m, and 5 m, in a soil with resistivity of 1000 Ωm and a relative permittivity of $\varepsilon_r = 10$ is illustrated in Fig. 3.28a and 3.28b. Increasing the length of the electrode decreases the voltage peak considerably. Furthermore, the time of voltage peak is delayed as the length of the electrode is increased. Regarding the accuracy of the methods, there is more inaccuracy for the lower lengths of the electrode, as shown in Table 3.6. Considering all the cases, the most inaccuracy of the RLC and transmission line theories is for higher soil resistivity, lower permittivity, and shorter electrodes. Moreover, the higher frequency content of the subsequent strokes, causes more inaccuracies in the theories.

3.5.3 Evaluation of Overvoltages as a Function of Soil Permittivity

In this section, the focus is on the calculation of the overvoltages for the grounding electrodes buried in soils with different permittivities, and the effect of electrode length and the soil conductivity on the extent to which the soil permittivity affects the overvoltages is

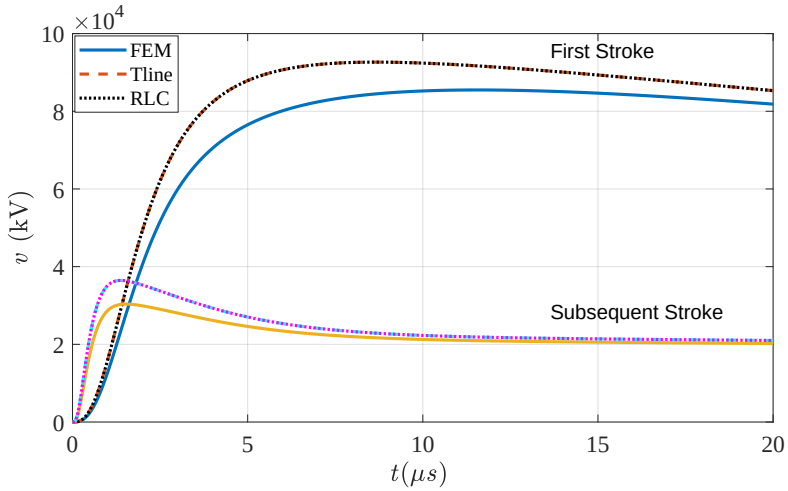

(a) $\varepsilon_r = 3$.

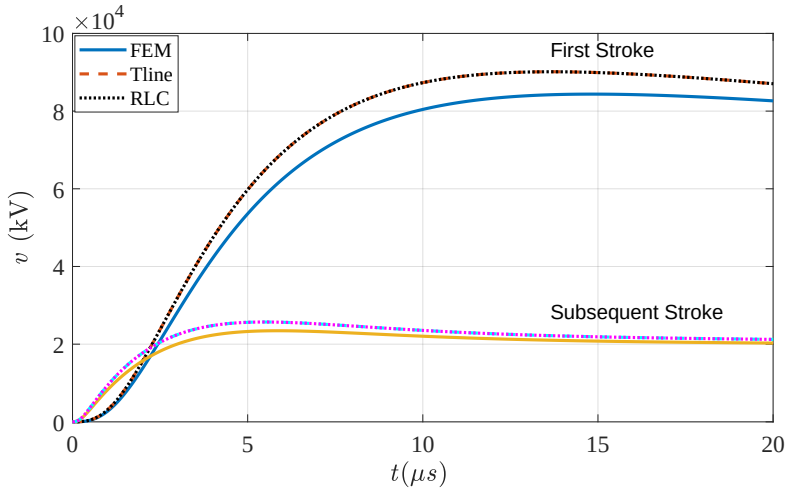

(b) $\varepsilon_r = 30$.

Fig. 3.27: First and subsequent voltage of a 3 m vertical electrode in a soil with $\rho = 10000\ \Omega$m and varying ε_r.

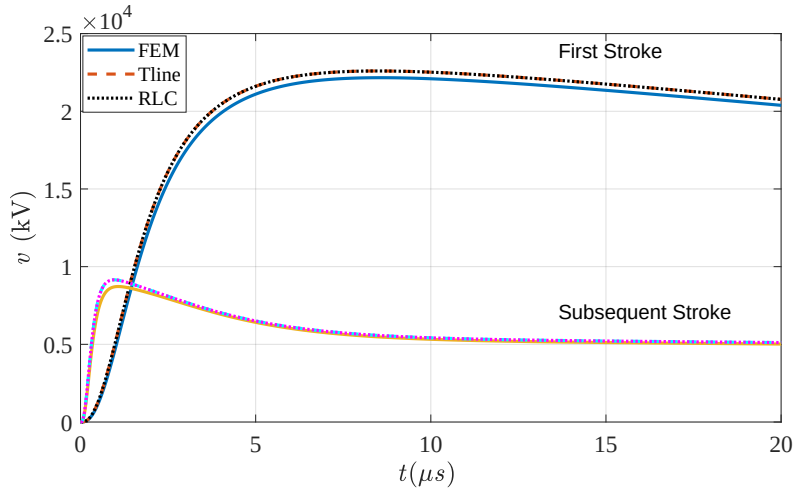

(a) $l = 1$ m.

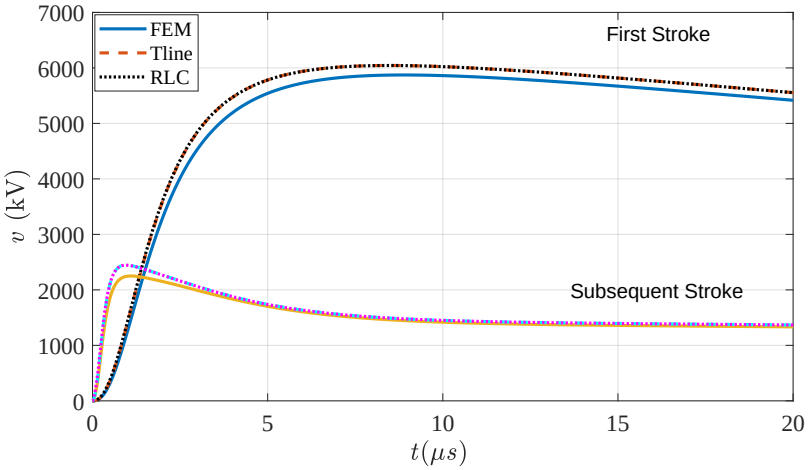

(b) $l = 5$ m.

Fig. 3.28: First and subsequent stroke voltage of a vertical electrode in a soil of $\rho = 1000$ Ωm and $\varepsilon_r = 10$.

investigated.

In Fig. 3.29, the induced voltage of a vertical electrode of length 1 m buried in soil with a resistivity of $\rho = 1000$ and $\rho = 10000$ Ωm and a varying relative permittivity is shown. The electrode is subjected to the first and subsequent lightning strokes. As expected, the effect of soil permittivity in the low resistivity soil ($\rho = 10$ Ωm) is negligible on the induced overvoltages and are not shown here. As the resistivity increases, there are two major effects on the voltages with varying soil permittivity: First, the peak of the voltage is considerably reduced as the relative permittivity is changed from $\varepsilon_r = 3$ to $\varepsilon_r = 30$ especially in the case of the subsequent strokes. The percentage of error is 3.5% and 24.86% for the first (Fig. 3.29b) and subsequent strokes (Fig. 3.29c), respectively when the soil resistivity is 10000 Ωm. This error is 2 and 6% for the soil of $\rho = 1000$ Ωm. This is in agreement with Fig. 3.22, where it was shown that the effect of soil permittivity is more pronounced at higher frequencies and more resistive soils. The second effect is the time at which the voltage reaches its peak. As the permittivity increases, the current peak is reached in a later time, which is again more affected in the case of a subsequent stroke. The first and subsequent current waveforms reach their peak in 8.38 μs and 0.83 μs, respectively. The time in which the peak of the voltages occrues is 3.30 is 11.56 μs for $\varepsilon_r = 3$ and 14.84 μs for $\varepsilon_r = 30$. For the overvoltages corresponding to the subsequent stroke, the time of peak changes from 1.53 μs to 5.86 μs. As the dielectric constant of the soil increases, the capacitive effect becomes more than the inductive effect, causing the voltage to lag more with respect to the current.

Another contributing parameter is the length of the electrode. Figure 3.30 shows the voltage of a 5 m vertical electrode buried in highly resistive soil ($\rho = 10000$ Ωm). A change of 2% and 16.86% of the voltage peak is observed as the permittivity is increased. In the first stroke lightning, it takes 11.24 and 13.74 μs for the voltage to reach its peak in a soil of

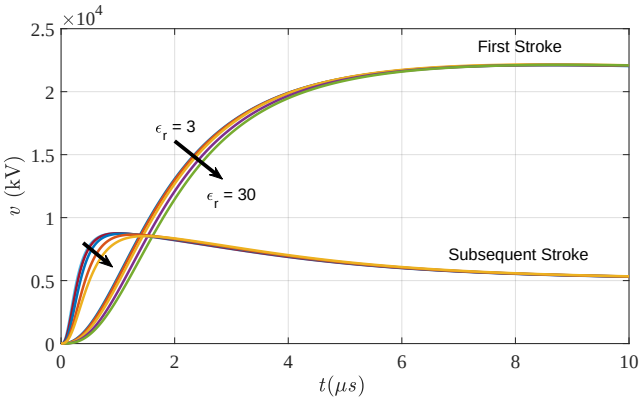

(a) $\rho = 1000\ \Omega$m.

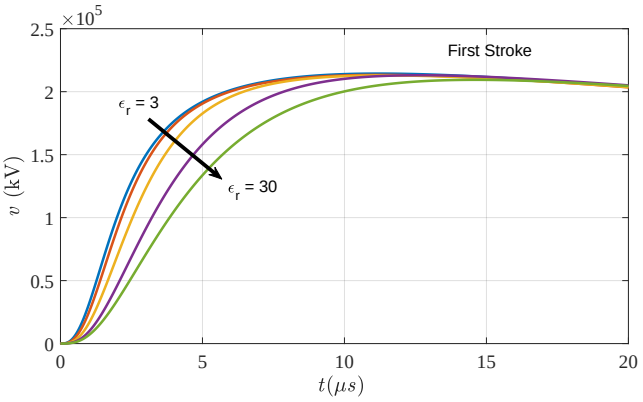

(b) First stroke for $\rho = 10000\ \Omega$m.

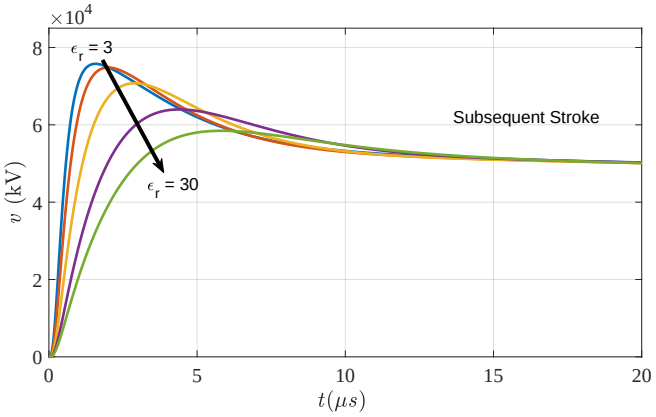

(c) Subsequent stroke for $\rho = 10000\ \Omega$m.

Fig. 3.29: First and subsequent stroke voltage of a 1 m vertical electrode in a soil with a relative permittivity of $\varepsilon_r = 3$, 5, 10, 20, and 30.

$\varepsilon_r = 3$ and $\varepsilon_r = 30$, respectively. In the case of a subsequent stroke, this time changes from 1.49 to 5.5 μs.

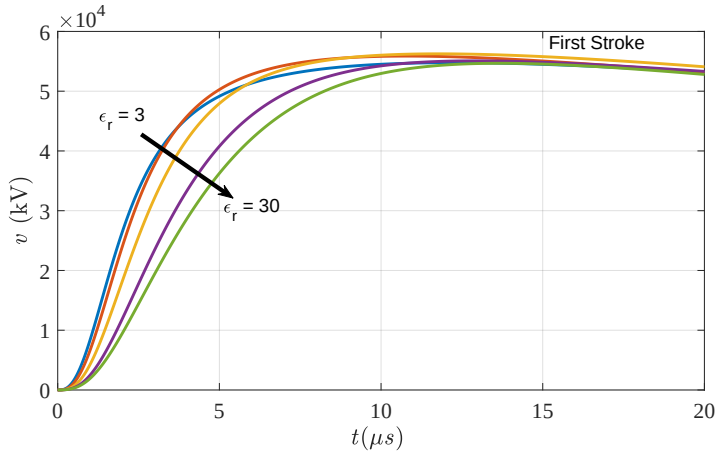

(a) First stroke.

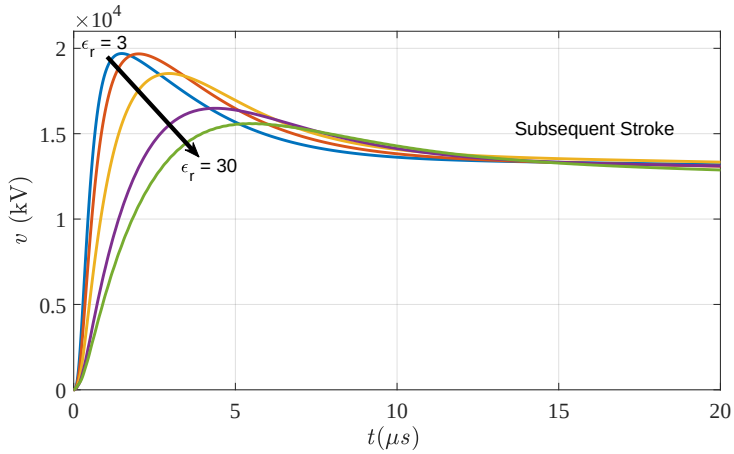

(b) Subsequent stroke.

Fig. 3.30: First and subsequent stroke voltage in a 5 m vertical electrode in a soil with $\rho = 10000\ \Omega$m and a relative permittivity of between 3 to 30.

3.6 Summary

In this chapter, a full-wave simulation model was developed based on FEM to obtain the tower-footing grounding impedance. Formulation of the problem and a sensitivity analysis were provided to obtain the optimum value of the affecting parameters on the accuracy of the simulation model. The obtained frequency-domain results were then fitted using vector fitting and approximated with a rational function approximation. Next, recursive convolution was used to obtain the time-domain results. The simulation results were compared to that of theoretical approaches, *i.e.* circuit and transmission line theories. The effect of the length of vertical and horizontal electrodes buried in soil with several different electrical parameters was studied. Both constant and frequency dependent soil resistivity and permittivity were considered.

Chapter 4
Transmission Tower Surge Impedance

The calculation of overvoltages in power transmission lines struck by lightning has been the subject of many researches in the past decades. The accurate representation of the transmission line tower and its grounding system is an essential part of studying the transient behavior of the power system. The advances made in the protection mechanisms require a greater precision in the calculations concerning the transmission line tower.

The approaches for modeling transmission line towers can be divided into three categories: (i) theoretical, (ii) numerical, and (iii) experimental that are performed/implemented either in the time [70, 72, 77, 78, 80, 81, 85–87, 92, 130–133] or frequency domains [71, 95, 134]. The numerical analyses are based on a) the Method of Moments (MOM) [134–136], b) Finite Element Method (FEM) [137,138], c) Hybrid Electromagnetic Model (HEM) [139], or d) Finite Different Time Domain (FDTD) method. [93,94,140–143]. Experimental measurements have been performed on full scale towers [88,89,143–145] or scaled towers [78,89,131,146,147]. Regardless of the approach, the aim of such analysis is to either find an equivalent impedance or derive an equivalent electric circuit for the transmission line tower with the same response as the measured waveforms. In the theoretical approaches, it is not possible to consider

all the tower details, such as its cross arms or bracings. Furthermore, the tower body is approximated by simple geometries such as a cylinder (*e.g.* [77]) or cone (*e.g.* [78]). There are only a few experimental studies on a limited number and types of in-service towers as such measurements require an outage and are quite costly. Due to the restrictions of the theoretical and experimental approaches, developing an automated process for the numerical analysis of transmission towers is receiving more attention in recent years.

In this chapter, following a thorough overview of the existing models for the transmission line towers and their underlying assumptions, a numerical method based on thin wire approximation of the tower is presented. The Method of Moments (MOM) through Numerical Electromagnetic Code (NEC4) is used to determine the surge impedance of a double circuit transmission line tower either above a perfect electric conductor (PEC) ground or with grounding electrodes buried in lossy ground. The developed model is verified by simulating cylinders of different heights and comparing the results with the measurements available in the literature. Counterpoise grounding electrodes of different lengths (from 5 to 20 m) are considered in soil with resistivity of 100 and 1000 Ωm.

4.1 Verification of the Numerical Analysis

Measurement of the tower surge impedance is performed in two ways: one is the *direct method* [131, 144], where a current pulse is injected into the tower top and the voltage between the tower top and a reference voltage measuring wire is measured using a voltage divider. The other method is the *reflection method* [148], where a steep-front traveling wave is injected into the tower top using a wire, and the reflected wave is observed to estimate the transient impedance of the tower. In this thesis, the former method of measurement

is implemented using numerical simulations, since the reflection method is only valid when evaluating the reflection of waves from adjacent towers [149]. The simulations are performed using Numerical Electromagnetic Code (NEC-4), which is based on the thin wire approximation and the numerical solution of integral equations by means of the Method of Moments (MOM) [150]. Measurements of the surge characteristics of cylinders with different heights and radii performed by Hara *et al.* [96] are employed to validate the accuracy of the numerical simulations. In the measurements of [96], the electrodes are placed on a 12×10 m^2 iron plate as the ground as shown in Fig. 4.1. The current is applied to the top of the vertical conductor by a current lead extended horizontally 9 m away. The voltage is measured using a voltage probe in the gap between the top of the cylindrical conductor and a voltage reference wire, which is horizontally extended to the remote ground and it is perpendicular to the current lead wire to minimize the coupling effects. Both the current and voltage wires are attached vertically to the ground at their ends, using a matching resistance (R_c) to avoid reflections.

The measurement performed on a 3-m high cylinder with a radius of 2.5 mm is considered for the numerical analysis in NEC4. A 10 kΩ resistance is inserted between the top of the electrode and end of the voltage reference wire. The voltage is evaluated by calculating the

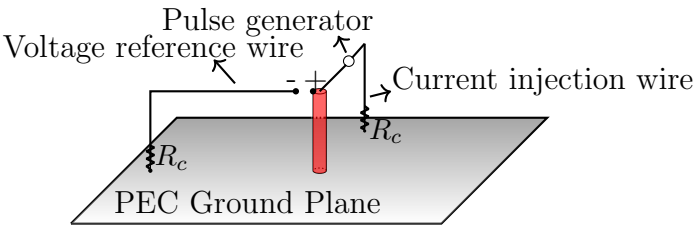

Fig. 4.1: Setup for the measurement of surge characteristics of a vertical cylinder by direct method as performed by Hara *et al.* in [96].

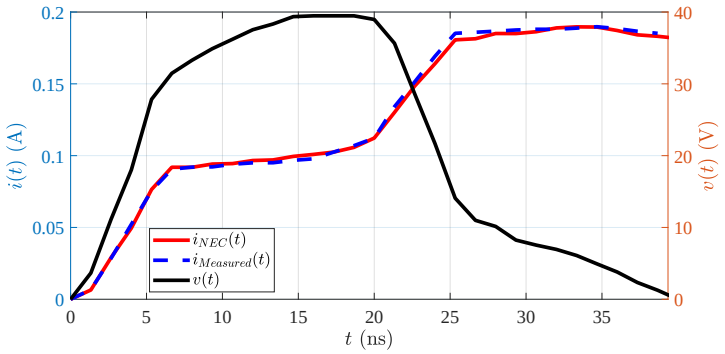

Fig. 4.2: Voltage at the top of the cylinder in reference to remote ground (right axis) and measured (Hara's) and simulated current (left axis) injected at the top of a 3-m cylinder on a PEC ground.

current flowing through this resistor. It shown that the value of the voltage-measuring probe has no significant impact on the measurement if its internal capacitance is less that a certain limit [151]. Finally, the inverse Fourier transform is used to obtain the time domain voltage and current.

The voltage waveform shown in Fig. 4.2, adopted from [96], is used as the input to the system. Figure 4.2 shows the measured and simulated currents injected at the top of the cylinder that shows the accuracy of simulation results, in terms of both the waveshape and magnitude. The measured current initially rises for 5 ns and remains almost constant till $t = 20$ ns that is when the reflected wave from the ground reaches the top of the cylinder.

4.2 Results and Discussions

In this section, firstly, the simulation results are presented for vertical cylinders and the double-circuit tower (shown in Fig. 4.8) on a PEC ground. The dependence of time-domain surge impedance and the effect of tower elements are investigated. Finally, the effect of lossy

ground on the simulated results is presented and discussed.

4.2.1 Dependence of Time-Domain Surge Impedance on the Excitation Waveshape

In this section, we also employ the measurements of Hara *et al.* [96] are considered to show the dependence of time-domain impedance definitions on the waveshape of the excitation. In [96], the so-called *maximum surge impedance*, as given in (2.1c), was used. A step input current with a rise time of 5 ns is applied to the cylinder (see Fig. 4.1) and the surge impedance is calculated at $t_0 = 2h/c$, where h is the height of the cylinder and c is the speed of light. For the case of a cylinder with a height of 15 m and a radius of 25.4 mm, the measured surge impedance is 320 Ω [96]. The same cylinder is simulated in NEC4 in the frequency range of 0.1 to 250 MHz. The length of the current and voltage leads are 115 m, so that the reflected waves do not affect the results until 760 ns. Step currents with various rise times from $t_r = 10$ to 80 ns are injected into the top of the cylinder. The values of t_r are less than the round-trip travel time of the wave along the cylinder, which is equal to $t_0 = 100$ ns. As a result, the effect of grounding system appears after the peak of the voltage waveform. The voltage at the top of the cylinder relative to the voltage reference wire is shown in Fig 4.3. The rise time of the voltage waveform is almost equal to the rise time of the injected current and there is a reflection from the ground at $t_0 = 100$ ns. Calculating the surge impedance of the tower for the considered excitations using (2.1c), Z varies from 324.6 to 293Ω, which is equal to a variation of 9.7%, when the rise time is increased from 10 to 80 ns. Considering a double exponential excitation, which is commonly used in lightning studies, the surge impedance defined by (2.1c) decreases from 316.8 Ω for a a rise time of $T_1 = 10\,\mu$s to 232.5 Ω for a double exponential waveform with a rise time of $T_1 = 200\,\mu$s.

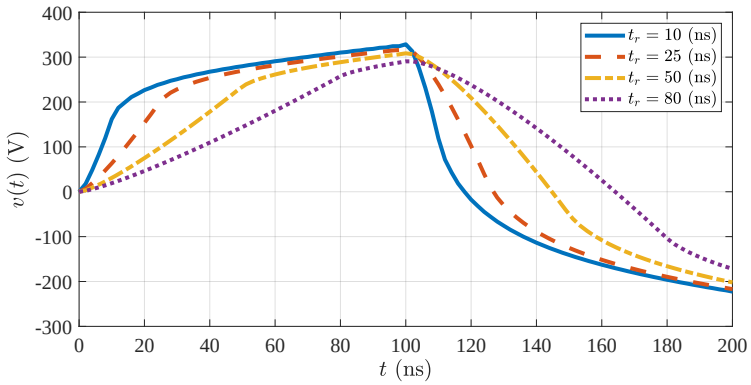

Fig. 4.3: Simulated voltage at the top of a 15-m vertical cylinder in response to pulse currents of 1 A in magnitude and rise time of t_r injected at the tower top.

4.2.2 Effect of Tower Elements

Generally, a typical transmission line tower consists of a main body (green in Fig. 1A), a cage (blue), cross arms (red), and slant and horizontal elements (also blue). In this thesis, the double circuit tower CAD file (in '.step' format) has been used to generate the wire diagram of the tower. This provides a detailed model of the tower for the numerical simulations by NEC4. It also enables the sensitivity study with regards to the level of detail required for an accurate simulation. The tower is simulated in NEC4 in the frequency range of 0.1 to 240 MHz with four level of details. Firstly, only the main legs with a height of 24.01 m are considered (*Case 1*). Next, the tower cage is added to the main legs, making the tower height equal to 42.51 m (*Case 2*). In *Case 3*, the cross arms are added to the geometry, and finally, the shield wire cross arms, bracings, and horizontal elements are taken into account in *Case 4*. The simulation configuration is the same as that shown in Fig. 4.1 and the horizontal extension of the leads is 200 m far from the top of the geometry. In the simulations performed in this section, to achieve a desirable resolution in the frequency

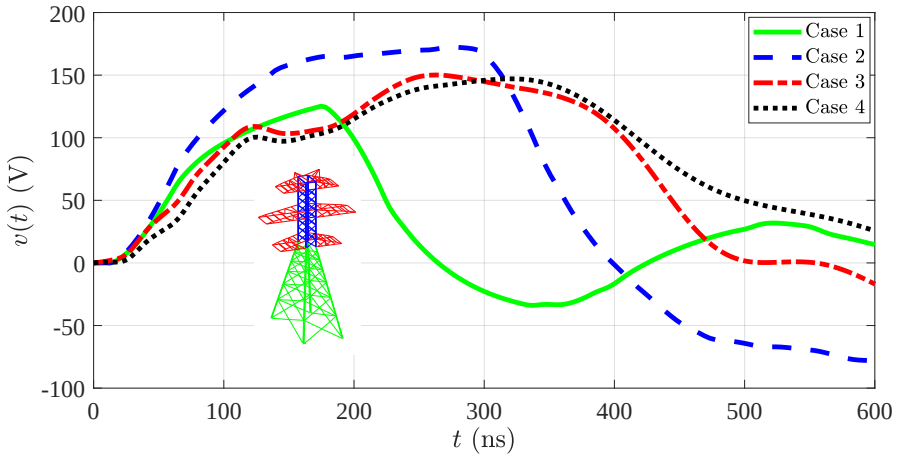

Fig. 4.4: The effect of tower elements on the voltage at the top of the structure for a ramp current with a rise time of $t_r = 50$ ns injected into the structure.

domain, 800 frequency points are used.

Two ramp currents with a magnitude of 1 A and rise times of $t_r = 50$ and 150 ns are used as the current waveform injected into the top of the structure through the current lead wire. Assuming that the waves propagate through the tower structure at the speed of light, the travel time $t_0 = 2h/c$ in Cases 1, 2, and 3 should be 160, 283 and 300 ns, respectively. The voltage at the top of the structure is shown in Fig. 4.4 for $t_r = 50$ ns. The surge impedance of each structure calculated using (2.1c) at $t_0 = 2h/c$ and also the apparent propagation speed (v_0), that is when we consider a straight vertical conductor, relative to the speed of light (c) are given in Table 4.1. It can be seen that the inclusion of the cross arms in the model decreases the tower surge impedance by 16.1% in the case of fast-rising currents ($t_r = 50$ ns) and 10.9% in the case of a excitation with a rise time of $t_r = 150$ ns. This is in agreement with previous measurements that considered the tower cross arms as capacitively-loaded stubs in parallel with the tower body [78]. Figure 4.5 shows the voltage at

Table 4.1: Surge impedance and wave propagation speed of the double circuit tower when different level of details for the tower are considered.

Geometry	$Z_{50}(\Omega)$	$Z_{150}(\Omega)$	$v_0/c(\%)$
Case 1	106.3	103	90.8
Case 2	172.4	164.1	91
Case 3	153.7	136.5	87
Case 4	145.9	137.2	84

the tower of Case 3 when the rise time of the excitation ramp current is 1 ns. The reflections observed in the waveshape show a negative reflection coefficient from the end of the cross arms [78]. The travel time of the upper cross arm, considering a propagation speed equal to the speed of light is 38.67 ns, which is in agreement with the reflections observed in this figure. However, such reflections will have no considerable effect in the case of currents with higher rise times. This shows that the extent of which each tower element affects the tower surge impedance depends on the excitation waveshape. The tower in Cases 3 and 4 have almost a similar surge impedance for all waveshapes. This can be justified by considering

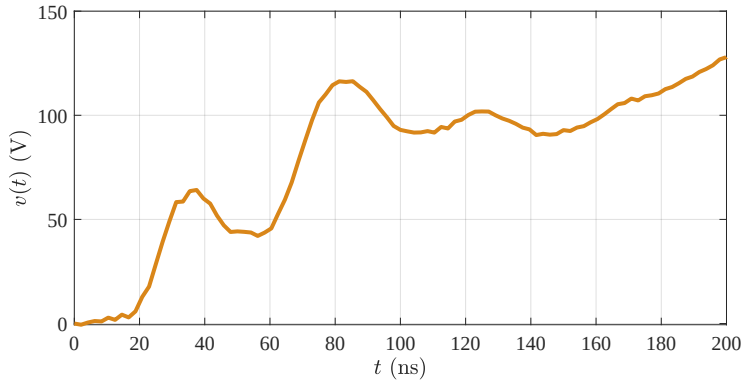

Fig. 4.5: Negative reflections from the end of tower cross arms when a fast rising current is applied to the tower top in case 3.

the opposing effects that adding the shield wire cross arms and tower bracings have on the impedance of the tower [134]. In all four cases, the apparent travel speed is lower than 91% of the speed of the light due to the presence of different tower elements that increase the propagation path of the waves.

4.3 Comparison of Theoretical and Simulation Results

In this section, to assess the accuracy of different tower models on the prediction of tower top voltage, they are compared with the numerical results for the case of the vertical cylinders with heights of 15, 45, and 90 m. They are also compared with the numerical results for the case of the double circuit tower over a lossy ground.

4.3.1 Vertical Cylinders

Figures 4.6a and 4.6b show the voltage at the top of the cylinder for the case of a vertical cylinder with a height of 15 m on a PEC ground when injected with currents with rise times of $t_r = 80$ and $t_r = 10$ ns, respectively. This figure presents a comparison of 11 of existing models with that obtained using NEC4. The predicted waveform of the theoretical solutions is closer to that obtained by NEC4 when the rise time of the injected current is 80 ns (see Fig. 4.6a). Whereas, in the case of a rise time of 10 ns, the calculated waveshapes using the theoretical models are step-like and are different from the simulated voltage in NEC4, which shows a slower rise-time and decay. This is due to the fact that the early-time electromagnetic fields around the cylinder is different from TEM but the theoretical models assume the electromagnetic fields are always TEM.

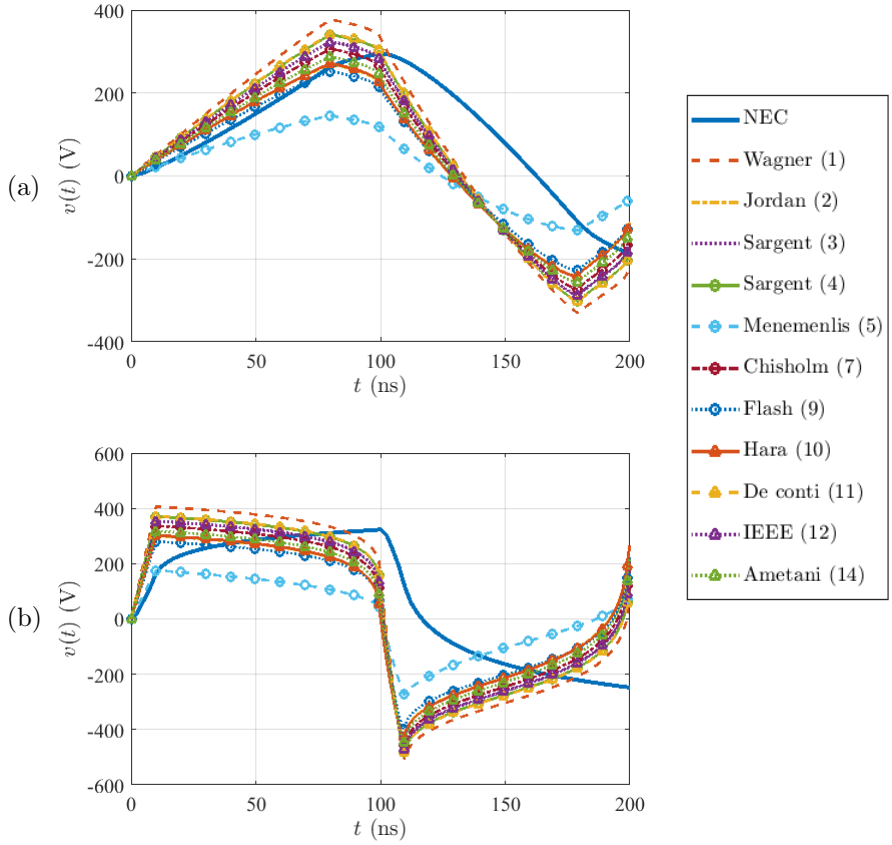

Fig. 4.6: The voltage at the top of a 15-m cylinder obtained by numerical analysis and also with the 4 most accurate ones between the models of Tables 2.1 and 2.2. The excitation is a ramp current with a rise time of (a) $t_r = 80$ ns and (b) $t_r = 10$ ns.

4.3.2 Double Circuit Tower

Figure 4.7a shows the voltage at the top of the double circuit tower obtained using NEC and theoretical approaches 4 and 7 from Table 2.1 and 14 and 17 from Table 2.2, for which we used the method of characteristics of partial differential equations theory [152] (Sec. 7). A rise time of $t_r = 150$ ns is considered such that the rise time is less than the travel time. In the theoretical approaches, the wave propagation speed is assumed to be the speed of light,

however, in the numerical result shown in Fig. 4.7a, the apparent wave speed is equal to 87% of the speed of light. This is in agreement with measurements which suggest 80% [72], 71%, 76%, 81% and 89% of the speed of the light [144]. This justifies why the zero crossing of the NEC result is at a later time in comparison to the theoretical results. The multiconductor model of Ametani [95] and the model of Hara & Yamamoto [85] show the closest values of the surge impedance (relative difference of 5.3% and 6.8%).

Now, let's consider the complete model of the double-circuit tower with all its details with the same current injected to the top of the tower. The multistory models of Table 2.3 are compared with the numerical analysis in Fig. 4.7b. Regarding the voltage peak, the closest predicted values are by the models of Yamada [89] (error of 2.8%) and Motoyama (error of 8.4%) [90]. Considering the waveshape of the voltage, the models of Yamada and Motoyama are closer than the others ones to the one predicted by NEC. However, the model of Hashimoto [93] shows a closer decaying part than the other models. As stated in [93], this is due to the modification in the derivation of this model in order to reproduce the gradual decay of the measured voltages. All of the multistory models of Table 2.3 require "tuning" based on measured waveforms from a specific tower structure, whereas our approach based on numerical simulation solely requires the geometrical information of the tower. For example, the model of Ishii which has a large overestimation of the voltage, was derived for Japanese 500 kV [88] and UHV towers [89] that are taller (62.8 and 140.5 m) than the typical double circuit towers like the one considered in this chapter (45.1 m). The results shown in this section, demonstrate the multistory models of Table 2.3 have limited applicability.

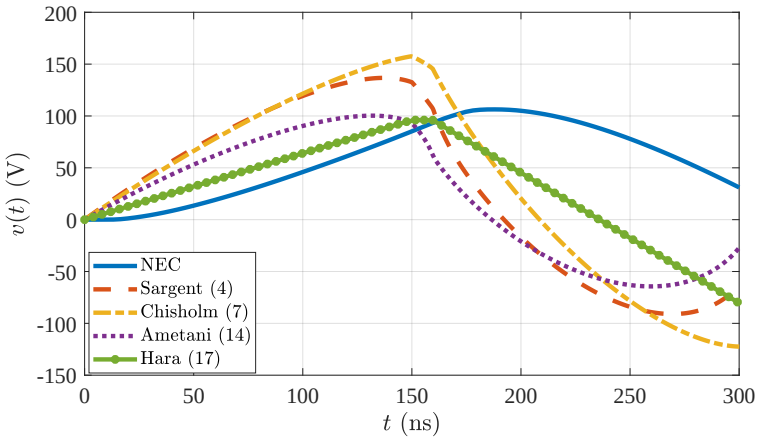

(a)

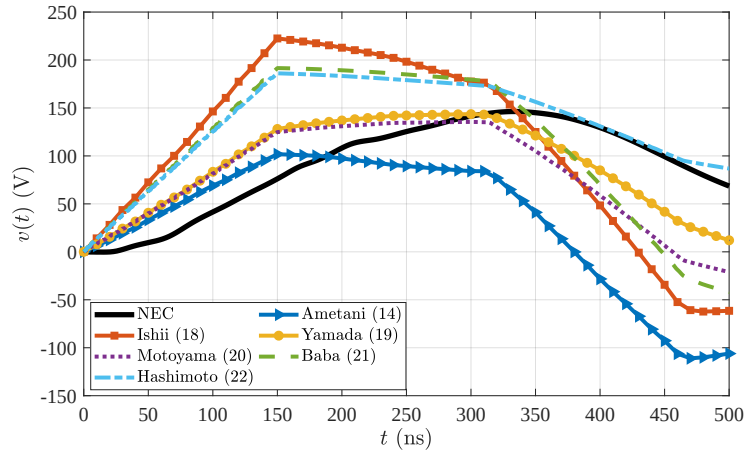

(b)

Fig. 4.7: The voltage at the top of the structure of Case 1 (a) and Case 4 (b) in response to a ramp excitation of rise time $t_r = 150$ ns.

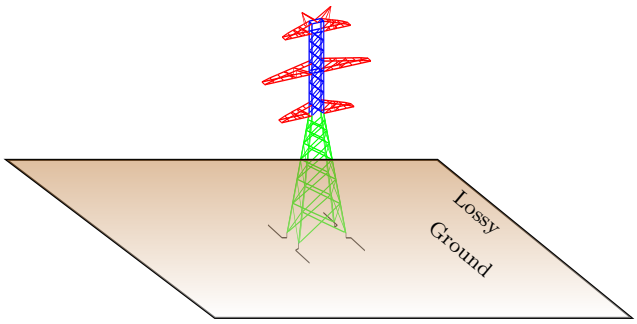

Fig. 4.8: The wire diagram of the double circuit tower generated by an automated procedure to be used in numerical simulations by NEC4. Sections of the tower, identified by different colors, and counterpoise grounding electrodes buried in lossy ground are shown.

4.4 Effect of Grounding System

In the previous sections and most previous studies (*e.g.* [78,85,92]), the ground was assumed to be a Perfect Electric Conductor (PEC). However, in reality the conductivity of ground is finite. In this section, we consider a lossy ground where counterpoise grounding electrodes, 1, 2, 5, 10 and 20 m in length, are considered as the grounding system of the tower (see Fig. 4.8). The burial depth of the electrode is assumed to be 1 m with an optimized opening angle of the electrodes of 45° [138]. Two soil resisitivities of 100 and 1000 Ωm are considered. The grounding system is a vertical electrode with a short length and then extends horizontally. The vertical part should be defined symmetrically with respect to ground in NEC4. Fig. 4.9a shows the simulated and theoretical voltage at the top of the tower when counterpoise grounding electrodes of 20 m in length buried in soil with a resistivity of 100 Ωm are considered. To obtain the response of theoretical tower models, first an electromagnetic simulation is performed on counterpoise grounding electrodes using the model presented in [31], to obtain their low frequency resistance. The obtained values agree well to the analytical formula provided in IEEE Std. 1243 [79]. This resistance is added to

the tower models and the simulation is performed in PSCAD/EMTDC. The injected current is a 2/50 μs double exponential with a peak of 1 A, and a shunt internal resistance of 5 kΩ [153] is considered to have the same condition as the numerical simulation. The most noticeable difference between an ideal and lossy ground is the difference in the peak of the voltages predicetd by theories that is less in the case of a lossy ground but still considerable. Considering the NEC results as the reference, the models of Baba [135] and Yamada [89] produce the closest results considering both the peak of the voltage and its waveshape. The difference in the peak of the voltage is 2.5% and 5.6%, respectively. Assuming a soil resisitivity of 1000 Ωm, the same tower models as above generate the closest results to those generated by NEC (see Fig. 4.9b). However, the difference (9.41% for Baba [135] and 20.45% for Yamada [89]) is higher as the resistivity of the soil is increased. In general, the theoretical tower models are a fast way to have an estimation of the developed over-voltages on a transmission tower, but they are not accurate for all tower models and the value of circuit elements need to be tuned for every topology of the tower using field measurements. Furthermore, the effect of excitation waveshape on the accuracy of predicted overvoltages is another challenge for the theoretical tower models.

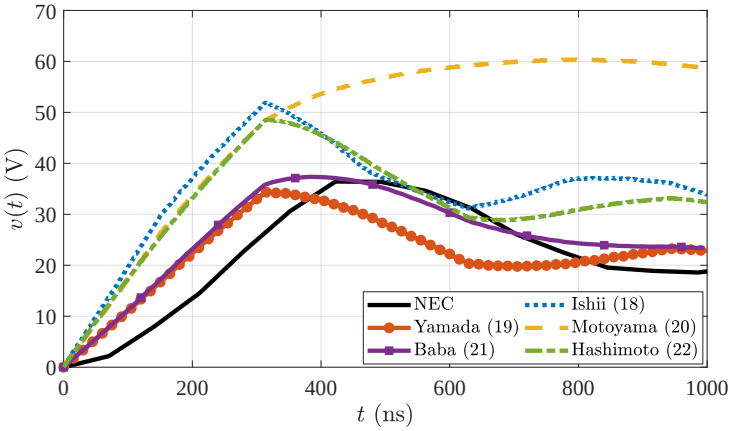

(a)

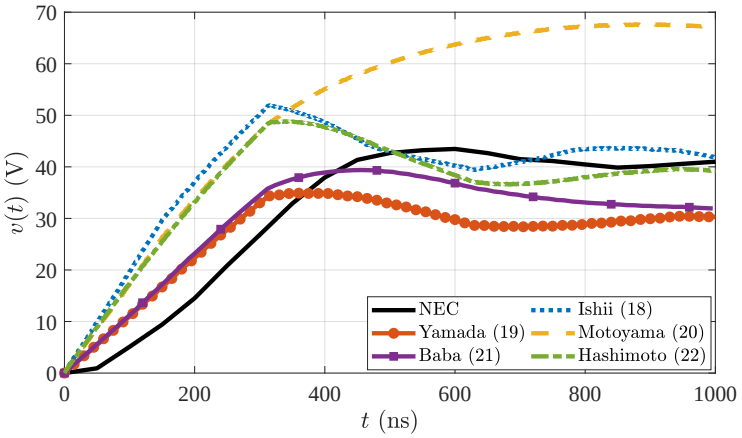

(b)

Fig. 4.9: The simulated and theoretical voltage at the top of the double circuit tower considering counterpoise grounding electrodes (20 m) in a soil with resistivity of (a) $\rho = 100\ \Omega$/m and (b) $\rho = 1000\ \Omega$/m and in response to double exponential current of $2/50\ \mu$s with a magnitude of 1 A.

4.5 Summary

In this section, a detailed wire-model of a typical 400 kV double-circuit tower with a height of 45.1 m was generated using an automated process that employs the CAD drawing of the tower. The wire model was then used in NEC4 to calculate the transient tower top-voltage considering the finite conductivity of the ground and grounding electrodes. It was shown that the definition of tower surge impedance based on time domain voltage and current has a main disadvantage of being dependent on the excitation waveshape and rise time. Following a review of existing transmission tower models, they were compared with the results of NEC4 for the case of a simple cylinder and the 400 kV double-circuit tower. Regarding the peak of the tower top voltage, the theoretical models could provide close predictions to that of NEC4. Considering the voltage waveshape, theoretical models were not able to generate results close to those determined by NEC4 in the case of fast-front currents, because the initial electromagnetic field around the cylinder is not TEM. In the case of the double-circuit tower on a PEC ground, the models of Yamada [89] (difference of -2.8%) and Motoyama [90] (difference of -8.4%) had the closest similarity to NEC4 results with regards to the calculated voltage peak.

The proposed model based on NEC is capable of considering the effect of the finite conductivity of the ground. In order to compare this model for the case of a lossy ground, a grounding resistance was added to the theoretical models. The models of Baba [135] (difference of $+2.5\%$) and Yamada [89] (difference of -5.6%) provide closer peak values to that of NEC4, although the error can not be considered as negligible (when $\rho = 1000\ \Omega m$, the error is -9.41 and -20.45%, respectively). The previous models of transmission towers were derived based on either electromagnetic field analysis on a simplified model of the tower (approximated by a cone or cylinder), or by a trial-and-error process to find the

resistance and inductance values of the circuit such that they produce similar waveforms as the measurements. The multistory tower models may be able to provide accurate results if the circuit values are tuned, but the process of such tunning is not well established. This chapter demonstrated that such models cannot provide accurate resutls in the case of a typical double-circuit tower that they have not been tuned for. The proposed process in this thesis has the advantage of needing only the geometry of the tower and it can be further applied to any other type of transmission towers.

Chapter 5
Black-Box Model of Tower

5.1 Introduction and Background

Direct lightning strikes to transmission towers are one of the main cause of outages in high voltage transmission lines. Three mechanisms are responsible for such outages, namely, i) flashover, ii) midspan-flashover, and iii) backflashover (BF) [3]. Flashovers occur when lightning strikes the overhead conductors, due to either the absence of shield wires or a shielding failure. Installation of properly-located overhead ground wires (OHGW) above the phase conductors reduce the risk of flashovers [79]. For transmission lines with very long spans, such that the negative reflection from adjacent towers arrive after the voltage has reached its peak, the lightning strikes to ground wires might produce a high voltage difference between the ground wire and the nearest phase conductor, leading to the so-called midspan-flashover. However, midspan flashovers do not occur frequently as they can be mitigated by reducing the sag of shield wires and increasing the distance between the shield and phase wires at the midspan [3]. The backflashover, which is the prevailing mechanism leading to outages in high voltage transmission lines, is caused when the lightning strikes

the top of the tower or the shield wires near the tower [154]. In this case, the flow of the lightning current through the tower and the grounding system may result in a voltage rise of the tower and increasing the voltage difference across the strings of insulators. The backflashover occurs if the induced overvoltage across the string of insulators result in a breakdown.

Two widely-accepted methodologies, documented in IEEE standard 1243 [79] and CIGRÈ Technical Brochure 63 [84], are commonly used in electromagnetic transient (EMT)-type simulators to calculate the developed transient voltage across a string of insulators and determine the backflashover rate (BFR) of transmission lines. There are several simplifications adopted in the derivation of such theoretical approaches, which highly affect their accuracy, leading to an inaccurate predication of BFR [155]. In these methodologies, the transmission tower is represented by the simplified model of Sargent [72] and Chisholm [78] in IEEE and CIGRÈ documents, respectively. However, such representation has been shown to have a considerable error in the calculation of the developed transient voltages [156]. One other simplification used in these methodologies is the representation of the grounding system by a resistance equal to the low frequency value of the grounding impedance that does not represent the frequency response of an actual grounding system [31].

In this section, a black-box model for the prediction of BFR is developed by simulating a detailed representation of a tower and its grounding system based on the numerical solution of full-wave Maxwell's equations in the frequency domain using the Finite Element Method (FEM). The system is modeled as a seven-port network, with an input port at the tower top (lightning strike point), and six other ports whose current represents the current of the string of insulators. Once a transfer function relating the output ports to the input port is determined using the numerical simulation, Vector Fitting [97] is employed to obtain the

state-space form of the system as a multiport network in the form of a black-box. The state-space form of the multiport network is interfaced with an electromagnetic transient simulator (PSCAD-EMTDC in this section) using Norton equivalent circuit and convolution operator [99]. The meaning of black-box representation of the tower in here means that the time-domain implementation is in the way that the end-user of EMT-type simulators has no access to the electrical details of what is inside the box (tower).ˆa The proposed model enables the incorporation of the frequency dependence of soil electrical parameters that is known to have a considerable effect on the transient behavior of the grounding system [31] and the high frequency response of the power system [157]. Using the proposed electromagnetic model allows one to consider the coupling between different elements of the system and also the propagation effects with no approximation.

To demonstrate the applicability of the proposed model, the physical geometry of a typical 400-kV double-circuit tower is considered taking all its details into account. Two OHGWs, six overhead conductors, and the grounding system of the tower consisting of counterpoise electrodes of different lengths buried in lossy ground are considered as shown in Fig. 5.1a. The overhead line is terminated by a matching network on both sides to avoid reflections (see Fig. 5.1b). Simulations are performed in the frequency range of 10 kHz to 10 MHz considering the frequency dependence of soil electrical parameters using the causal model of Alipio and Visacro [158]. A low-frequency soil relative permittivity of $\varepsilon_r = 10$, and resistivity of $\rho = 100$, $1,000$, and $5,000$ Ωm are considered. The frequency-domain transfer functions are then calculated numerically and used to model the tower as a black-box for time-domain simulations. To assess the occurrence of a BF across the string of insulators, the existing models that correlate the time-domain overvoltage and time-to-flashover can be employed that include the volt-time curve method [159–165], the disruptive effect (DE)

model [166–174], and the leader progration (LP) model [84, 175–178]. Here, a backflashover analysis is performed using the first lightning strokes measured at two different stations, namely, Morro do Cachimbo [68] and Monte San Salvatore [179], and employing the DE and LP methods.

The outcome of this section is a model for the double-circuit tower in EMT-type simulators, where the end user of the model doesn't need to use any electromagnetic field solver. The voltage across insulator strings can be obtained when different currents are injected in to the tower top under different soil conditions, and the optimum length of the counterpoise electrodes can be determined to ensure a desired outage rate.

5.2 Transmission Tower Full-Wave Model

To assess the transient response of a transmission tower in the event of a lightning strike to the tower top, a rigorous full-wave electromagnetic model is proposed. Let us assume that the permittivity, conductivity, and permeability of the medium (*i.e.* air, soil, and metal in this case) are ε, σ, and μ, respectively. Using Finite Element Method (FEM), the wave equation given by 3.12a is solved numerically in the frequency domain [118]. A typical 400 kV double-circuit tower made of steel and with a height of $h = 45.1$ m is considered here as shown in Fig. 5.1. The specifications of the two OHGWs and the phase conductors are provided in Table 5.1 [180]. The eight conductors are grounded at 100 m away from the tower through a matching network to avoid reflections from both ends of the line [181]. The lightning channel is represented by a vertical perfectly conducting wire attached to the top of the tower through a port (representing a voltage source with magnitude of 1 V) with an internal impedance of 500 Ω. Considering the surge impedance of the connecting wire ($60 \ln 2h/r = 518.8\Omega$),

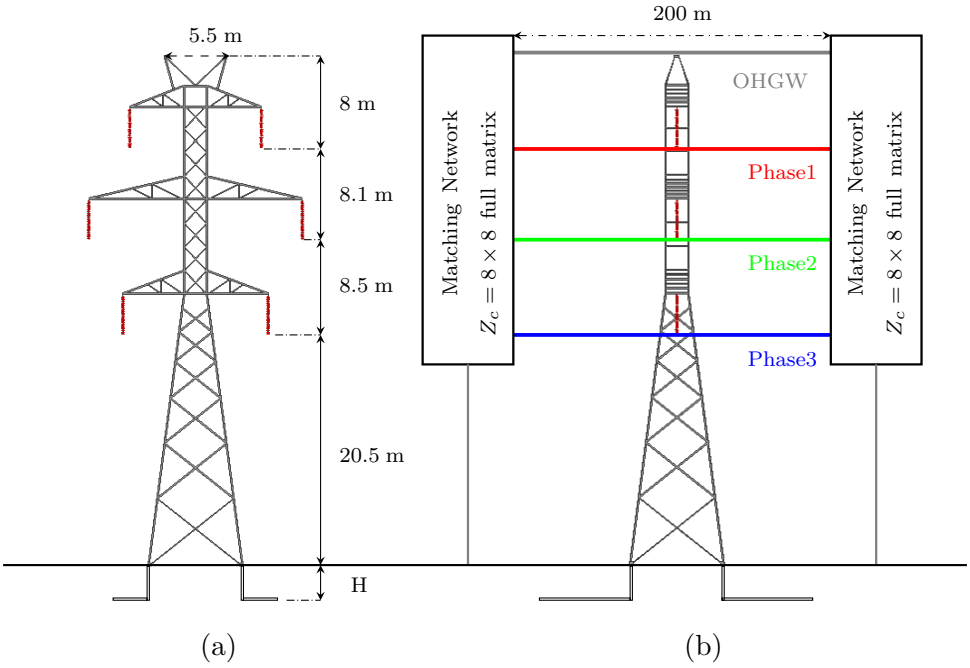

Fig. 5.1: Geometry of the 400 kV double circuit tower considered in the simulations, (a) front view, and (b) side view showing the shield wires, overhead phase conductors and the terminating network.

Table 5.1: The characteristics of shield wires and conductors.

	Type	Diameter (mm)	DC Resistance in 20° (Ω/km)
Phase conductors	CURLEW	31.63	0.05501
Shield wires	94S	12.6	0.642

the input impedance of the channel Z_{ch} seen by the tower is 1018 Ω, which is in the range of measured lightning channel impedance on instrumented towers [182–187]. Furthermore, Datsios *et al.* has shown that higher values of channel impedance have a negligible effect on the calculated BFR [188].

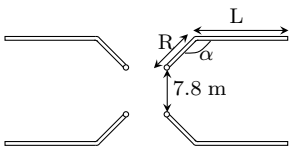

Fig. 5.2: The grounding system consisted of counterpoise electrodes considered in the simulations. The adjacent tower legs are 7.8 m apart, R is the opening length, α opening angle, and L is the length of electrodes.

A grounding system consisting of counterpoise electrodes are considered as shown in Fig. 5.2. The burial depth and the length of electrodes are represented by H, and L, respectively. The opening angle is α and the opening length is R. To consider the frequency dependency of soil electrical parameters in the simulations, according to the recommendation of CIGRÈ [157], the causal model of Alipio and Visacro [158] is employed here that are given by

$$\rho(f) = \rho_0 \left[1 + 4.7 \times 10^{-6} \times \rho_0^{0.73} \times f^{0.54}\right]^{-1} \tag{5.1a}$$

$$\varepsilon_r(f) = 9.5 \times 10^4 \times \rho_0^{-0.27} \times f^{-0.46} + 12. \tag{5.1b}$$

In order to perform simulations using FEM, the simulation space has to be truncated. Uniaxial Perfectly Matched Layer (UPML) is used as the absorbing boundary condition that prevent the reflection of the electromagnetic waves from the truncation boundary [189]. The UPML will be a fictitious anisotropic material, causing zero reflection regardless of frequency and the angle of incidence [189]. The amount of memory required for simulations can reach up to 1 TB, because of the level of details considered.

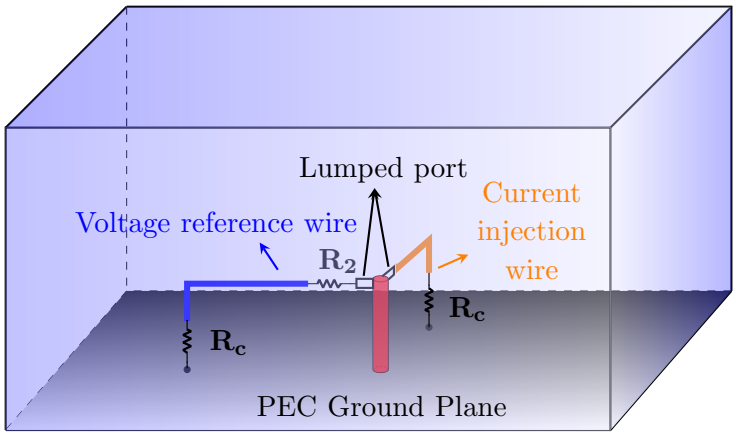

Fig. 5.3: Implementation of the Setup for the measurement of voltage and current at the top of a verical cylinder for FEM analysis. This configuration is the measurement setup used by Hara *et al.* in [96].

5.3 Verification of the Numerical Simulation Model

The accuracy of the proposed simulation model is verified employing the measurements performed by Hara *et al.* [96] on cylinders of different heights and radii. In the measurements, the cylinders are placed on an iron plate. The current is injected into the top of the vertical cylinders using a horizontal wire and a pulse generator with an interal resistance of 5 kΩ. A voltage probe is inserted between the top of the cylinder and a horizontal voltage reference wire to measure the voltage in reference to remote ground. Both the wires are grounded by a matching resistance (R_c) to avoid reflections.

The measurement of [96] is simulated using the proposed model where a 3-m high cylinder with a radius of 2.5 mm is located on a Perfect Electric Conductor (PEC) ground (see Fig. 5.3). A port with an internal resistance of $R_1 = 5$ kΩ is inserted between the top of the cylinder and the current injection wire, which applies a voltage difference of 1 V. The injected current is then equal to the admittance seen by this port in the frequency domain. To

measure the voltage, a second port is used in series with a resistance of $R_2 = 10$ kΩ between the top of the cylinder and the voltage reference wire. The second port has no voltage difference between its ends and it is only used to calculate the current passing through R_2. If the mutual addmitance between these two ports is equal to Y_{21}, the voltage across R_2 is equal to $R_2 Y_{21}$. The simulation is performed in the frequency range of 100 kHz to 400 MHz, and PML is used at the boundaries to simulate open air. A distance of λ, equal to the wavelength at the lowest frequency of interest, is considered between the PML interface and the cylinder [190]. Once the frequency-domain voltage and current at the top of the cylinder are determined, inverse Fourier transform is used to obtain time-domain values. Figure 5.4 shows the measured voltage at the top of the electrode, adopted from [96], and the measured and simulated currents. Both the waveshape and magnitude of the simulated current are reasonably similar to the measured one. The reflection from the ground at $t = 20$ ns is also observed in both of the current waveforms. This verification is used to determine the optimum value of different parameters affecting the accuracy of the simulation, such as the distance that should be considered for placing the PML material away from the radiating object (vertical cylinder).

5.4 Crossarm String of Insulators

To incorporate the string of insulators in the simulation, each string of insulators is implemented as a lumped capacitance. This reduces the required memory and simulation time significantly. The geometry of cap-and-pin insulator string of standard disks (254 mm $\times$ 146 mm) [79] is generated considering all its details as shown in Fig. 5.5a. One of the parameters of great importance in the design of each disk is the leakage distance (L) (see

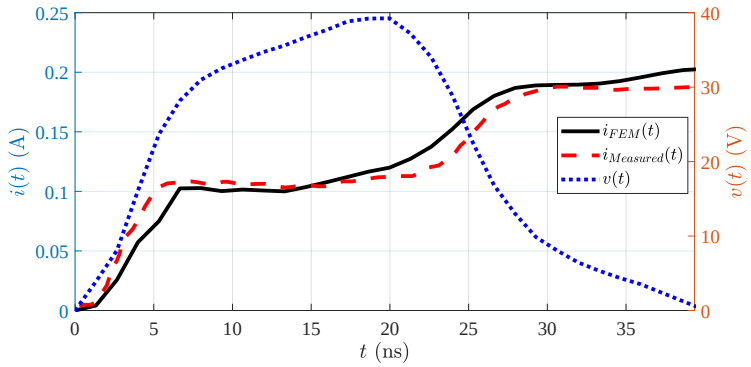

Fig. 5.4: Voltage at the top of the cylinder in reference to remote ground (right axis) and measured and simulated current (left axis) injected at the top of a 3-m cylinder on a PEC ground.

Fig. 5.5a). The reason is that the fast flashovers tend to hug the leakage distance instead of going through the dry-arc distance (M) (see Fig. 5.5b) [173]. In the insulator string considered here, $L = 326$ mm. The number of disks in an insulator string depends on several factors, such as the nominal voltage of the system, the leakage distance of each disk and the pollution level. According to the IEC 60815 standard [191], and assuming a medium pollution level, a minimum nominal specific creepage distance of 20 mm/kV is employed. For the 400 kV system considered here, it requires 24 disks in each string of insulators, which is in agreement with the typical line insulation provided by IEEE [79]. Next, an electrostatic analysis is performed to obtain the equivalent capacitance of the string of 24 insulators. Using an electrostatic analysis, an equivalent capacitance of 1.26 pF is obtained per string. This is a more realistic representation of the string of insulators as compared to modeling it as a resistance (*e.g.* 100 kΩ resistance in [134]). The value of the equivalent capacitance is assigned to a sheet of a height equal to the length of the string of 24 insulators (3.51 m), inserted between each crossarm and the corresponding phase conductor. The voltage across

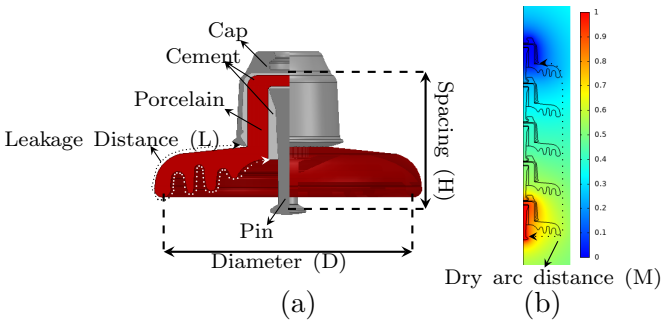

Fig. 5.5: (a) Geometry of a cap-and-pin insulator, (b) static distribution of electric potential (V) around a string of insulators, where 0 and 1 V are applied to the first cap and last pin, respectively. (For the sake of demonstration, a string of 5 disks is shown here. In the actual simulations, a string of 24 insulators has been considered.)

the insulator string is obtained by defining a port of small electrical size ($0.01\lambda_{min}$) in series with the lumped capacitor, and calculating the current going through the port in the frequency range of interest. This size of the port ensures that there would be no problem associated with the definition of voltage at high frequencies between distant terminals [69].

5.5 Assessment of Insulator Flashover

There are two different measures which specify the lightning impulse strength of high voltage insulators, namely, the critical flashover voltage (CFO) [79], and the basic insulation level (BIL) [192]. The CFO and the BIL are the peak value of a standard impulse wave for which the insulation structure exhibits a 50% and 10% probability of failure, respectively [192]. For the 400 kV system considered here, the BIL and the CFO are equal to 1425 kV [192] and 1568 kV [174], respectively. Such a value of CFO is in the range of previous measured values (1638 and 1726 kV), performed on 400 kV insulator strings [193].

When an string of insulators is subjected to overvoltages, the probability of the oc-

currence of a backflashover can be assessed using different approaches, such as the volt-time curve method [159–165], the disruptive effect (DE) model (also called the integration method) [166–174], and the leader progration (LP) model [84, 175–178]. This section briefly introduces each approach to assess the BF performance of a string of insulators.

5.5.1 Volt-Time Curve

The voltage-time curve relates the peak value of the applied voltage across the insulator to the time to flashover (t_b) [84]. These curves are obtained by performaing measurements on different type of gaps (rod-rod or rod-plane) or insulator strings. The volt-time characteristic adopted here is described as [174]

$$V_{\mathrm{FO}}(t_b) = (0.58 + \frac{1.39}{t_b^{0.5}}) \times \mathrm{CFO} \tag{5.2}$$

where V_{FO} is the flashover strength in kV, t is the time to flashover in μs, and CFO is the critical flashover voltage of the system in kV. However, there are disadvantages associated with such an approach [79]. Firstly, the volt-time curves have been derived based on measurements employing the 1.2/50 μs standard lightning impulse voltage, therefore, they are only valid for standard lightning-impulse waveshapes [79]. Secondly, the volt-time curve relates voltage and time values that do not refer to the same time instant that introduces further inaccuracies. As such, the volt-time curve method is not used for the BF assessment.

5.5.2 Disruptive Effect (DE) Method

The disruptive effect (DE) model, which is also called the integration method, was first proposed by Witzke and Bliss [168, 169]. The integration method was derived based on

Table 5.2: Values of the integration method parameters to be used in (5.3).

Model	n	V_0 (kV)	DE_b (kV$^n\mu$s)
Caldwell [165]	1	0.86CFO	$1.29\mathrm{CFO}^{1}$
IEEE [171]	2.5	0.48CFO	$1.62\mathrm{CFO}^{2.5}$
Hileman [174]	1.36	0.77CFO	$1.15\mathrm{CFO}^{1.36}$

measurements under standard lightning impulse, however, it can be used to assess the performance of gaseous, liquid or solid insulation under non-standard fast-front overvoltages as well [79]. In contrast to the volt-time curve approach, the integration method takes into account the effect of the waveform of the overvoltages in the whole time range, and not only the peak value. In this method, it is assumed that there is a minimum voltage V_0, which must be exceeded before any breakdown process can start. The time to breakdown t_b depends on both the magnitude and duration of the applied voltage above V_0. Determination of the dielectric strength of the insulation requires the calculation of the disruptive effect constant given by [79]

$$D = \int_{t_0}^{t_b} (V(t) - V_0)^n \, dt \tag{5.3}$$

where t_0 is the time after which the voltage $V(t)$ exceeds the minimum required voltage V_0 and n is a constant. The disruptive effect constant, D, must be greater than a value called base disruptive effect (DE_b) in order for any flashover to occur. There has been several justification for the accuracy of the integration method for the prediction of the insulator behavior under non-standard lightning impulse waveforms [165–167, 194]. Values for V_0, n, and DE_b are proposed in the literature [165–174]. In this section, the values suggested by Caldwell [165], IEEE [171], and Hileman [174] are used as given in Table 5.2.

5.5.3 Leader Progression (LP) Model

This model is derived based on the physical process of the breakdown, consisting of three phases: corona inception, streamer propagation, and leader progression [84]. The time to flashover t_b is the sum of the time of these three processes. Based on measurements on different gap configurations (rod-rod or rod-plane), a time-domain equation is developed for the leader progression velocity in the air gap as a function of the applied electric field (voltage). Table 5.3 contains the corresponding leader progression velocity expressions for negative flashover based on the models of CIGRÈ [84], Shindo [175], and Pigini [176]. In each time step ($t = t_0$), the leader velocity (v) is obtained, knowing the applied voltage (V) at that time. Leader length (x) at the next time step ($t = t_0 + \Delta t$) is calculated as follows:

$$x(t_0 + \Delta t) = x(t_0) + v\Delta t. \tag{5.4}$$

Following this iterative procedure, the time to breakdown, which is the time required for the leader to cross the air gap length, is obtained [175]. Figure 5.6 shows the volt-time curve of the 400 kV insulator string with a length of 3.51 m calculated based on the models of Tabs. 5.2 and 5.3. There is a noticeable difference between the volt-time curves obtained by these approaches, and the effect will be discussed on the prediction of BFR later.

5.6 Results and Discussion

In this section, numerical simulations are performed using the proposed model in the range of 10 kHz to 10 MHz. Grounding electrodes of different lengths, $L = 2, 5, 10, 15, 25, 40$ m, are considered. The other parameters of the electrodes are $H = 1$ m, $R = 1$ m, and the

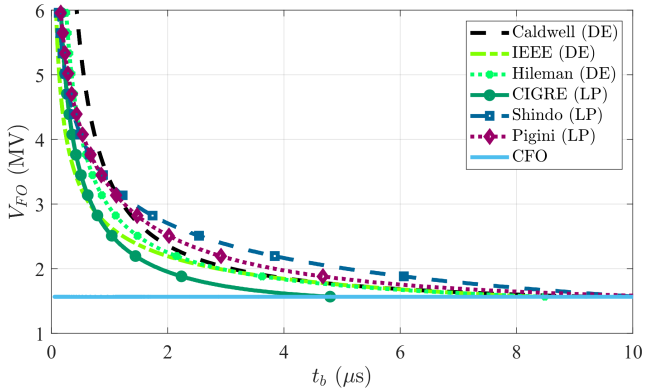

Fig. 5.6: Volt-time curves of 400 kV transmission line insulator string with a length of 3.51 m. Disruptive effect and leader progression models are shown with (DE) and (LP), respectively.

Table 5.3: The expression for the leader velocity in LP breakdown models.

Model	Leader velocity
CIGRÈ	$v = 1.3V(V/(D-x) - 600)$ Flashover condition: $x \geq D$
Shindo	$v = 0.05V^2/(D-2x) + 25 \times 10^{-10}V^2vx/(D(D-2x))$ Flashover condition: $2x \geq D$
Pigini	$v = 170D(V/(D-x) - 560)\exp(1.5 \times 10^{-3}V/D)$ Flashover condition: $x \geq D$

radius of the electrodes is 20 mm (see Fig. 5.2). An opening angle of $\alpha = 45°$ is adopted as an optimized value [195]. A low-frequency soil relative permittivity of $\varepsilon_r = 10$ and three values of low-frequency soil resistivity (100, 1,000, and 5,000 Ω m) are considered. Once the frequency domain transfer functions relating the current of the input port (at the tower top) to the current going through the insulator strings are obtained, the procedure described in [99] is used to interface the transmission tower black-box model to a time-domain simulator (PSCAD-EMTDC in this section). This procedure consists of fitting the frequency-domain transfer functions with rational function approximations, and then deriving a state-space

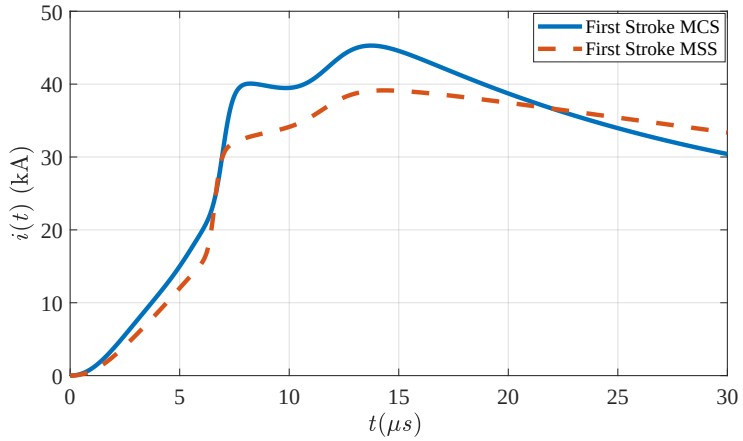

Fig. 5.7: Representation of double-peaked first lightning strokes corresponding to the median current peak measured at Morro do Cachimbo [68] and Monte San Salvatore [179] stations.

form for the system. The input currents are the typical double-peaked first lightning strokes measured at Morro do Cachimbo [68] ("MCS") and Monte San Salvatore [179] ("MSS") stations, which are synthesised using a sum of Heidler functions as described in [196] and shown in Fig. 5.7. The string of insulators is represented by a 1.26 pF capacitor. Figure 5.8 shows the voltage across the upper insulator string when the injected current at the tower top is the median current measured at the MCS station, and for different lengths of counterpoise grounding electrodes buried in soil with resistivity of 100, 1,000, and 5,000 Ωm, respectively. Regarding the waveshape of the voltage induced across the insulator string, one can see that it is closer to the waveshape of the lightning current in the case of higher soil resistivity (*i.e.* 5,000 Ωm). As the length of counterpoise electrode increases, the induced voltage tends to decrease, which shows the importance of grounding system in diminishing the overvoltages due to lightning strikes to transmission towers. However, the rate of such reduction is less for higher lengths of electrodes, and even insignificant if the so-called *effective length* of

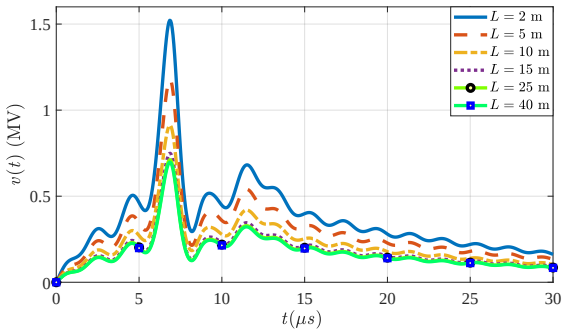

(a)

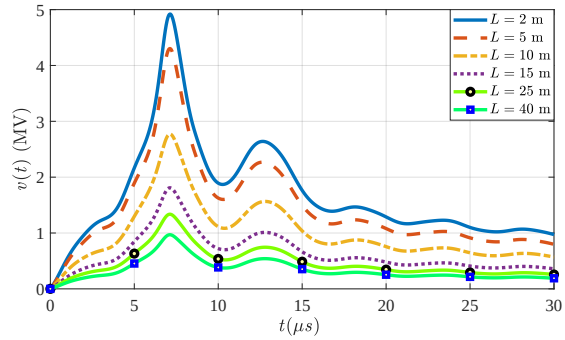

(b)

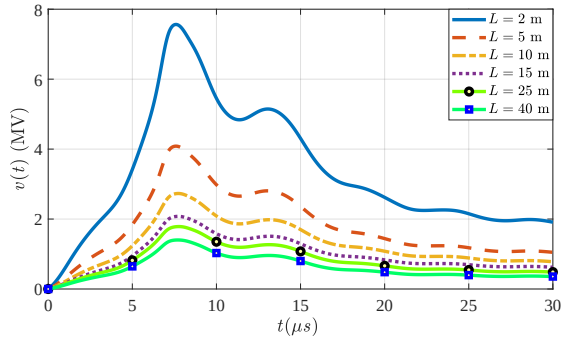

(c)

Fig. 5.8: Simulated voltages across the top insulator string in the 400 kV double circuit tower as a function of the length of counterpoise grounding electrodes. The input current is the median current measured at MCS station, and the soil resistivity is (a) 100, (b) $1,000$, and (c) $5,000$ Ωm.

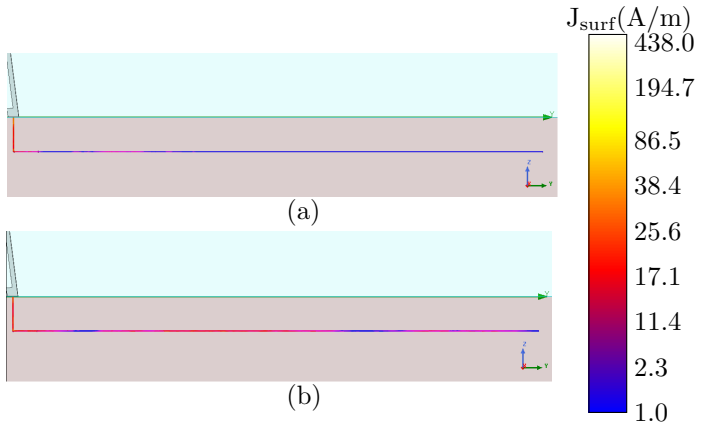

Fig. 5.9: Magnitude of the current density on the surface of a 15-m conuterpoise grounding electrode at frequency of 5.5 MHz and in soil with a low-frequency resistivity of (a) 100, and (b) $5,000$ Ωm. The magnitude of the applied voltage at the tower top is 10 kV.

counterpoise electrodes is reached [139, 197]. To illustrate the electrode's effective length, Fig. 5.9 shows the current density on the surface of a 15-m counterpoise electrode attached to a tower leg and buried in soil with resistivity of 100 Ωm (Fig. 5.9a) and $5,000$ Ωm (Fig. 5.9b). The applied voltage at the tower top has a magnitude of 10 kV with a frequency of 5.5 MHz. One can see that only a small portion (around one third) of the length of the electrode is responsible for dissipating most of the current through the soil of lower resistivity (*i. e.* 100 Ωm). However, in a soil resistivity of $5,000$ Ωm, there is a considerable current density on the surface of the electrode at its end.

5.6.1 Backflashover Assessment

Once the time-domain voltages are obtained, the occurrence of a backflashover across the insulator string is assessed by applying the DE and LP methods described in Sec. 5.5, considering both the currents of MCS and MSS stations. The correlation between the peak

of the lightning current and its front time is disregarded [198], and the current is increased up to a level that causes flashover of the insulator string of the overhead line based on each model. Tables 5.4 and 5.5 show the minimum critical current (I_c) causing insulator flashover, considering counterpoise grounding electrodes of length 5 and 40 m, respectively. Furthermore, using a probabilistic evaluation [129] based on the measured distribution of negative downward first strokes in the two locations, the percentage of the lightning currents expected to exceed the critical current in amplitude are calculated and shown in these tables. It can be seen that the value of the critical current varies significantly among the flashover models. Such differences are of major importance in insulation coordination studies. In general, the leader development models predict much higher values of the critical current as compared to DE models. This can be due to the fact that in LP models, the electric field strength, E_0, required for the leader onset decreases as the length of the insulator string increases. Another source of difference is that the applicability of LP models to overhead transmission line insulator strings has some limitations. The model of Pigini has been derived based on measurements on air gaps [176]. Also, the model of Shindo refers to rod-rod air gaps shorter than 3 m [175]. On the other, the predictions provided by the DE models, that are based on measurements on string of insulators, in Tables 5.4 and 5.5 can be considered more reliable. According to these tables, the model of IEEE predicts the least critical current in all the considered cases, while the model of Shindo leads to the highest values of the critical current.

The probability of occurrence of a BF is dependent on the region where the transmission line is located. The critical current is higher at MCS than at MSS if all other conditions, such as the soil resistivity and length of grounding electrodes are identical. This difference is higher when the soil resistivity increases. Since the MCS station is located in Brazil, which

is a tropical region, there is an intense average lightning activity (keraunic level) [84]. The higher number of lightning strikes per unit time per unit area and also the higher portion of lightning currents leading to a BF leads to a considerably higher BFR at MCS station than at MSS station.

Employing 5-m long counterpoise electrodes is shown to be very inefficient in all soil resistivities at both stations, even for soil with a resistivity as low as 100 Ωm. Increasing the length of the grounding electrode to 40 m results in a considerable decrease in the probability of occurrence of a BF in a soil of low resistivity (*i. e.* 100 Ωm). This probability is less than 8% according to the flashover models (except the model of IEEE), concluding that 40 m counterpoise electrodes are suitable for reliable performance of the line in a soil resistivity of 100 Ωm. However, in higher soil resistivities, even such length of electrode cannot provide the needed low grounding impedance and the probability of a BF is more than 10%. Using longer counterpoise electrodes, changing the electrode arrangement, or installing surge arresters can be a remedy for this situation.

Table 5.4: Minimum backflashover current causing flashover of the insulator string for the 400 kV overhead transmission line. Counterpoise grounding electrodes with length of 5 m are considered.

$i(t)$	$\rho(\Omega m)$	Caldwell		IEEE		Hileman		CIGRÈ		Shindo		Pigini	
		I_c(kA)	%($I > I_c$)	I_c(kA)	%($I > I_c$)	I_c(kA)	%($I > I_c$)	I_c(kA)	%($I > I_c$)	I_c(kA)	%($I > I_c$)	I_c(kA)	%($I > I_c$)
MCS	100	51.87	36.4	28.95	87.5	46.44	47.5	103.42	1.7	128.72	0.3	116.73	0.8
	1,000	18.19	99.0	11.92	99.7	16.71	99.5	29.10	87.2	32.51	80.3	31.50	82.42
	5,000	12.23	99.6	3.62	99.9	8.60	99.9	24.00	94.8	28.08	89.0	25.81	92.5
MSS	100	45.92	27.8	25.63	75	41.12	36.3	108.59	0.7	133.09	0.2	121.43	0.4
	1,000	13.76	97.9	7.68	99.9	12.32	98.8	28.92	66.1	32.2	57.2	31.35	59.4
	5,000	11.35	99.3	3.98	99.9	8.73	99.9	24.46	78.2	28.18	68.1	26.97	71.4

[1] For a better visualization, the different range of lightning strokes leading to a BF are shown with different colors: green: $0-10\%$, yellow: $10-30\%$, orange: $30-50\%$, red: $>50\%$

Table 5.5: Minimum backflashover current causing flashover of the insulator string for the 400 kV overhead transmission line. Counterpoise grounding electrodes with length of 40 m are considered.

$i(t)$	$\rho(\Omega m)$	Caldwell		IEEE		Hileman		CIGRÈ		Shindo		Pigini	
		I_c(kA)	%($I > I_c$)	I_c(kA)	%($I > I_c$)	I_c(kA)	%($I > I_c$)	I_c(kA)	%($I > I_c$)	I_c(kA)	%($I > I_c$)	I_c(kA)	%($I > I_c$)
MCS	100	87.60	4.5	58.90	25.04	78.80	7.8	208.63	<0.1	251.43	<0.1	231.07	<0.1
	1,000	63.03	19.9	35.18	74.2	56.44	28.7	125.38	0.5	137.81	0.2	134.80	0.3
	5,000	43.57	54.0	24.32	94.5	39.01	64.9	76.42	9	77.19	8.6	79.18	7.61
MSS	100	77.54	4.2	43.28	32.3	69.43	6.9	200.33	<0.1	241.88	<0.1	222.00	<0.1
	1,000	62.04	10.7	34.62	50.9	55.54	15.8	125.28	0.3	136.65	0.2	134.75	0.2
	5,000	44.79	29.6	25.00	76.7	40.10	38.4	77.17	4.3	74.95	4.9	79.12	3.8

[1] For a better visualization, the different range of lightning strokes leading to a BF are shown with different colors: green: $0-10\%$, yellow: $10-30\%$, orange: $30-50\%$, red: $>50\%$

5.7 Summary

In this ection, a detailed full-wave simulation model was proposed to obtain the equivalent black-box model of transmission towers for the calculation of the transient voltage across the insulator strings. All details of the transmission tower, the real representation of tower-footing grounding electrodes, frequency dependence of soil electrical parameters, shield wires and phase conductors are considered in this simulation model. The user of the black-box model can apply any arbitrary current at the tower top, and calculate the induced voltage across the insulator strings, without the need to perform any electromagnetic fields simulation. The model was applied to a typical 400 kV double circuit tower, and the time domain voltages across the insulator strings were calculated considering various soil resistivity values and length of counterpoise grounding electrodes. Two available measurements in the literature at Monte San Salvatore (MSS) and Morro do Cachimbo (MCS) stations on downward negative first lightning strokes were used as the input current injected at the tower top. Next, the minimum critical current leading to a flashover was calculated employing the disruptive effect (DE) and leader propagation (LP) flashover models. The predicted current varies significantly among these models, with the LP methods leading to much higher values in comparison to the DE methods. The least critical current was obtained by applying the IEEE DE method. The lightning performance of the line was shown to be dependent on the location where it is installed, because of the various waveshapes of lightning current and the probabilistic distribution of the characterizing parameters, such as its peak value and rise time. The length of counterpoise grounding electrodes was shown to be highly affecting in mitigating the overvoltages. Electrodes of 5 m in length were shown to be insufficient in even lower soil resistivity. Increasing this length to 40 m, decreased the precentage of lightning current leading to a flashover to 7.8% and below, in soil resistivity of 100Ωm. However, the

performance of such length of electrode in a soil resistivity of $1,000$, and $5,000\Omega$m is not satisfactory, and it should be further increased to ensure an acceptable rate of outage.

Chapter 6
Concluding Remarks

6.1 Conclusions

In this thesis, EMT-compatible models were developed for tower-footing grounding electrodes and transmission line tower along with its grounding system. A simulation model was developed for the analysis of grounding electrodes where full-wave Maxwell's equations were solved using Finite Element Method (FEM) in commercial software HFSS. Vertical and horizontal grounding electrodes of various length buried in soil were studied considering both constant and frequency dependent soil electrical parameters. A broad range of values for the soil resistivity and relative permittivity were considered, to take into account the effect of soil water content on the transient response of grounding electrodes. In the frequency domain, the input impedance of grounding electrodes is constant up to a certain frequency, known as characteristic frequency. At higher frequencies, the electrode has a capacitive or inductive behavior, depending on the electrode length and soil resistivity. This results in significantly different behavior from that obtained by considering a resistive model for the grounding electrode. Furthermore, it was shown that the frequency dependence of soil electrical pa-

rameters have a considerable effect on the grounding impedance, especially with a higher soil resistivity. The frequency-domain response of vertical and horizontal electrodes of the same length were found to be very similar to each other. The effect of varying the soil relative permittivity, which is dependent on the soil water content was found to be significant.

The second part of the thesis was focused on transmission line towers. An automated process was developed to obtain the wire network equivalent of transmission line towers, which were used in simulations using NEC4. To verify the simulation model, a simple structure was implemented in NEC4, and the results were compared with the available measurements. Next, a 400 kV double circuit tower was considered and the results obtained by the thin wire approximation were compared with those obtained by theoretical tower models. Both PEC and lossy ground were considered. It was found that the results of theoretical models are different from those obtained using NEC4 when the injected current to the tower top has a short rise time. This is because the low frequency approximations that the theoretical approaches are based on, and the fact that such models are developed based on a very restricted number of measurements on one type of transmission tower.

In the last part of the thesis, a black-box model for transmission line towers was developed to be used in EMT-type simulators. First, a rigorous full-wave simulation model was developed for the simulation of electromagnetic waves around the tower. All tower details, tower-footing grounding electrodes, frequency dependence of soil electrical parameters, and shield wires and overhead phase conductors were considered in the model with no approximation. Several length of counterpoise grounding electrodes and soil electrical parameters were considered. The accuracy of the model was verified by reproducing measured voltage and currents. To obtain the multi-port equivalent of the tower, 7 ports were considered in the simulations. A port at the tower top, representing the injection of current at the tower top,

and 6 ports whose current was equal to the current going through the string of insulators. Vector Fitting was then used to approximate the frequency-domain response with rational functions and the state-space model of the tower was developed. Using this model, the end user does not need to perform any electromagnetic simulation. Finally, the developed model was used to obtain the time-domain induced voltage across the string of insulators, and different models for the assessment of flashover across the insulators were used. The lightning data taken from two different locations were used to assess the probability of occurrence of backflashover under different conditions of soil resistivity and length of grounding electrodes. Considering the generality of the proposed model, the developed model can be considered as a considerable improvement in lightning studies.

6.2 Future Work

In this section, future studies and possible extensions of this research are recommended.

1. In the simulation of the transmission line tower, the adjacent towers were not considered, and the transmission lines were grounded through a matching network to avoid reflections. The reason was that considering the adjacent towers increases the required computational time and recourse considerably. The negative reflection from adjacent towers can be considered in future studies.

2. The simulation can be done considering a higher length of the counterpoise electrodes and a higher number of soil resistivity, to derive equations relating the soil resistivity to the effective length of grounding electrodes, or an equation to be used to determine the required length of electrode to ensure a specific outage rate for the transmission line.

3. The developed model can be used to simulate other type of transmission line towers, to create a complete library of towers to be used in transient electromagnetic simulations.

4. Since the numerical simulations of this thesis were all performed in the frequency domain, inclusion of soil ionization was not an option. However, as the amplitude of the injected current into the system increases, soil ionization occurres and can affect the grounding impedance and the induced voltage across the insulator strings.

5. A multi-layer soil, which represents the reality to a better extent compared to a homogeneous one, can be easily incorporated into the simulation model of the transmission tower.

6. A lightning stroke can also hit the shield wires at the midspan, which was not considered in this thesis. In this case, a shielding failure can happen.

Chapter 7

Appendix A

7.1 Description of the Method of Characteristics

The theoretical models of transmission line towers (Sec. 2.3), provide a surge impedance for the tower as a function of its height. In this case, the surge impedance varies at different heights. This is equivalent to a non-uniform transmission line having a varying per-unit-length parameters at different heights. In this case, the the differential changes in the line voltage and current are given by

$$\frac{\partial V(z,t)}{\partial z} + L(z)\frac{\partial i(z,t)}{\partial t} + Ri(z,t) = 0 \tag{7.1a}$$

and

$$\frac{\partial i(z,t)}{\partial z} + C(z)\frac{\partial V(z,t)}{\partial t} = 0 \tag{7.1b}$$

where $V(z,t)$ and $i(z,t)$ are the voltage and current along the line, respectively. The method of characteristics aims at transforming these partial differential equations of the transmission

line into ordinary differential equations that are easily integrable.

Consider the following matrix from (7.1a) and (7.1b) [152]:

$$\begin{bmatrix} 0 & L(z) \\ C(z) & 0 \end{bmatrix} \tag{7.2}$$

where its eigenvalues are:

$$\lambda_{(\pm)} = \pm\sqrt{L(z)C(z)}. \tag{7.3}$$

Next, the following two relationships are introduced from the eigenvalues:

$$\frac{dt}{dx} = \lambda_{(+)} \tag{7.4a}$$

$$\frac{dt}{dx} = \lambda_{(-)} \tag{7.4b}$$

The solution of these two expressions, is a pair of Ordinary Differential Equations (ODEs) as follows:

$$t - \sqrt{L(z)C(z)}z = \alpha \tag{7.5a}$$

$$t + \sqrt{L(z)C(z)}z = \beta \tag{7.5b}$$

where α and β are real constants. These two expressions are two families of lines in the z-t plane, and they serve as a new coordinate system for (7.1a) and (7.1b). Performing this coordinate change, (7.1a) and (7.1b) become:

$$\frac{dV}{dz} + Z_W\frac{di}{dz} + Ri = 0 \tag{7.6a}$$

and

$$\frac{dV}{dz} - Z_W \frac{di}{dz} + Ri = 0 \tag{7.6b}$$

where Z_W is the surge impedance given by

$$Z_W = (L(Z)/C(Z))^{1/2} \tag{7.7}$$

Solving (7.6a) and (7.6b) by integration, one can find the voltage and current along the non-uniform transmission line representing the transmission line tower. The excitation should be modeled as a current source in parallel with the equivalent impedance of the lightning channel.

References

[1] "List of major power outages," https://en.wikipedia.org/wiki/List_of_major_power_outages.

[2] V. Cooray, *Lightning protection*. London, United Kingdom: The Institution of Engineering and Technology, 2010.

[3] S. Visacro, "Direct strokes to transmission lines: Considerations on the mechanisms of overvoltage formation and their influence on the lightning performance of lines," *J. Lightning Res.*, vol. 1, pp. 60–68, 2007.

[4] F. H. Silveira, S. Visacro, A. De Conti, and C. R. De Mesquita, "Backflashovers of transmission lines due to subsequent lightning strokes," *IEEE Transactions on Electromagnetic Compatibility*, vol. 54, no. 2, pp. 316–322, 2012.

[5] S. Visacro, *Lightning: An engineering approach*. Sao Paulo, Brazil: Ed. ArtLiber, 2005.

[6] R. Rudenberg, *Electrical shock waves in power systems*. London, United Kingdom: Harvard university press, 1968.

[7] R. Verma, "Impulse impedance of buried ground wire," *IEEE Transactions on Power Apparatus and Systems*, vol. PAS-99, no. 5, pp. 2003–2007, 1980.

[8] A. F. Otero, J. Cidras, and J. L. del Alamo, "Frequency-dependent grounding system calculation by means of a conventional nodal analysis technique," *IEEE Transactions on Power Delivery*, vol. 14, no. 3, pp. 873–878, 1999.

[9] M. Ramamoorty, M. M. B. Narayanan, and S. Parameswaran, "Transient performance of grounding grids," *IEEE Transactions on Power Delivery*, vol. 4, no. 4, pp. 2053–2059, 1989.

[10] A. Geri, "Behaviour of grounding systems excited by high impulse currents: The model and its validation," *IEEE Transactions on Power Delivery*, vol. 14, no. 3, pp. 1008–1017, 1999.

[11] J. Cidras, A. Otero, and C. Garrido, "Nodal frequency analysis of grounding systems considering the soil ionization effect," *IEEE Transactions on Power Delivery*, vol. 15, no. 1, pp. 103–107, 2000.

[12] R. Zeng, X. Gong, and J. He, "Lightning impulse performance of grounding grids for substations considering soil ionization," *IEEE Transactions on Power Delivery*, vol. 15, no. 2, pp. 667–675, 2008.

[13] Z. Feng, X. Wen, and X. Tong, "Impulse characteristics of tower grounding devices considering soil ionization by the time-domain difference method," *IEEE Transactions on Power Delivery*, vol. 30, no. 4, pp. 1906–1913, 2015.

[14] E. D. Sunde, *Earth conduction effects in transmission systems.* New York, Dover: New York: Dover, 1968.

[15] L. V. Bewley, *Traveling waves on transmission systems.* New York, Wiley: New York: Dover, 1951.

[16] ——, "Theory and tests of the counterpoise," *Electrical Engineering*, vol. 53, pp. 1163–1172, 1934.

[17] A. D. Papalexopoulos and A. P. Meliopoulos, "Frequency dependent characteristics of grounding systems," *IEEE Transactions on Power Delivery*, vol. 2, no. 4, pp. 1073–1081, 1987.

[18] Y. Liu, N. Theethayi, and R. Thottappillil, "An engineering model for transient analysis of grounding system under lightning strikes: Nonuniform transmission-line approach," *IEEE Transactions on Power Delivery*, vol. 20, no. 2, pp. 722–730, 2005.

[19] V. Z. Annenkov, "Calculating the impulse impedance of long groundings in poor conducting soil," *Electrichestvo*, vol. 11, pp. 62–79, 1974.

[20] C. Mazzetti and G. M. Veca, "Impulse behaviour of grounded electrodes," *IEEE Transactions on Power Apparatus and Systems*, vol. PAS-102, no. 9, pp. 3148–3156, 1983.

[21] R. Velazquez and D. Mukhedkar, "Analytical modeling of grounding electrodes," *IEEE Transactions on Power Apparatus and Systems*, vol. 103, no. 6, pp. 1314–1322, 1984.

[22] S. Chiheb, O. Kherif, and M. Teguar, "Impedance nature of long horizontal grounding electrode employing TLM," *International Conference on Electrical Sciences and Technology*, pp. 1–4, 2018.

[23] ——, "Transient behavior of vertical grounding electrode under impulse current," *International Conference on Electrical Engineering ICEE-B*, pp. 1–5, 2017.

[24] Z. Shi, L. Liu, and P. Xiao, "Applying transmission line theory to study the transmitting turn-off current in a long grounded wire," *IEEE Transactions on Antennas Propagation*, vol. 65, no. 10, pp. 5112–5122, 2017.

[25] S. Bourg, B. Sacepe, and T. Debu, "Deep earth electrodes in highly resistive ground: Frequency behavior," *Proceedings IEEE International Symposium Electromagnetic Compatibility*, pp. 584–589, 1995.

[26] S. S. Devgan and E. R. Whitehead, "Analytical models or distributed grounding systems," *IEEE Transactions on Power Apparatus and Systems*, vol. PAS-92, no. 5, pp. 1763–1770, 1973.

[27] F. Mentre and L. Grcev, "EMTP-based model for grounding system analysis," *IEEE Transactions on Power Delivery*, vol. 9, no. 4, pp. 1838–1849, 1994.

[28] Y. Liu, M. Zitnik, and R. Thottappillil, "An improved transmission-line model of grounding system," *IEEE Transactions on Electromagnetic Compatibility*, vol. 43, no. 3, pp. 348–355, 2001.

[29] B. Nekhoul, C. Guerin, and P. Labie, "A finite element method for calculating the electromagnetic fields generated by substation grounding systems," *IEEE Transactions on Magnetics*, vol. 31, no. 3, pp. 2150–2153, 1995.

[30] B. Nekhoul, P. Labie, and F. X. Zgainski, "Calculating the impedance of a grounding system," *IEEE Transactions on Magnetics*, vol. 32, no. 3, pp. 1509–1512, 1996.

[31] B. Salarieh, H. M. J. De Silva, and B. Kordi, "Wideband EMT-compatible model for grounding electrodes buried in frequency dependent soil," *Int. conf. Power Systems Transients (IPST2019) - Proc.*, 2019, Paper 19IPST081.

[32] M. Akbari, K. Sheshyekani, and M. Alemi, "The effect of frequency dependence of soil electrical parameters on the lightning performance of grounding systems," *IEEE Transactions on Electromagnetic Compatibility*, vol. 33, no. 4, pp. 739–746, 2013.

[33] J. Arajo, A. R., S. Kurokawa, and M. Seixas, C., "Overvoltage analysis of transmission towers considering the influence of tower footing impedance," *International Symposium on Lightning Protection*, pp. 1–6, 2017.

[34] A. Sunjerga, F. Rachidi, and M. Rubinstein, "Calculation of the grounding resistance of structures located on elevated terrain," *IEEE Transactions on Electromagnetic Compatibility*, pp. 1–5, 2018.

[35] L. Qi, X. Cui, and Z. Zhao, "Grounding preformance analysis of the substation grounding grids by finite element method in frequency domain," *IEEE Transactions on Magnetics*, vol. 43, no. 4, pp. 1181–1184, 2007.

[36] F. E. Asimakopoulou, V. T. Kontargyri, and I. F. Gonos, "Transient behavior of grounding systems embedded in different earth structures," *7th International Mediterranean Conference and Exhibition on Power Generation, Transmission, Distribution and Energy Conversion*, 2010.

[37] J. P. Plumey, D. Roubertou, and J. Fontaine, "High frequency harmonic input impedance of an antenna embedded in a conducting half-space," *International Zurich Symposium on Electromagnetic Compatibility*, 1983.

[38] D. Roubertou, J. Fontaine, and J. P. Plumey, "Harmonic input impedance of earth connections," *IEEE International Symposium on Electromagnetic Compatibility*, pp. 717–720, 1984.

[39] L. Grcev and F. Dawalibi, "An electromagnetic model for transients in grounding systems," *IEEE Transactions on Power Delivery*, vol. 5, no. 4, pp. 1773–1781, 1990.

[40] L. Grcev, "Computer analysis of transient voltages in large grounding systems," *IEEE Transactions on Power Delivery*, vol. 11, no. 2, pp. 815–823, 1996.

[41] ——, "Time and frequency dependent lightning surge characteristics of grounding electrodes," *IEEE Transactions on Power Delivery*, vol. 24, no. 4, pp. 2186–2196, 2009.

[42] L. Grcev and M. Heimbach, "Frequency dependent and transient characteristics of substation grounding system," *IEEE Transactions on Power Delivery*, vol. 12, pp. 172–178, 1997.

[43] L. Grcev and M. Popov, "On high frequency circuit equivalents of a vertical ground rod," *IEEE Transactions on Power Delivery*, vol. 20, no. 2, pp. 1598–1603, 2005.

[44] L. Grcev, A. Kuhar, and V. Arnautovski-Tasova, "Evaluation of high-frequency circuit models for horizontal and vertical grounding electrodes," *IEEE Transactions on Power Delivery*, vol. 33, no. 6, pp. 3065–3074, 2018.

[45] L. Grcev, "Modeling of grounding electrodes under lightning currents," *IEEE Transactions on Electromagnetic Compatibility*, vol. 51, no. 3, pp. 559–571, 2009.

[46] M. Alemi and K. Sheshyekani, "Wide-band modeling of tower-footing grounding systems for the evaluation of lightning performance of tranmission lines," *IEEE Transactions on Electromagnetic Compatibility*, vol. 57, no. 6, pp. 1627–1636, 2015.

[47] A. Sunjerga, D. Gazzana, and D. Poljak, "Tower and path-dependent voltage effects on the measurement of grounding impedance for lightning studies," *IEEE Transactions on Electromagnetic Compatibility*, vol. 61, no. 2, pp. 409–418, 2018.

[48] B. Honarbakhsh, H. Karami, and K. Sheshyekani, "Direct characterization of grounding system wide-band input impedance," *IEEE Transactions on Electromagnetic Compatibility*, vol. 60, no. 1, pp. 292–293, 2018.

[49] F. Dawalibi, A. Selby, and R. G. Olsen, "Electromagnetic-fields of energized conductors," *IEEE Transactions on Power Delivery*, vol. 8, no. 3, pp. 1275–1284, 1993.

[50] H. Karami, K. Sheshyekani, and F. Rachidi, "Mixed-potential integral equation for full-wave modeling of grounding systems buried in a lossy multilayer stratified ground," *IEEE Transactions on Power Delivery*, vol. 59, no. 5, pp. 1505–1513, 2017.

[51] R. Olsen and M. C. Wilis, "A comparison of exact and quasi-static methods for evaluating grounding systems at high frequencies," *IEEE Transactions on Power Delivery*, vol. 11, no. 2, pp. 1071–1081, 1996.

[52] K. Tanabe and A. Asakawa, "Computer analysis of transient performance of grounding grid element based on the finite-difference time-domain method," *IEEE International Symposium on Electromagnetic Compatibility*, pp. 209–212, 2003.

[53] K. Tanabe, "Novel method for analyzing the transient behavior of grounding systems based on the finite-difference time-domain method," *IEEE Power Engineering Society Winter Meeting*, pp. 1128–1132, 2001.

[54] Y. Baba, N. Nagaoka, and A. Ametani, "Modeling of thin wires in a lossy medium for FDTD simulations," *IEEE Transactions on Electromagnetic Compatibility*, vol. 47, no. 1, pp. 54–60, 2005.

[55] H. Chen and Y. Du, "Lightning grounding grid model considering both the frequency-dependent behavior and ionization phenomenon," *IEEE Transactions on Electromagnetic Compatibility*, vol. 61, no. 1, pp. 157–165, 2019.

[56] A. Yutthagowith, N. Ametani, A., and N., "Application of the partial element equivalent circuit method to analysis of transient potential rises in grounding systems," *IEEE Transactions on Electromagnetic Compatibility*, vol. 53, no. 13, pp. 726–736, 2011.

[57] H. Lu, Z. Feng, and X. Tong, "Observation and analysis of the sparkover around grounding electrode under impulse current," *IET Generation, Transmission, and Distribution*, vol. 11, no. 8, pp. 1997–2002, 2017.

[58] E. Y. Ryabkova and V. M. Mishkin, "Impulse characteristics of high voltage transmission line tower groundings in homogeneous soil," *Electrichestvo*, vol. 8, pp. 67–70, 1976.

[59] S. Sekioka, T. Sonoda, and A. Ametani, "Experimental study of current-dependent grounding resistance of rod electrode," *IEEE Transactions on Power Delivery*, vol. 20, no. 2, pp. 1569–1576, 2005.

[60] S. Sekioka, H. Hayashida, and T. Hara, "Measurements of grounding resistances for high impulse currents," *IEEE Generation, Transmission, and Distribution*, pp. 693–699, 1998.

[61] D. S. Gazzana, A. Smorgonskiy, and N. Mora, "An experimental field study of the grounding system response of tall wind turbines to impulse surges," *Electric Power Systems Research, Elsevier*, pp. 219–225, 2018.

[62] A. A. R. Zohdy, "The auxiliary point method of electrical sounding interpretation, and its relationship to the Dar Zarrouk parameters," *Geophysics*, vol. 30, no. 4, pp. 644–660, 1965.

[63] C. E. F. Caetano, R. Batista, and J. O. S. Paulino, "A simplified method for calculating the impedance of vertical grounding electrodes buried in a horizontally stratified multilayer ground," *International Conference on Lightning Protection, ICLP*, 2018.

[64] H. Karami and K. Sheshyekani, "Harmonic impedance of grounding electrodes buried in a horizontally stratified multilayer ground: A Full-Wave Approach," *IEEE Transactions on Electromagnetic Compatibility*, vol. 60, no. 4, pp. 899–906, 2018.

[65] S. Chiheb, O. Kherif, and M. Teguar, "Transient behaviour of grounding electrodes in uniform and in vertically stratified soil using state space representation," *IET Science, Measurement, and Technology*, vol. 12, no. 4, pp. 427–534, 2018.

[66] M. Ghomi, H. Mohammadi, and H. Karami, "Full-wave modeling of grounding system: Evaluation the effects of multi-layer soil and length of electrode on ground potential rise," *International Conference on Power Systems Transients, IPST*, pp. 1–6, 2019.

[67] R. L. Smith-Rose, "Electrical measurements on soil with alternating currents," *Institute of Electrical Engineers, Proceedings of the Wireless Section of the Institution*, vol. 9, no. 27, pp. 293–309, 1934.

[68] S. Visacro, A. Soares Jr., M. A. O. Schroeder, L. C. L. Cherchiglia, and V. J. de Sousa, "Statistical analysis of lightning current parameters: Measurements at Morro de Cachimbo Station," *Journal of Geophysical research*, vol. 109, no. 1, pp. 1–11, 2004.

[69] L. Grcev and F. Rachidi, "On tower impedances for transient analysis," *IEEE Transactions on Power Delivery*, vol. 19, no. 3, pp. 1238–1244, 2004.

[70] C. F. Wagner and A. R. Hileman, "A New Approach to the Calculation of the Lightning Performance of Transmission Lines III-A Simplified Method: Stroke to Tower," *Transactions of the American Institute of Electrical Engineering Part III: Power Apparatus and System*, vol. 79, no. 16, pp. 589–603, 1960.

[71] F. P. Dawalibi, W. Ruan, S. Fortin, J. Ma, and W. K. Daily, "Computation of power line structure surge impedances using the electromagnetic field method," *Proceedings of IEEE/Power Engineering Society, Transmission and Distribution Conference*, vol. 2, pp. 663–668, 2001.

[72] M. A. Sargent and M. Darveniza, "Tower Surge Impedance," *IEEE Transactions on Power Apparatus and System*, vol. PAS-88, no. 5, pp. 680–687, 1969.

[73] F. Heidler, "Calculation of lightning current parameters," *IEEE Transactions on Power Delivery*, vol. 14, no. 2, pp. 399–404, 1999.

[74] C. R. Paul, *Analysis of multiconductor transmission lines.* IEEE Press, 2007.

[75] J. G. Anderson, A. R. Hileman, and W. Chisholm, "A Simplified Method for Estimating Lightning Performance of Transmission Lines," *IEEE Transactions on Power Apparatus and System*, vol. PAS-104, no. 4, pp. 918–932, 1985.

[76] C. Menemenlis and Z. T. Chun, "wave propagation on nonuniform lines," *IEEE Transactions on Power Apparatus and System*, vol. PAS-101, no. 4, pp. 833–839, 1982.

[77] W. A. Chisholm and Y. L. Chow, "Travel time of transmission towers," *IEEE Trans. Power App. Syst.*, vol. PAS-104, no. 10, pp. 2922–2928, 1985.

[78] W. A. Chisholm, Y. L. Chow, and K. D. Srivastava, "Lightning surge response of transmission towers," *IEEE Trans. Power App. Syst.*, vol. PAS-102, no. 9, pp. 3232–3242, 1983.

[79] IEEE Std. 1243, *Guide for improving the lightning performance of Transmission Lines.* IEEE, 1997.

[80] A. De Conti, S. Visacro, A. Soares, and M. A. O. Schroeder, "Revision, extension, and validation of Jordan's formula to calculate the surge impedance of vertical conductors," *IEEE Trans. Electromagn. Compat.*, vol. 48, no. 3, pp. 530–536, 2006.

[81] H. Takahashi, "Confirmation of the error of Jordan's formula on tower surge impedance," *The Journal of the Institute of Electrical Engineers of Japan*, vol. 114-B, pp. 112–113, 1994.

[82] C. A. Jordan, "Lightning computations for transmission lines with overhead ground wires," *General Electric Rev.*, vol. 37, no. 4, pp. 180–186, 1934.

[83] Z. G. Datsios and P. N. Mikropoulos, "Effect of tower modelling on the minimum backflashover current of overhead transmission lines," *19th Int. Symp. on High Voltage Eng. (ISH)*, no. August, 2015.

[84] CIGRE WG01 SC33, "Guide to procedures for estimating the lightning performance of transmission lines, A. Eriksson (CH), L. Dellera (IT), G. Baldo (IT), C. H. Bouquegneau (BE), H. Darvenisa (AU), J. Elovaara (FI), E. Garbagnati (IT), C. Gary (FR)," *Cigré Tb 63*, vol. 01, no. October, p. 64, 1991.

[85] T. Hara and O. Yamamoto, "Modeling of a transmission tower for lightning-surge analysis," *IEE Proceedings - Gen. Trans. Dist.*, vol. 143, no. 3, p. 283, 1996.

[86] J. A. Gutiérrez, R. P. Moreno, J. L. Naredo, J. L. Bermúdez, M. Paolone, C. A. Nucci, and F. Rachidi, "Nonuniform transmission tower model for lightning transient studies," *IEEE Trans. Power Deli.*, vol. 19, no. 2, pp. 490–496, 2004.

[87] R. J. Gutiérrez, P. Moreno, L. Guardado, and J. L. Naredo, "Comparison of transmission tower models for evaluating lightning performance," *2003 IEEE Bologna PowerTech - Conf. Proc.*, vol. 4, pp. 339–344, 2003.

[88] M. Ishii, T. Kawamura, T. Kouno, E. Ohsaki, K. Murotani, and T. Higuchi, "Multistory Transmission Tower Model For Lightning Surge Analysis," *IEEE Transactions on Dielectric and Electrical Insulation*, vol. 18, no. 3, pp. 1855–1865, 2014.

[89] T. Yamada, A. Mochizuki, J. Sawada, E. Zaima, T. Kawamura, A. Ametani, M. Ishii, and S. Kato, "Experimental evaluation of a uhv tower model for lightning surge analysis," *IEEE Transactions on Power Delivery*, vol. 10, no. 1, pp. 393–402, 1995.

[90] H. Motoyama, K. Shinjo, Y. Matsumoto, and N. Itamoto, "Observation and analysis of multiphase back flashover on the Okushishiku test transmission line caused by winter lightning," *IEEE Trans. Power Del.*, vol. 13, no. 4, pp. 1391–1398, 1998.

[91] M. Ishii and Y. Baba, "Numerical electromagnetic field analysis on lightning surge response of tower with shield wire," *IEEE Power Engineering Review*, vol. 17, no. 1, p. 69, 2000.

[92] M. O. Goni and A. Ametani, "Analysis and estimation of surge impedance of tower," *Applied Computational Electromagn. Society*, vol. 24, no. 1, pp. 72–78, 2009.

[93] S. Hashimoto, Y. Baba, N. Nagaoka, A. Ametani, and N. Itamoto, "An equivalent circuit of a transmission-line tower struck by lightning," *2010 30th Int. Conf. Lightning Protection, ICLP 2010*, vol. 2010, pp. 2–7, 2017.

[94] T. Noda, "A tower model for lightning overvoltage studies based on the result of an FDTD simulation," *Electrical Engineers of Japan*, vol. 164, no. 1, pp. 8–20, 2008.

[95] A. Ametani, "Frequency-dependent impedance of vertical conductors and a multiconductor tower model," *IEE Proceedings - Generetaion, Transmission and Distribution*, vol. 141, no. 4, p. 339, 2002.

[96] T. Hara, O. Yamamoto, M. Hayashi, and C. Uenosono, "Empirical formulas of surge impedance for single and multiple vertical cylinders," *IEEJ Trans. Power Energy*, vol. 110, no. 2, pp. 129–137, 1990.

[97] B. Gustavsen and A. Semlyen, "Rational approximation of frequency domain responses by vector fitting," *IEEE Transactions on Power Delivery*, vol. 14, no. 3, pp. 1052–1061, 1999.

[98] T. Noda, "Identification of a multiphase network equivalent for electromagnetic transient calculations using partitioned frequency response," *IEEE Power Engineering Society General Meeting*, 2005.

[99] B. Gustavsen and H. M. J. D. Silva, "Inclusion of Rational Models in an Electromagnetic Transients Program: Y-Parameters, Z-Parameters, S-Parameters, Transfer Functions," *IEEE Transactions on Power Delivery*, vol. 28, no. 2, pp. 1164–1174, 2013.

[100] G. Antonini, "SPICE equivalent circuits of frequency-domain responses," *IEEE Transactions on Electromagnetic Compatibility*, vol. 45, no. 3, pp. 502–512, 2003.

[101] J. H. Scott, *Electrical and magnetic properties of rock and soil.* U. S. Geological Survey, 1983.

[102] L. A. Richards, *Diagnosis and improvement of saline and alkali soils.* U. S. Department of Agriculture, Agriculture Handbook, 1954.

[103] L. M. Thring, "Electrical measurements on soil with alternating currents," *Institute of Electrical Engineers*, vol. 9, no. 27, pp. 293–309, 1934.

[104] K. Roth, R. Schulin, H. Flühler, and W. Attinger, "Calibration of time domain reflectometry for water content measurement using a composite dielectric approach," *Water resources research*, vol. 26, no. 10, pp. 2267–2273, 1990.

[105] J. R. Wang and T. J. Schugge, "An empirical model for the complex dielectric permittivity of soils as a function of water content," *IEEE Transactions on Geoscience and remote sensing*, vol. 1, no. 4, pp. 288–295, 1980.

[106] J. H. Scott, R. D. Carroll, and D. R. Cunningham, "Dielectric constant and electrical conductivity measurements of moist rock: A new laboratory method," *U. S. Geological Survey*, vol. 72, no. 20, pp. 5101–5115, 1967.

[107] H. M. Mooney, "Magnetic susceptibility measurements in Minnesota," *U. S. Geophysics*, vol. 17, no. 3, pp. 531–543, 1952.

[108] L. L. Nettleton, *Geophysical prospecting for soil.* New York, McGwar Hill: Harvard university press, 1940.

[109] C. Portela, "Measurement and modeling of soil electromagnetic behavior," *IEEE International Symposium on Electromagnetic Compatibility*, vol. 2, pp. 1004–1009, 1999.

[110] S. F. Visacro, F. H. Silveira, S. Xavier, and H. B. Ferreira, "Frequency dependence of soil parameters: The influence on the lightning performance of transmission lines," *International Conference on Lightning Protection (ICLP)*, vol. 57, no. 3, pp. 1–4, 2012.

[111] J. H. Scott, R. D. Carroll, and D. R. Cunningham, *Dielectric constant and electrical conductivity of moist rock from laboratory measurements.* Kirtland AFB, NM: Sensor and Simulation Note 116, 1964.

[112] A. G. Pedrosa, A. R. S., and A. O. Schroeder, "Simulation of behavior electrical grounding: Comparative analysis for performance in frequency-domain," *International Workshop on Application, Modeling, and Simulation*, 2010.

[113] C. L. Longmire and H. J. Longley, *Time domain treatment of media with frequency dependent parameters.* Santa Barbara, CA, USA: Theoretical Notes 113, 1973.

[114] K. S. Smith and C. L. Longmire, *A universal impedance for soils.* Alexandria, VA, USA: Defense Nuclear Agency, 1975.

[115] M. A. Messier, *The propagation of an electromagnetic impulse through soil: Influence of frequency dependent parameters.* Santa Barbara, Ca, USA: Mssion Res. Corp., 1980.

[116] ——, *Another soil conductivity model.* Santa Barbara, Ca, USA: Mission Res. Corp., 1985.

[117] D. I. L. Villiers, "Analysis and design of conical transmission line power combiners," *University of Stellenbosch*, 2007.

[118] S. Ramo, J. R. Whinnery, and T. Duzer, *Fields and waves in communication electronics.* New York, Willey, 3rd edition, 1994.

[119] C. R. Paul, "Measurement and modeling of soil electromagnetic behavior," *IEEE Transactions on Microwave Theory and Techniques*, vol. 1, no. 1, pp. 307–333, 2010.

[120] P. Sumithra and D. Thiripurasundari, "A review on Computational Electromagnetics Methods," *Advanced Electromagnetics*, vol. 6, no. 1, pp. 42–55, 2017.

[121] *User's guide: High frequency structure simulator.* Ansys, 2014.

[122] C. Gary, "The impedance of horizontally buried conductors," *Proceedings of the First International Symposium: Lightning and Mountains*, pp. 148–151, 1994.

[123] L. Grcev, "Modeling of grounding electrodes under lightning currents," *IEEE Transactions on Electromagnetic Compatibility*, vol. 51, no. 3, pp. 559–571, 2009.

[124] ——, "Improved earthing system design practices for reduction of transient voltages," *Presented at the CIGRE*, 1998.

[125] S. Visacro and R. Alipio, "Frequency dependence of soil parameters: Experimental results, predicting formula and influence on the lightning response of grounding electrodes," *IEEE Transactions on Power Delivery*, vol. 27, no. 2, pp. 927–935, 2012.

[126] S. Visacro, "Response of Grounding Electrodes to Impulsive Currents: An Experimental Evaluation," *IEEE Transactions on Electromagnetic Compatibility*, vol. 51, no. 1, pp. 161–164, 2009.

[127] S. Visacro, M. H. M. Vale, N. Miguel B Guimarães, R. Araújo, W. L. F. Pinto, and R. S. Alípio, "The response of grounding electrodes to lightning currents : the effect of frequency-dependent resistivity and permittivity of soil," *30th International Conference on Lightning Protection - ICLP 2010*, vol. 2010, pp. 1–4, 2010.

[128] K. Berger, R. B. Anderson, and H. Kroninger, "Parameters of lighning flashes," *Electra*, vol. 41, pp. 23–37, 1975.

[129] P. Chowdhuri, J. G. Anderson, and W. A. Chisholm, "Parameters of lightning strokes: A review," *IEEE Transactions on Power Delivery*, vol. 20, no. 1, pp. 346–358, 2005.

[130] F. Rachidi, W. Janischewskyj, and A. M. Hussein, "Current and electromagnetic field associated with lightning-return strokes to tall towers," *IEEE Transactions on Electromagnetic Compatibility*, vol. 43, no. 3, pp. 356–367, 2001.

[131] F. A. Fisher, J. G. Anderson, and J. H. Hagenguth, "Determination of lightning response of transmission lines by means of geometrical models," *Transactions of the American Institute of Electrical Engineering Part III: Power Apparatus and System*, vol. 78, no. 4, pp. 1725–1734, 1959.

[132] M. T. Correia De Barros and M. E. Almeida, "Computation of electromagnetic transients on nonuniform transmission lines," *IEEE Trans. Power Del.*, vol. 11, no. 2, pp. 1082–1087, 1996.

[133] H. Motoyama and H. Matsubara, "Analytical and experimental study on surge response of transmission tower," *IEEE Trans. Power Del.*, vol. 15, no. 2, pp. 812–819, 2000.

[134] Y. Baba and M. Ishii, "Numerical electromagnetic field analysis of tower surge response," *IEEE Trans. Power Del.*, vol. 15, no. 3, pp. 1010–1015, 2000.

[135] Y. Baba and I. Masaru, "Tower Models for Fast-Front lightning currents," *IEE Japan*, vol. 120-B, no. 1, pp. 18–23, 2000.

[136] M. S. Yusuf, M. Ahmad, M. A. Rashid, and M. O. Goni, "Analysis of lightning surge characteristics on transmission tower," *Engineering Letters*, vol. 23, no. 1, pp. 29–39, 2015.

[137] P. C. A. Mota, M. L. R. Chaves, and J. R. Camacho, "Power Line Tower Lightning Surge Impedance Computation , a Comparison of Analytical and Finite Element Methods ." *2012 International Conference on Renewable Energies and Power Quality, ICREPQ'12*, no. March 2012, 2012.

[138] R. J. Anderson De Araujo, S. Kurokawa, C. M. D. Seixas, and B. Kordi, "Lightning-induced surge in transmission towers calculated using full-wave electromagnetic analysis and the method of moments," *2018 13th IEEE Int. Conf. Industry Applic., INDUSCON 2018 - Proc.*, pp. 943–948, 2019.

[139] A. Soares Jr., M. A. O. Schroeder, and S. Visacro, "Transient voltages in transmission lines caused by direct lightning strikes," *IEEE Trans. Power Del.*, vol. 20, no. 2, pp. 1447–1452, 2005.

[140] T. H. Thang, Y. Baba, N. Nagaoka, A. Ametani, N. Itamoto, and V. A. Rakov, "FDTD simulation of insulator voltages at a lightning-struck tower considering ground-wire corona," *IEEE Trans. Power Del*, vol. 28, no. 3, pp. 1635–1642, 2013.

[141] J. Takami, T. Tsuboi, K. Yamamoto, and S. Okabe, "Lightning Surge Response of a Double-Circuit Transmission Tower with Incoming Lines to a Substation through FDTD Simulation," *IEEE Trans. Dielectr. Electr. Insul.*, pp. 96–104, 2013.

[142] T. Noda, A. Tatematsu, and S. Yokoyama, "Improvements of an FDTD-based surge simulation code and its application to the lightning overvoltage calculation of a transmission tower," *Electric Power Systems Research*, vol. 77, pp. 1495–1500, 2007.

[143] H. Motoyama, Y. Kinoshita, K. Nonaka, and Y. Baba, "Experimental and analytical studies on lightning surge response of 500-kV transmission tower," *IEEE Trans. Power Del.*, vol. 24, no. 4, pp. 2232–2239, 2009.

[144] M. Kawai, "Studies of the Surge Response on a Transmission Line Tower," *IEEE Trans. Power App. Syst.*, vol. 83, no. 1, pp. 30–34, 1964.

[145] A. Ametani, K. Adachi, and T. Narita, "An Investigation of Surge Propagation Characteristics on an 1,100 kV Transmission Line," *The trans. Inst. of Elect. Eng. of Japan*, vol. 123, no. 4, pp. 513–519, 2003.

[146] J. L. Bermudez, J. A. Gutiérrez, W. A. Chisholm, F. Rachidi, and M. Paolone, "A Reduced-Scale Model to Evaluate the Response of Tall Towers Hit by Lightning," *Int. Symp. Power Quality (SICEL)*, no. January, 2001.

[147] J. Takami, T. Tsuboi, K. Yamamoto, S. Okabe, and Y. Baba, "Lightning surge characteristics on inclined incoming line to substation based on reduced-scale model experiment," *IEEE Trans. Dielectr. Electr. Insul.*, vol. 20, no. 3, pp. 739–746, 2013.

[148] G. D. Breuer, A. J. Schultz, R. H. Schlomann, and W. S. Price, "Field Studies of the Surge Response of a 345-Kv Transmission and ground wire," *Trans. American Inst. Elect. Eng. Part III: Power App. Syst.*, vol. 76, no. 3, pp. 1392–1396, 1957.

[149] Y. Baba and M. Ishii, "Numerical electromagnetic field analysis on measuring methods of tower surge impedance," *IEEE Trans. Power Del.*, vol. 14, no. 2, pp. 630–635, 1999.

[150] G. J. Burke, *Numerical Electromagnetic Code - (NEC-4) - Method of Moments, Part I: User's Manual*, Lawrence Livermore National Laboratory.

[151] P. Yutthagowith, A. Ametani, N. Nagaoka, and Y. Baba, "Influence of a measuring system to a transient voltage on a vertical conductor," *IEEJ Trans. Electr. Electr. Eng.*, vol. 5, no. 2, pp. 221–228, 2010.

[152] J. A. Gutiérrez, P. Moreno, J. L. Naredo, and J. C. Gutiérrez, "Fast transients analysis of nonuniform transmission lines through the method of characteristics," *Int. Journal Elect. Power Energy Syst.*, vol. 24, no. 9, pp. 781–788, 2002.

[153] *EPRI AC transmission line reference book-200kV and above.* Palo Alto, Dec. 2005.

[154] S. Visacro and F. H. Silveira, "Lightning performance of grounding systems of overhead lines," *2014 International Conference on Lightning Protection, ICLP 2014*, pp. 1386–1389, 2014.

[155] F. H. Silveira, S. Visacro, and R. E. Souza, "Lightning performance of transmission lines: Assessing the quality of traditional methodologies to determine backflashover rate of transmission lines taking as reference results provided by an advanced approach," *Electric Power Systems Research*, vol. 153, no. 2016, pp. 60–65, 2017.

[156] B. Salarieh, H. M. J. De Silva, and B. Kordi, "An Electromagnetic Model for the Calculation of Tower Surge Impedance Based on thin Wire Approximation," *Manuscript submitted for publication*, 2019.

[157] CIGRE WG C4.33, "Impact of soil-parameters frequency dependence on the response of grounding electrodes and on the lightning performance of electrical systems," *Cigré Tb 781*, vol. 01, no. October, p. 66, 2019.

[158] R. Alipio and S. Visacro, "Modeling the frequency dependence of electrical parameters of soil," *IEEE Trans. Electromagn. Compat.*, vol. 56, no. 5, pp. 1163–1171, 2014.

[159] I. S. Grant, J. G. Anderson, A. R. Hileman, W. Janischewskyj, G. E. Lee, V. J. Longo, W. Chisholm, D. Parrish, N. K. Roukos, C. T. Main, E. Whitehead, and J. T. Whitehead, "Simplified Method for Estimating Lightning Performance of Transmission Lines." *IEEE trans. power app. syst.*, vol. PAS-104, no. 4, pp. 919–932, 1985.

[160] A. F. Rohlfs and H. E. Fiegel, "Impulse flashover charactersitics of long strings of suspension insulators," *IEEE trans. power app. syst.*, vol. 76, no. 3, pp. 1321–1329, 1957.

[161] B. E. Kingsbury, "Suspension insulator flashover under high impulse voltages," *Transactions of American Institute of Electrical Engineers Part III: Power Apparatus and System*, vol. 76, no. 3, pp. 1429–1432, 1957.

[162] J. A. Rawls, J. W. Kalb, and A. R. Hileman, "Full scale surge testing of VEPCO 500-kV line insulation," *IEEE Transactions on power apparatus and system*, vol. 83, no. 3, pp. 245–250, 1964.

[163] W. C. Guyker, A. R. Hileman, and J. F. Wittibschlager, "Full-scale tests for the Allegheny power system 500-kV tower insulation system," *IEEE Transactions on power apparatus and system*, vol. PAS-85, no. 6, pp. 614–623, 1966.

[164] J. R. Fonseca, V. H. G. Andrade, P. C. V. Esmeraldo, and D. L. E. N., "Lightning impulse tests on tower models," *IEEE Transactions on power apparatus and system*, vol. PAS-103, no. 4, pp. 893–896, 1984.

[165] R. O. Caldwell and M. Darveniza, "Experimental and analytical studies of the effect of non-standard waveshapes on the impulse strength of external insulation," *IEEE Transactions on power apparatus and system*, vol. PAS-92, no. 4, pp. 1420–1428, 1973.

[166] M. Darveniza and A. E. Vlastos, "The generalized integration method for predicting impulse volt-time characteristics for non-standard wave shapes-A theoretical basis," *IEEE Tranactions on electrical insulation*, vol. 23, no. 3, pp. 373–381, 1988.

[167] A. R. Jones, "Evaluation of integration method for analysis of nonstandard surge voltages," *Transactions of American Institute of Electrical Engineering, Part III: Power Apparatus and Systems*, vol. 73, no. 2, pp. 984–990, 1954.

[168] R. L. Witzke and T. J. Bliss, "Surge protection of cable-connected equipment," *Transactions of American Institute of Electrical Engineers*, vol. 69, no. 1, pp. 527–542, 1950.

[169] ——, "Co-ordination of lightning arrestor location with transformer insulation level," *Transactions of the American Institute of Electrical Engineers*, vol. 69, no. 2, pp. 964–975, 1950.

[170] P. Chowdhuri, A. K. Mishra, and B. W. McConnell, "Volt-time characteristics of short air gaps under nonstandard lightning voltage waves," *IEEE Transactions on power delivery*, vol. 12, no. 1, pp. 470–476, 1997.

[171] IEEE, "task force 15.09 on nonstandard lightning voltage waves, Review of research on nonstandard lightning voltage waves," *Transactions on power delivery*, vol. 9, no. 4, pp. 1972–1981, 1994.

[172] W. A. Chisholm, J. G. Anderson, A. Philips, and J. Chan, "Lightning performance of compact lines," *Proceedings of the international symposium on lightning protection (SIPDA)*, pp. 45–64, 2009.

[173] W. A. Chisholm, "New challenges in lightning impulse flashover modeling of air gaps and insulators," *IEEE electrical insulation magazine*, vol. 26, no. 2, pp. 14–25, 2010.

[174] A. R. Hileman, *Insulation coordination for power systems.* CRC press/Taylor & Francis group, 1999.

[175] T. Shindo and T. Suzuki, "A new calculation method of breakdown voltage-time characteristics of long air gaps," *IEEE Transactions on power apparatus and system*, vol. PAS-104, no. 6, pp. 1556–1563, 1985.

[176] G. Pigini A .and Rizzi, E. Garbagnati, A. Porrino, G. Baldo, and G. Pesavento, "Performance of large air gaps under lightning overvoltages: experimental study and analysis of accuracy of predetermination methods," *IEEE Transactions on power delivery*, vol. 4, no. 2, pp. 1379–1392, 1989.

[177] H. Motoyama, "Experimental study and analysis of breakdown characteristics of long air gaps with short tail lightning impulse," *IEEE Transactions on power delivery*, vol. 11, no. 2, pp. 972–979, 1996.

[178] T. Mozumi, Y. Baba, M. Ishii, N. Nagaoka, and A. Ametani, "Numerical electromagnetic field analysis of archorn voltages during back-flashover on a 500-kV twin-circuit line," *IEEE Transactions on power delivery*, vol. 76, no. 1, pp. 207–213, 2003.

[179] R. B. Anderson and A. J. Eriksson, "Lightning parameters for engineering applications," *Electra*, vol. 69, no. 1, pp. 65–102, 1980.

[180] J. A. Martinez-Velasco, *Power system transients: Parameter determination.* CRC Press, 2009.

[181] J. Knockaert, J. Peuteman, J. Catrysse, and R. Belmans, "General equations for the charactersitc impedance matrix and termination network of multiconductor transmission lines," *Proc. IEEE Int. Conf. Indust. Tech.*, 2009.

[182] B. N. Gorin, V. I. Levitov, and A. V. Shkilev, "Lightning strikes to the Ostankino tower," *Electrichestvo*, no. 8, pp. 19–23, 1977.

[183] A. V. Gorin, B. N.and Shkilev, "Measurements of lightning currents at the Ostankino tower," *Electrichestvo*, no. 8, pp. 64–65, 1984.

[184] O. Beierl, "Front shape parameters of negative subsequent strokes measured at the Peissenburg tower," *in Proc. 21st Int. Conf. Lightning Protection*, pp. 19–24, 1992.

[185] W. Janischewskyj, V. Shostak, J. Barratt, A. M. Hussein, R. Rusan, and J. S. Chang, "Collection and use of lightning return troke parameters taking into account characteristics of the struck object," *in Proc. 23rd Int. Conf. Lightning Protection*, pp. 16–23, 1996.

[186] K. Ishimoto, T. Noda, M. Nakamura, and S. Maru, "Modeling of telecommunication cables with distribution lines for lightning overvoltage studies," *Int. conf. Power Systems Transients (IPST2011)*, 2011, Paper 11IPST044.

[187] H. Goshima, A. Asakawa, T. Shindo, H. Motoyama, A. Wada, and S. Yokoyama, "Characteristics of electromagnetic fields due to winter lightning stroke current to high stack," *IEJ Trans. Power Energy*, vol. 120-B, no. 1, pp. 44–49, 2000.

[188] Z. G. Datsios, P. N. Mikropoulos, and T. E. Tsovilis, "Effects of Lightning Channel Equivalent Impedance on Lightning Performance of Overhead Transmission Lines," *IEEE Trans. Electromagn. Compat.*, vol. PP, pp. 1–8, 2019.

[189] Z. Chen and X. Wu, "An Adaptive Uniaxial Perfectly Matched Layer Method for Time-Harmonic Scattering Problems," *Journal of Numerical mathematics: theory, methods and applications*, vol. 1, no. 2, 2008.

[190] I. Bardi and Z. Cendes, "New directions in HFSS for designing microwave devices," *Microwave journal*, vol. 7, no. August, 1998.

[191] C. Bayliss and B. Hordy, *Transmission and distribution electrical engineering.* Newness; 4th edition, 2011.

[192] IEEE, *Standard for insulation coordination-definitions, principles and rules.* IEEE std. C.62.82.1, 2010.

[193] D. F. Grcic, B. F. Grcic, and I. Uglesic, "Lightning critical flashover voltage pf high voltage insulators: laboratory measurements and calculations," *International review of electrical engineering (I.R.E.E.)*, vol. 7, no. 2, pp. 4321–4328, 2012.

[194] A. Ancajima, A. Carrus, E. Cinieri, and C. Mazzetti, "Behavior of MV insulators under lightning-induced overvoltages: experimental results and reproduction of volt-time characteristics by disruptive effect models," *IEEE Trans. Power Del.*, vol. 25, no. 1, pp. 221–230, 2010.

[195] A. R. de Araújo, S. Kurokawa, C. M. Seixas, and B. Kordi, "Optimization of tower-footing grounding impedance for guyed-V transmission towers," *Electric Power Systems Research*, vol. 177, no. June, p. 105947, 2019.

[196] A. De conti and S. Visacro, "Analytical representation of single- and double-peaked lightning current waveforms," *IEEE Trans. Electromagn. Comp.*, vol. 49, no. 2, pp. 488–451, 2007.

[197] S. Visacro and F. Silveira, "Lightning performance of transmission lines: Methodology to design grounding electrodes to ensure an expected outage rate ," *IEEE Trans. power del.*, vol. 30, no. 1, pp. 237–245, 2015.

[198] J. Takami and S. Okabe, "Observational results of lightning current on transmission towers," *IEEE Trans. power del.*, vol. 22, no. 1, pp. 547–556, 2007.